

Next-To-Leading-Order Matching Conditions in Extended Higgs Sectors

Master's Thesis of

Martin Gabelmann

at the Department of Physics
Institute for Theoretical Physics (ITP)

Reviewer: Prof. Dr. M. M. Mühlleitner
Second reviewer: Prof. Dr. U. Nierste
Advisor: Dr. F. Staub

16. August 2017 – 14. August 2018

I declare that I have developed and written the enclosed thesis completely by myself, and have not used sources or means without declaration in the text.

Karlsruhe, 14.08.2018

.....

(Martin Gabelmann)

Contents

1. Introduction	1
1.1. Effective Field Theories	3
1.1.1. Example: B decays	3
1.1.2. The APPELQUIST CARAZZONE Theorem	6
1.1.3. (Non-)Decoupling in the Scalar Sector	7
1.1.4. Integrating out Heavy Degrees of Freedom	9
1.2. The Standard Model of Particle Physics	10
1.2.1. Notation and Definitions	11
1.2.2. Electroweak Symmetry Breaking in the SM	13
1.2.3. The Standard Model as an Effective Theory	15
1.3. The Minimal Supersymmetric Standard Model	16
1.3.1. Particle Content	17
1.3.2. The MSSM Lagrangian	19
1.3.3. Electroweak Symmetry Breaking in the MSSM	20
1.3.4. Tree-Level Masses and Mixing Matrices	21
1.3.5. SUSY Breaking and UV Completions	23
1.4. The Next-To Minimal Supersymmetric Standard Model	23
1.4.1. Particle Content	24
1.4.2. Tree-Level Masses and Mixing Matrices	25
1.5. Supersymmetry without Natural Scalars	27
1.6. Higher-Order Threshold Corrections in Supersymmetric Models	28
1.6.1. Dimensional Regularization and Dimensional Reduction	28
1.6.2. Threshold Corrections to Gauge Couplings	29
1.7. Effective Higgs Masses in Supersymmetric Models	29
1.7.1. General Overview	29
1.7.2. Status Quo in SARAHS/SPHENO	31
2. Scalar Matching Conditions at Next-to Leading Order	35
2.1. Topologies and Generic Diagrams and their Amplitudes	35
2.1.1. Generic Tree-Level Graphs	36
2.1.2. Generic One-Loop Graphs	37
2.2. Loop Functions with vanishing External Momenta	39
2.3. A Toy-Model with Two Real Singlets	43
2.3.1. Tree-Level Matching	43
2.3.2. One-Loop Amplitudes	44
2.4. Implementation in SARAHS/SPHENO	47

3. Validation: High-Scale Supersymmetry	49
3.1. High-Scale MSSM: an Overview	49
3.2. Non-Minimal SUSY: Matching the NMSSM to the SM	51
3.2.1. Tree-Level Mass Spectrum at the Matching Scale	52
3.2.2. Matching to the SM	53
3.2.3. The Singlet Decoupling Parametrisation	54
3.2.4. Numerical Analysis	55
3.3. High-Scale MSSM with Low m_A : Matching to a 2HDM	57
3.3.1. The Low-Energy Lagrangian	58
3.3.2. Tree-Level Matching	59
3.3.3. One-Loop Matching	60
4. Application: Split Supersymmetry	63
4.1. Non-Minimal Split SUSY: The Split NMSSM	64
4.1.1. The NMSSM at m_{SUSY}	65
4.1.2. Parameter Counting	66
4.1.3. The Split NMSSM at m_t	67
4.2. One-Loop Matching of the Scalar Sector	71
4.2.1. Quartic Couplings	71
4.2.2. Trilinear Couplings	73
4.3. Numerical Analysis of the Split NMSSM Matching	73
4.3.1. Example spectrum	74
4.3.2. Parameter Scan	77
4.3.3. Top-Down Versus Simplified Models: the Advantage of Matching	84
5. Summary and Outlook	89
A. Appendix	91
A.1. Topologies	91
A.1.1. Notation	91
A.1.2. Generic Tree-Level Graphs	91
A.1.3. Generic One-Loop Graphs	93
A.2. Loop Functions with vanishing External Momenta	95
A.2.1. Definition of the Loop Functions	95
A.2.2. One- and Two-Point Integrals	95
A.2.3. Triangle Integrals	96
A.2.4. Box Integrals	97
A.2.5. Derivatives of the One- and Two-Point Functions	98
A.3. The SARAH Extension Manual	98
A.3.1. The SARAH NLO Matching Interface	98
A.3.2. Reserved Variables	104
A.3.3. Example Usage	105
Bibliography	107

1. Introduction

The idea of formulating physical laws describing nature in an effective rather than a fundamental way was already present in the ancient Greece. With the discovery of advanced mathematical and experimental tools *modern physics* is able to hypothesize and falsify microscopic theories as well as to perform the *classical* limit, if appropriate, and give a connection to physical phenomena at macroscopic scales. In this manner the scattering of two objects can be described by classical mechanics rather than quantum mechanics (QM) if their DE BROGLIE wavelength $\lambda = \hbar/p$, where p is the momentum and $\hbar \approx eV \cdot \mu\text{m}$ the PLANCK constant, is much smaller than their spatial size. One advantage of the classical limit is not only due to simpler mathematics in the effective description, but also due to the breakdown of QM in this kinematic regime. For example, when describing an electron radiating a low-energy photon in QM, the expansion of the probability function in the coupling constant e suffers from a logarithmic divergence indicating a breakdown of the description. It was shown in Ref. [1] that this divergence can be avoided by a classical expansion in $e\omega/m_e$ because the electron mass m_e is much larger than the radiated energy ω .

Quantum field theory (QFT) emerges from the ideas of quantum mechanics, field theory and special relativity. It does include quantum corrections within a perturbative quantization of the fields and contains the classical limit corresponding to the zeroth order in this expansion. The Standard Model of particle physics (SM) is a gauge theory which describes many experimental results with tremendous precision and is one of the most precisely tested theories. However, the SM is not able to predict the correct relic abundance of Dark Matter particles $\Omega h^2 \approx 0.12$ [2], nor does it explain the baryon asymmetry observed in the universe. There are also theoretical reasons for physics beyond the SM (BSM) such as theorists hope to formulate a *theory of everything*, that is to combine gravity with electroweak and strong interactions, the hierarchy problem or the strong Charge-Parity (CP) problem. Thus, the SM can also be seen as an effective description of nature which works under certain conditions only, namely at low interaction energies.

Effective field theories (EFT) assume that one of these conditions is the presence of a mass hierarchy in the theory. This makes an expansion of observables in the ratio between masses and momenta of heavy and light states possible. Although it appears to be analogous to the classical limit of QM, EFTs are still QFTs which are renormalizable at each order in perturbation theory (which is called non-renormalizability). The SM itself has many mass hierarchies spanning from a few keV (ignoring neutrino masses) up to $O(100 \text{ GeV})$. This is why EFT techniques were already successfully applied and developed in the context of high precision experiments studying the SM properties at very different scales. Hence, EFTs are very powerful and well understood tools for the search of new physics (NP) if further mass hierarchies are involved.

With the discovery of a scalar resonance h with mass $m_h \approx 125$ GeV [3, 4] at the Large Hadron Collider (LHC) the last missing piece of the SM and the first elementary scalar particle was found. Six years after the Higgs boson discovery, m_h turned into a precision observable with an experimental uncertainty of a few hundred MeV [2]. This strengthens the question whether further scalar fields may be realized in nature as they are a necessity in many BSM models. However, the presence of null-results in LHC BSM searches yield strong constraints on the masses of e.g. additional colored particles of up to a few TeV [5]. This implies large quantum corrections on m_h in BSM models where the Higgs mass is not a free parameter. Indeed, it was shown in Ref. [6] that conventional fixed order computations of m_h in the Minimal Supersymmetric Standard Model (MSSM) suffer from large logarithms and an EFT computation is more precise if the BSM mass scale is above 1 TeV. Thus, for any BSM model with a large mass gap between the new BSM scale and the electroweak scale, an EFT matching procedure between the SM scalar sector and the scalar sector of the BSM model under consideration must be applied in order to decrease the theoretical uncertainty in the prediction of m_h . Since experimental bounds on uncolored BSM particles are often still below the TeV scale, it could happen that m_h must be computed along with further light scalar states within an EFT which is not the SM but a model with an extended Higgs sector.

Supersymmetric models have an extended Higgs sector compared to the SM as well as additional colored particles. Furthermore, they also yield relations between the scalar and other sectors of the theory, which otherwise would be independent in a non-supersymmetric EFT. Thus, the matching of supersymmetric theories with large mass hierarchies onto low-energy EFTs is competitive to ordinary high precision calculations of m_h . Matchings can also significantly reduce the parameter space of the EFTs, which gives a further possibility to distinguish between BSM models with different heavy states, even if only the experimental signatures from light particles are in reach. These advantages have already been studied for the simplest supersymmetric models in the past [7–10]. However, there are aspects which were only partially addressed in the literature. On the one hand, the simplest models still have open questions which can be answered in non-minimal models. On the other hand, there are too many -if not infinite- realizations of non-minimal models with an increasing complexity in computation. In addition, there are many possibilities to accommodate different mass hierarchies, i.e. it is possible to construct different low-energy EFTs of one specific theory. This makes it relatively time consuming to study non-minimal models, since there are no automation mechanisms available for performing a precise matching of scalar sectors containing more than one Higgs doublet. However, spectrum generators such as SARAH/SPHENO [11–14] compute mass spectra at fixed order for a large class of BSM models even at two-loop level. Hence, it is a natural step to extend these tools, such that they are able to perform an EFT matching between models at higher scales. This Master thesis covers the theoretical grounds needed for such a matching between two arbitrary scalar sectors at the one-loop level as well as the implementation in SARAH/SPHENO.

The thesis is organized as follows. Chapter 1 introduces the concept of effective field theories as well as the notation and motivations of the SM and its supersymmetric extensions. Chapter 2 describes the implementation in SARAH/SPHENO and gives a detailed example

of a toy model matching. Chapter 3 and 4 contain supersymmetric applications of the matching procedure. Conclusions are presented in chapter 5.

1.1. Effective Field Theories

Effective Field Theories have a long tradition and many applications in different fields of particle physics. In the following, we will give a modern example of an EFT, based on Ref. [15], before formulating general statements.

1.1.1. Example: B decays

Quarks are subject to strong interactions and can form unstable hadronic states such as mesons, composed of a quark-antiquark pair, and can decay into virtual SM vector bosons. The vector bosons can then further decay into a pair of leptons, for example. Fig. 1.1a shows the decay of a B^+ meson, composed of a \bar{b} and a u quark, into a tau τ^+ and a tau neutrino ν_τ through a W^+ exchange. The physically relevant scales for this process are the scale of Quantum Chromodynamics (QCD) Λ_{QCD} at which hadrons begin to form and the quark/meson masses, which describe the hard process. Since the mass of the W^+ boson is much larger than these scales $m_W \approx 90 \text{ GeV} \gg 0.2 \text{ GeV} \approx \Lambda_{\text{QCD}}$ as well as the external momenta ($p^2 \ll m_W^2$), one can expand the W^+ boson propagator

$$\frac{g_{\mu\nu}}{p^2 - m_W^2} = -\frac{g_{\mu\nu}}{m_W^2} \left(1 + \mathcal{O}\left(\frac{p^2}{m_W^2}\right) \right), \quad (1.1)$$

where $g_{\mu\nu}$ is the MINKOWSKI metric. The first term in this expansion is seen as a local effective vertex. The corresponding FEYNMAN graph is shown in Fig. 1.1b. According to the rules of perturbation theory, this vertex is generated by an operator containing four fermion fields

$$\mathcal{L}_{\text{EFT}} \supset \frac{C_{bu\tau\nu}}{m_W^2} (\bar{b}_L \gamma_\mu u_L) (\tau_L^+ \gamma^\mu \nu_L), \quad (1.2)$$

where the gamma matrices γ_μ have been contracted with the help of $g_{\mu\nu}$ and no W -bosons are present in \mathcal{L}_{EFT} at all. The WILSON coefficient $C_{bu\tau\nu}$ has to be determined by performing the calculation in Fig. 1.1a using the momentum expansion. This procedure is called *matching*.

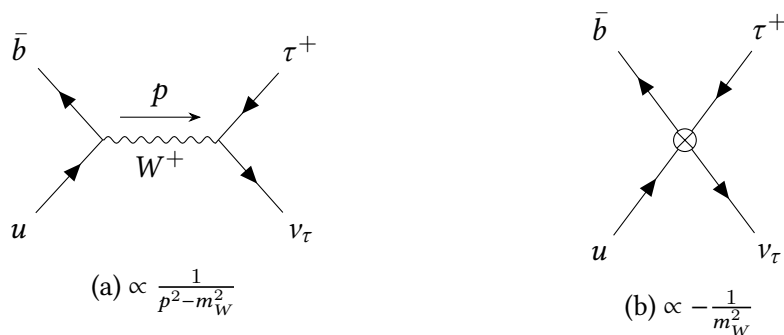


Figure 1.1.: Decay of a B^+ meson into a tau and a tau neutrino computed at tree level in the (a) SM (b) effective description, where the W^+ boson has been integrated out.

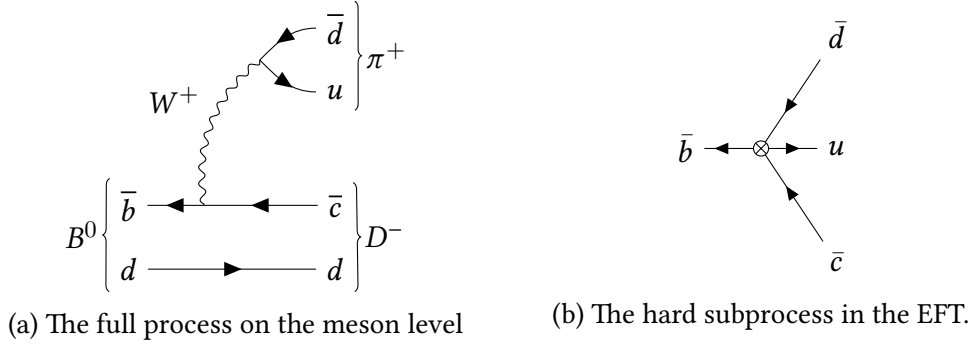
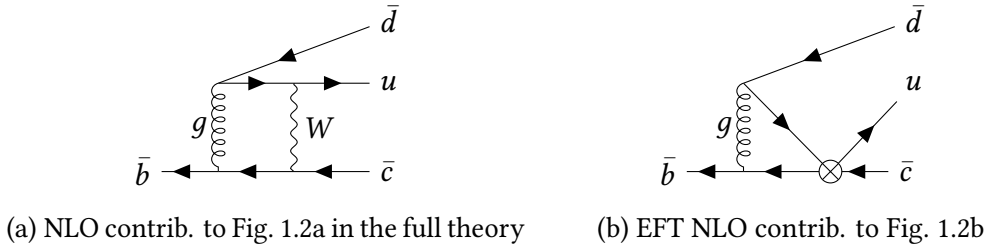
Since the calculation with the full Lagrangian containing the W boson field is not that difficult, one may ask about the advantage of the matching and using \mathcal{L}_{EFT} instead. To address this question, we consider the hadronic B^0 decay into a D^- and a π^+ meson in Fig. 1.2a in the full theory. The hard process of the decay, involving the W^+ boson is very similar to the leptonic decay. Thus, one can again shrink the heavy propagator to a local point interaction described by an effective Lagrangian, see Fig. 1.2b. Since the final state is now also colored, QCD corrections are important. Fig. 1.3a shows such a correction in the full theory with an additional internal gluon line. The diagram may be computed with the use of dimensional regularization (DREG) which introduces the renormalization scale Q . Although without physical relevance in the first place, Q should be of the order of the physical process under consideration e.g. the mass of the decaying particle. All physical parameters $g_j(Q_i)$ of the theory measured at scales Q_i need to be evolved to the scale Q of the experiment using renormalization group equations (RGE). Thus, in the full theory the one loop matrix element involves very different scales

$$\mathcal{M}_{b \rightarrow cdu}^{\text{full}, (1)} \propto \alpha_s(Q) \log \frac{m_b^2(Q)}{m_W^2(Q)} \quad (1.3)$$

where $m_b(m_b) \approx 4.2 \text{ GeV}$ is the bottom mass, α_s is the strong coupling constant and an on-shell b -quark $p^2 \approx m_b^2(Q)$ has been used. This rather large logarithm indicates a breakdown of the perturbative expansion. To perform a meaningful expansion, the different scales need to be separated, which is done using the EFT. At the scale $Q_{\text{match}} \approx m_W$, the coefficient $C_{bcdu}^{(1)}(Q_{\text{match}})$ is calculated at one-loop by equating the one-loop EFT diagram Fig. 1.3b with the full calculation Fig. 1.3a expanded in $\frac{p^2}{m_W^2}$. In the next step, the result of the one-loop matched coupling is run down to $Q \approx \mathcal{O}(m_b)$ using the RGEs of \mathcal{L}_{EFT} . The calculation based on \mathcal{L}_{EFT} does not contain any large logarithm

$$\mathcal{M}_{b \rightarrow cdu}^{\text{EFT}, (1)} \propto C_{bcdu}(Q) \log \frac{m_b(Q)}{Q}. \quad (1.4)$$

One may wonder if there are large logarithms $\propto \log \frac{Q_{\text{match}}}{m_b}$ present at the matching scale. Indeed, in each of the one-loop diagrams of Figs. 1.3a and 1.3b such a log arises. However,


 Figure 1.2.: The decay $B^0 \rightarrow \pi^+ D^-$.

 Figure 1.3.: The $b \rightarrow cud$ transition at NLO QCD in the full theory (a) and the EFT (b).

we will later give a general argument stating that the two theories must yield the same results in the infra-red (IR) limit i.e. if $p^2, m_b^2 \rightarrow 0$. Thus, all large logarithms must cancel when equating the two diagrams because those are only due to the mass gap between m_b and Q_{match} (but not m_W and Q_{match} , which are of the same size). Furthermore, one should stress that the ultra-violet (UV) behavior is not necessarily the same in both descriptions, as \mathcal{L}_{EFT} introduces new counter terms for the effective four fermion operators at each order in perturbation theory.

A different way of understanding how the scales have been separated is by writing the large log as

$$\log \frac{m_b}{m_W} = \underbrace{\log \frac{m_b}{Q}}_{\text{long distance}} + \underbrace{\log \frac{Q}{m_W}}_{\text{short distance}}, \quad (1.5)$$

where the first term corresponds to long distance contributions, canceling in the matching but later entering the calculation of hadronic matrix elements at $Q \approx m_b$ in the EFT. The second term corresponds to short distance physics absorbed in the WILSON coefficients at the matching scale $Q \approx m_W$.

We have seen that an EFT description can improve the calculation of an SM process involving different scales. However, also NP may contribute to the considered processes. For example, the W^+ boson in Fig. 1.1a may be replaced by a new charged scalar field like it is predicted in many BSM models. In a usual *bottom-up* approach the prediction of $C_{bu\tau\nu}^{SM}$ is compared with the experiment. The remaining parameter space for the BSM model under consideration can then be deduced by performing a matching. However,

care has to be taken if general statements from global fits on a large set of coefficients are made. Without performing a matching of the corresponding operators to a UV complete model, the WILSON coefficients are treated as independent. This is usually not the case in UV complete models, as they incorporate more symmetries than the SM and thus can give correlations between certain coefficients. This will be shown in the last chapter of this thesis.

1.1.2. The Appelquist Carazzone Theorem

The observations of the previous example have been formulated for general cases in 1977 by APPELQUIST and CARAZZONE [16]. The *decoupling theorem* states that

Any renormalizable QFT described by $\mathcal{L}_{H+L} = \mathcal{L}_H + \mathcal{L}_L$ with heavy \mathcal{L}_H and light \mathcal{L}_L fields turns for small external momenta into a theory composed of light fields only, $\mathcal{L}_{EFT} = \mathcal{L}_L + \mathcal{L}_L^{(5)} + \mathcal{L}_L^{(6)}$, including additional non-renormalizable operators $\mathcal{L}_L^{(n>4)}$.

There exists an on-shell renormalization scheme such that $\mathcal{L}_L^{\text{ren}} \equiv \mathcal{L}_{EFT}^{\text{ren}}$.

The crucial point is that the non-renormalizable operators $\mathcal{L}^{(n>4)}$ are suppressed by the masses m_H^{-n} of the heavy fields. Thus, for $m_H \rightarrow \infty$, the higher-dimensional operators decouple from the theory without influencing physical low-energy observables.

The low-energy effective theory, described by $\mathcal{L}_{EFT}(m_L)$, of any renormalizable theory, described by $\mathcal{L}_{L+H}(m_H, m_L)$, must be renormalizable in the decoupling limit $m_H \rightarrow \infty$.

Although the original theorem was given within an on-shell renormalization scheme, it was shown that also the $\overline{\text{MS}}$ scheme in fact obeys the decoupling theorem [17]. In particular, this is only possible if non-local contributions, which mix heavy and light fields, are included in the matching. The consequence for a diagrammatic calculation is that diagrams involving internal heavy as well as internal light propagators have to be included. Section 1.1.4 will introduce various methods on how to derive \mathcal{L}_{EFT} from \mathcal{L}_{L+H} .

Since supersymmetric theories are of particular interest in this thesis, we want to stress that also a supersymmetric version of the decoupling theorem [18] exists.

As a result of the decoupling theorem, one can impose the matching condition for all one-particle-irreducible (1PI) correlation functions of the full theory and the EFT

$$\Gamma_i^{\text{full}}(p^2) \Big|_{p^2=0} = \Gamma_i^{\text{EFT}}(p^2) \Big|_{p^2=0}. \quad (1.6)$$

Since the EFT is a renormalizable theory for $m_H \rightarrow 0$, also the renormalization condition which ensures a proper canonically normalized kinetic term has to be matched

$$\partial_{p^2} \Gamma_i^{\text{full}}(p^2) \Big|_{p^2=0} = \partial_{p^2} \Gamma_i^{\text{EFT}}(p^2) \Big|_{p^2=0}. \quad (1.7)$$

The IR safety of the decoupling theorem ensures that all p^2 dependent parts (which are in addition potentially IR divergent) in the matching conditions Eqs. (1.6) and (1.7) cancel, i.e. the low-momenta regions of the two theories are identical. Those contributions which are not canceled in the matching conditions are called *threshold corrections*. They connect the UV behaviour of the full theory to the parameters of the EFT.

Accordingly, a concrete matching needs to disentangle all non-local (p^2 -dependent) parts of the full theory (which correspond to the 1PIs in the EFT) from the local (p^2 -independent) parts, which are absorbed into the WILSON coefficients. Chapter 2 gives the details how this can be achieved in a generic way at one-loop order.

1.1.3. (Non-)Decoupling in the Scalar Sector

There are a few subtle situations where heavy particles do not decouple. A case of non-decoupling is for example, if $m_H \rightarrow \infty$ would break a symmetry of the low-energy theory, making it inconsistent.

For instance, consider a toy-model composed of a heavy scalar Φ and a light scalar φ , both charged under the same \mathbb{Z}_2 symmetry:

$$\mathcal{L}_{UV} = \sum_{S=\Phi,\varphi} \left(\frac{1}{2} \partial_\mu S \partial^\mu S - \frac{1}{2} m_S^2 S^2 - \lambda_S S^4 \right) - m_{\Phi\varphi}^2 \Phi\varphi - \lambda_{\Phi\varphi} \Phi^2 \varphi^2, \quad m_\Phi \gg m_\varphi. \quad (1.8)$$

The result of the decoupling should yield a single scalar φ^4 theory

$$\mathcal{L}_{EFT} = \frac{1}{2} \partial_\mu \varphi \partial^\mu \varphi - \frac{1}{2} m_\varphi^2 \varphi^2 - \lambda_{EFT} \varphi^4 \quad (1.9)$$

which is also \mathbb{Z}_2 invariant. A proper decoupling requires $m_{\Phi\varphi} \ll m_\Phi$, since large mixing destroys the picture of a well separated mass hierarchy. Thus, we set $m_{\Phi\varphi} = 0$ in the following. At tree level, it follows from Eq. (1.6) that $\lambda_{EFT} \equiv \lambda_\varphi$ whereas at one-loop order one expects corrections of the form

$$\delta\lambda_\varphi \propto \frac{1}{16\pi^2} \lambda_{\Phi\varphi}^2 \log \frac{m_\Phi^2}{Q^2} \quad (1.10)$$

which does not decouple because φ^4 is a renormalizable operator. One could argue that there is still a renormalization scheme where λ_φ is chosen such that all threshold corrections from the heavy field are absorbed into its tree-level value. However, we will see that in supersymmetric theories, the quartic couplings are governed by the gauge structure of the theory and thus they do not have this freedom.

In the following we distinguish between two cases where the \mathbb{Z}_2 symmetry is broken by the vacuum expectation value (VEV) of

- (i) the heavy field $\langle \Phi \rangle = v_\Phi$ or
- (ii) the light field $\langle \varphi \rangle = v_\varphi$,

so that the symmetry breaking is either of the order

(i) $m_\Phi^2 \propto v_\Phi^2 \lambda_\Phi$ or

(ii) $m_\varphi^2 \propto v_\varphi^2 \lambda_\varphi$.

In both cases the \mathbb{Z}_2 breaking introduces effective trilinear couplings proportional to a quartic coupling times a VEV. We examine each case separately:

(i) $\langle \Phi \rangle = v_\Phi, \langle \varphi \rangle = 0$

The effective trilinear coupling yields a new tree-level contribution to the quartic coupling λ_{EFT} through an internal Φ propagator, similar to Fig. 1.1a. The contribution is proportional to $\frac{v_\Phi^2 \lambda_{\Phi\varphi}^2}{m_\Phi^2}$. However, it is $v_\Phi \propto \mathcal{O}(m_\Phi)$ and thus the contribution to λ_{EFT} does not decouple but keeps constant in the decoupling limit.

Another issue is that the mass eigenvalue, which is supposed to be light $m_{\text{light}}^2 = m_\varphi^2 + v_\Phi^2 \lambda_{\Phi\varphi}$, leads to a fine-tuning condition between the tree-level parameters m_φ and v_Φ . However, the actual problem arises at the one-loop level, where \mathbb{Z}_2 -breaking terms for the light field are radiatively generated by diagrams like the one shown in Fig. 1.4.

By dimensional arguments, the contribution from the diagram in Fig. 1.4 is $\propto \frac{v_\Phi^3 \lambda_{\Phi\varphi}^3}{m_\Phi^2}$ which also does not necessarily decouple because v_Φ and m_Φ are correlated. Thus \mathcal{L}_{EFT} would suffer from diverging (or large) trilinear couplings in the decoupling limit, which cannot be compensated (fine-tuned) as there is no such tree-level vertex. Hence, the low-energy theory cannot be described by \mathcal{L}_{EFT} .

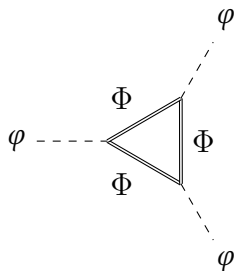


Figure 1.4.: Radiatively generated \mathbb{Z}_2 -breaking operator. Since there are no other scales involved, the diagram must scale as $\propto \frac{v_\Phi^3 \lambda_{\Phi\varphi}^3}{m_\Phi^2}$ leaving a mass parameter of $\mathcal{O}(m_\Phi)$ in the EFT. The doubled lines denote heavy propagators.

(ii) $\langle \Phi \rangle = 0, \langle \varphi \rangle = v_\varphi$

If the light scalar obtains a VEV $v_\varphi \propto \mathcal{O}(m_\varphi)$ clearly all new \mathbb{Z}_2 -breaking contributions from the heavy scalar are suppressed by $v_\varphi^2/m_\Phi^2 \rightarrow 0$ and vanish the decoupling limit. This is precisely because there is not connection between the \mathbb{Z}_2 -breaking scale v_φ (which is supposed to be a good symmetry of \mathcal{L}_{EFT}) and the decoupling scale m_Φ .

We conclude, that it is of particular importance at which scale the (soft) symmetry breaking occurs and if there are potential contributions to mass parameters in the low-energy Lagrangian. Care has to be taken if the breaking scale coincides with the decoupling scale and inconsistencies occur if the symmetry of the tentative low-energy Lagrangian is broken at the decoupling scale.

1.1.4. Integrating out Heavy Degrees of Freedom

This paragraph introduces various methods for constructing a low-energy Lagrangian from a theory with a significant mass hierarchy. We discuss the advantages and disadvantages of the different techniques and argue why we have chosen the diagrammatic method for our calculation.

1.1.4.1. Covariant Derivative Expansion

The path integral formalism, introduced in QFT by FEYNMAN [19], connects an n -point correlation function with the generating functional $Z[J]$, which is a functional integral over all field configurations Φ

$$Z[J] = \int \mathcal{D}\Phi e^{iS[\Phi, J]}, \quad (1.11)$$

where $S = \int d^4x \mathcal{L} + J \Phi$ is the action and J is an external current. The idea is to isolate the heavy field configurations $\mathcal{D}_\Phi = \mathcal{D}_{\Phi_{\text{heavy}}} \cdot \mathcal{D}_{\Phi_{\text{light}}}$ and *integrate out* all heavy degrees of freedom Φ_{heavy} in a gauge-covariant way. The integration is done perturbatively which is why the technique is also called *covariant derivative expansion* (CDE). The result is an effective generating functional where the integration over an effective action S_{eff} containing light degrees of freedom takes place.

A generic approach to perform the construction of S_{eff} using CDE techniques was given in Ref. [20]. However, it was shown in Refs. [21, 22] that this general ansatz does not work if the heavy fields couple linearly to light fields. Hence, no *mixed loops* containing both, heavy and light propagator lines are accounted for.

Ref. [23] showed that CDE techniques can in principle take care of mixed loops, although the modifications on the standard procedures are quite involved and difficult to generalize. Indeed, there are also diagrams like Fig. 1.5a which have no mixed loops but a linear heavy-light-light coupling involved. This type of diagram is called *one-particle-reducible* (1PR) and is complementary to the 1PI diagram. 1PR diagrams are important for a matching and generated at one loop by 1PIs connected to a tree-level vertex through a heavy propagator line.

1.1.4.2. The Coleman-Weinberg Potential

Another possibility to compute S_{eff} was given in 1973 by COLEMAN, WEINBERG [24] and JACKIW [25]. The result is a closed form of the one-loop *effective potential* $\Delta V^{(1)}$, which is the summation over all one-loop 1PI graphs in the limit of $n \rightarrow \infty$ external scalars and vanishing external momenta. Effective operators containing ϕ_1, \dots, ϕ_m scalar fields are thus given by the derivative $\frac{\partial^m \Delta V^{(1)}}{\partial \phi_1 \dots \partial \phi_m}$.

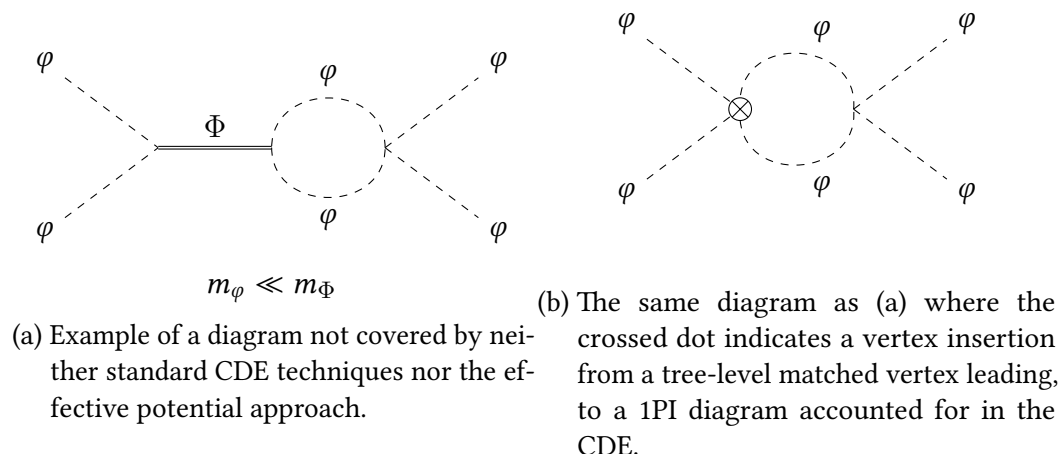


Figure 1.5.: Two examples for (a) one-particle-reducible (1PR) and (b) a one-particle-irreducible diagram in the full theory and the EFT, respectively.

Today the effective potential is known up to three-loop order for a general QFT [26], which makes it an appealing candidate for a generic matching. However, with the effective potential method one can only account for the first matching condition Eq. (1.6), but not for the second one, because it is only the generator of all 1PI diagrams. Thus, wave function renormalization constants have to be determined in a separate calculation. In addition, the effective potential would need further modifications in order to also account for 1PR diagrams.

1.1.4.3. Diagrammatic Method

Computing FEYNMAN graphs has a long tradition in particle physics and involves many standard techniques such as *dimensional regularization* (*dimensional reduction*, respectively), PASSARINO-VELTMAN reduction, FEYNMAN parameters etc. Although this machinery might look much more involved than e.g. the effective potential approach, it is well known and already automatized at the one-loop order with computer tools such as FEYNARTS [27] and FORMCALC [28]. Furthermore, it is straightforward to disentangle the contributions of one-loop corrections from light, mixed light-heavy, and heavy particles in the loop.

We summarize our comparison in Table 1.1, where the ability to include the different pieces necessary for a complete matching are marked for the effective potential, the CDE and the diagrammatic method. The comparison was made with the focus on the implementation of the approach into a generic spectrum generator. We conclude that under this assumption the diagrammatic method fits best for our purposes.

1.2. The Standard Model of Particle Physics

This section introduces notations and definitions concerning the SM as well as describes the mechanism of spontaneous symmetry breaking in the electroweak sector, i.e. electroweak

	Eff. Pot.	CDE	Diagrammatic
1PI	✓	✓	✓
1PR	?	?	✓
WFR	×	?	✓
mixed loops	✓	?	✓

Table 1.1.: Comparison between the three considered matching methods: the effective potential (eff. pot.), the covariant derivative expansion (CDE) and a calculation of FEYNMAN diagrams. The abbreviations indicate the inclusion of the following diagrams: 1PI = one-particle-irreducibles, 1PR = one-particle-reducibles, WFR = loops on external legs, mixed loops = loops containing heavy and light fields. Entries marked with "✓" are suited while those with a "×" do miss the feature completely. The "?" means, that it is technically possible but not (yet) suitable for a generic implementation.

symmetry breaking (EWSB). As an example, the generation of gauge boson masses is discussed, while the fermion sector is introduced in the gauge basis only.

1.2.1. Notation and Definitions

The SM is a gauge theory with the gauge group $G_{\text{SM}} = SU(3) \times SU(2) \times U(1)$, the corresponding gauge fields and gauge couplings $g_{1,2,3}$ are listed in Table 1.2 whereas matter fields are listed in Table 1.3. In addition to the gauge symmetries, the SM has many approximate global symmetries starting from a $U(3)^5$ in the family space of the matter fields. These global symmetries are broken by the hierarchy in the 3x3 YUKAWA matrices $Y_{l,d,u}$ which couple fermions to the Higgs field responsible for their mass generation. Further tree-level input parameters of the SM are found in the Higgs potential which connects the mass parameter μ and the quartic Higgs self-coupling λ through EWSB to the Higgs mass m_h and its VEV v .

The Lagrangian of the SM in unitarity gauge with suppressed generation, color and isospin indices reads

$$\begin{aligned}
 \mathcal{L}_{\text{SM}} = & (D_\mu H)^\dagger (D^\mu H) - \mu^2 H^\dagger H - \frac{1}{2} \lambda^2 |H^\dagger H|^2 \\
 & - \frac{1}{4} g_{\mu\nu} g^{\mu\nu} - \frac{1}{4} W_{\mu\nu} W^{\mu\nu} - \frac{1}{4} B_{\mu\nu} B^{\mu\nu} \\
 & + i \bar{l} \not{D} l + i \bar{e} \not{D} e + i \bar{q} \not{D} q + i \bar{u} \not{D} u + i \bar{d} \not{D} d \\
 & - Y_d q H d - Y_u q H^\dagger u - Y_l l H e,
 \end{aligned} \tag{1.12}$$

where the covariant derivative D_μ is determined by the gauge structure listed in Table 1.2

$$D_\mu = \partial_\mu - ig_1 Y B_\mu - i \frac{g_2 \sigma_i}{2} W_\mu^i + i \frac{g_3 \lambda_a}{2} g_\mu^a \quad (1.13)$$

with the Hypercharge operator Y and the PAULI (GELL-MANN) matrices τ^i (λ_a). The $SU(2)$ doublets are

$$H = (G^+, H^0)^T, \quad q = (u_L, d_L)^T \quad \text{and} \quad l = (v_L, l_L)^T, \quad (1.14)$$

whereas $d \equiv \bar{d}_R$, $u \equiv \bar{u}_R$ and $e = \bar{e}_R$ are the right handed $SU(2)$ singlets. There are no right handed neutrino singlets ν_R . Thus, there is no possibility to construct DIRAC mass terms for neutrinos, whereas quark and lepton masses are generated through the YUKAWA couplings in the third line of Eq. (1.12) through EWSB.

The covariant derivative in Eq. (1.12) depends on the quantum numbers of the matter fields it is acting on. The charges under the SM gauge groups are listed in Table 1.3. If a field is a singlet, denoted by a $\mathbf{1}$, under the symmetry group, the corresponding term in D_μ vanishes.

Field	Gauge Group	Coupling	Name
B	$U(1)$	g_1	hypercharge
W	$SU(2)$	g_2	isospin
g	$SU(3)$	g_3	color

Table 1.2.: Gauge fields in the Standard Model. Lorentz, isospin and color indices are suppressed.

Field	Spin	Generations	$U(1) \otimes SU(2) \otimes SU(3)$
H	0	1	$(\frac{1}{2}, \mathbf{2}, \mathbf{1})$
q	$\frac{1}{2}$	3	$(\frac{1}{6}, \mathbf{2}, \mathbf{3})$
l	$\frac{1}{2}$	3	$(-\frac{1}{2}, \mathbf{2}, \mathbf{1})$
d	$\frac{1}{2}$	3	$(\frac{1}{3}, \mathbf{1}, \bar{\mathbf{3}})$
u	$\frac{1}{2}$	3	$(-\frac{2}{3}, \mathbf{1}, \bar{\mathbf{3}})$
e	$\frac{1}{2}$	3	$(1, \mathbf{1}, \mathbf{1})$

Table 1.3.: Matter field content in the Standard Model.

1.2.2. Electroweak Symmetry Breaking in the SM

Gauge boson mass terms are forbidden when enforcing local invariance of the SM symmetry groups. This is in conflict with the massive vector bosons observed at particle colliders. The Higgs mechanism [29–31] does not only allow for gauge invariant mass generation, it also connects the masses of the gauge bosons to the size of symmetry breaking of the Higgs boson vacuum. This connection makes the SM a predictive model and is one of the key features responsible for its enormous success.

We start by decomposing the neutral Higgs component into its real and imaginary part. If $\mu^2 < 0$, the real part of H gets a non-zero vacuum expectation value (VEV)

$$\langle H \rangle = \frac{1}{\sqrt{2}} \begin{pmatrix} 0 \\ v \end{pmatrix}. \quad (1.15)$$

Expanding H around v yields

$$H = \begin{pmatrix} G^+ \\ H^0 \end{pmatrix} = \begin{pmatrix} G^+ \\ \frac{v+h+iG^0}{\sqrt{2}} \end{pmatrix} \quad (1.16)$$

where h is the SM Higgs field and $G^{0,\pm}$ are the GOLDSTONE modes which provide longitudinal degrees of freedom for the massive vector bosons.

The minimum condition of the Higgs potential $V(H)$, given in the first line of Eq. (1.12), yields a relation between the Higgs mass m_h , its VEV and the quartic self-coupling

$$\begin{aligned} \left. \frac{\partial V(H)}{\partial H} \right|_{H=\langle H \rangle} &= \mu^2 \langle H \rangle^\dagger + \lambda (\langle H \rangle^\dagger \langle H \rangle) \langle H \rangle^\dagger = 0 \\ \Leftrightarrow \langle H \rangle^\dagger \langle H \rangle &\equiv \frac{v^2}{2} = -\frac{\mu^2}{\lambda} \\ \Rightarrow V \left(H^0 \approx \frac{v+h}{\sqrt{2}} \right) &\supset \frac{1}{2} v^2 \lambda h^2 + \frac{\lambda}{8} h^4 + \frac{\lambda v}{2} h^3, \end{aligned} \quad (1.17)$$

such that we obtain the tree-level relation

$$m_h^2 = v^2 \lambda. \quad (1.18)$$

To calculate the gauge boson masses at tree-level, we consider the covariant derivative acting on the real part of the H^0 Higgs component after EWSB

$$\begin{aligned} D_\mu H &\supset \left(\partial_\mu - i \frac{g_2 \sigma_i}{2} W_\mu^i - i \frac{g_1}{2} B_\mu \right) \begin{pmatrix} 0 \\ \frac{v+h}{\sqrt{2}} \end{pmatrix} \\ &= \begin{pmatrix} 0 \\ \frac{\partial_\mu h}{\sqrt{2}} \end{pmatrix} - i \frac{(v+h)}{2} \begin{pmatrix} \frac{g_2}{\sqrt{2}} (W_\mu^1 - i W_\mu^2) \\ \frac{1}{\sqrt{2}} (g_1 B^\mu - g_2 W_3^\mu) \end{pmatrix}, \end{aligned} \quad (1.19)$$

which leads to the definition of the charged W bosons

$$W_\mu^\pm = \frac{W_\mu^1 \mp iW_\mu^2}{\sqrt{2}}. \quad (1.20)$$

The fields W_3 and B are rotated into the mass basis by the weak mixing angle θ_w ,

$$\begin{aligned} \begin{pmatrix} Z_\mu \\ A_\mu \end{pmatrix} &= \begin{pmatrix} \cos \theta_w & -\sin \theta_w \\ \sin \theta_w & \cos \theta_w \end{pmatrix} \begin{pmatrix} W_\mu^3 \\ B_\mu \end{pmatrix} \\ &= \frac{1}{\sqrt{g_1^2 + g_2^2}} \begin{pmatrix} g_2 W_\mu^3 - g_1 B_\mu \\ g_2 W_\mu + g_1 B_\mu \end{pmatrix}. \end{aligned} \quad (1.21)$$

By squaring Eq. (1.19), we find mass terms for the rotated gauge fields Z and the W^\pm while A is interpreted as the massless photon

$$(D^\mu H)^\dagger (D_\mu H) \supset \mathcal{L}_{\text{Mass}}^{\text{Gauge}} = \underbrace{\left(\frac{g_2 v}{2}\right)^2}_{M_W^2} W_\mu^+ W^{-\mu} + v^2 \underbrace{\frac{g_1^2 + g_2^2}{8}}_{\frac{1}{2}M_Z^2} Z_\mu Z^\mu. \quad (1.22)$$

Using the definition of the electric charge

$$e \equiv g_2 \sin \theta_w = g_1 \cos \theta_w = \frac{g_1 g_2}{\sqrt{g_1^2 + g_2^2}} \quad (1.23)$$

it follows from Eq. (1.22) that

$$\frac{M_W^2}{M_Z^2 \cos^2 \theta_w} = 1 \equiv \rho. \quad (1.24)$$

The ρ parameter is one of the most precisely known observables of the SM [2]

$$1 - \rho^{\text{exp}} = (-3.9 \pm 1.9) \cdot 10^{-4} \quad (1.25)$$

and thus a common quantity used in the search for NP. The reason for $\rho \approx 1$ is a global $SU(2) \times SU(2)$ *custodial symmetry* [32] which is broken by $g_1 \neq 0$. In general, any BSM model should respect this symmetry at tree-level to avoid large deviations from one. The ρ parameter receives additional quantum corrections in the SM as well as BSM models that have a sector that couples to the SM gauge sector. Since the ρ parameter is precisely measured, those loop corrections must be taken into account

$$\rho^{\text{NLO}} = \frac{1}{1 - \Delta\rho}, \quad \Delta\rho = \frac{\Pi_Z^{(1),\text{T}}(0)}{m_Z^2} - \frac{\Pi_W^{(1),\text{T}}(0)}{m_W^2}, \quad (1.26)$$

where $\Pi_{W,Z}^{(1),\text{T}}$ are the transverse one-loop W and Z boson self-energies in the SM or BSM. The custodial symmetry is also broken by $Y_d \neq Y_u$ i.e. the mass difference of for example

the top and bottom quark entering the self-energies. The one-loop correction of any non-degenerate $SU(2)$ doublet with masses m_1 and m_2 reads [2]

$$\Delta\rho \propto m_1^2 + m_2^2 - \frac{4 m_1^2 m_2^2}{m_1^2 - m_2^2} \log \frac{m_1^2}{m_2^2} \geq (m_1 - m_2)^2. \quad (1.27)$$

Since the custodial symmetry is broken by dimensionless parameters, it is not necessarily connected to a certain breaking scale but only to the degree of mass non-degeneracy of the doublet components. In case of any BSM model containing non-degenerate $SU(2)$ doublet components, the contribution to the ρ -parameter does not decouple as $m_1 \rightarrow \infty$ but only if $m_1 \rightarrow m_2$.

1.2.3. The Standard Model as an Effective Theory

As already mentioned in the introductory example, a bottom-up approach parametrizes the effects of not-too-heavy and not-too-light new physics by non-renormalizable operators which are suppressed by the new mass scale m_{BSM} . Under the assumption that the SM is the correct EFT (no further light particles to be found at colliders), one can construct all possible higher dimensional operators from SM fields that are LORENTZ invariant and respect the symmetries of the SM. Because of the power suppression, an expansion of the form

$$\mathcal{L}_{\text{EFT}} = \mathcal{L}_{\text{SM}} + \sum_{n=1}^{\infty} \mathcal{L}_{\text{Eff}}^{(n+4)}, \quad (1.28)$$

$$\mathcal{L}_{\text{Eff}}^{(n)} = \sum_i \frac{\alpha_i}{m_{\text{BSM}}^n} \mathcal{O}^{(n)} \quad (1.29)$$

where α_i are dimensionless couplings, is appropriate. The leading contributions come from dimension $n = 5, 6, \dots$ operators. At dimension five level, there is only one such operator, responsible for neutrino MAJORANA masses, the WEINBERG operator. At dimension six, there are already more than 50 independent operators [33, 34] (and even more if lepton flavour conservation is relaxed), one of them

$$\mathcal{O}_6 = \frac{c_6}{m_{\text{BSM}}^2} |H^\dagger H|^3 \quad (1.30)$$

built from the Higgs doublet only.

After spontaneous symmetry breaking (SSB) the operator \mathcal{O}_6 contributes with

$$\mathcal{L}_{\text{SM}}^{\text{EFT}} \supset \underbrace{\left(\frac{\lambda}{2} + \overbrace{\frac{15 c_6 v^2}{8 m_{\text{BSM}}^2}}^{\mathcal{O}_6} \right)}_{\lambda_{\text{EFT}}} h^4 \quad (1.31)$$

to the quartic Higgs coupling of the effective Lagrangian, which gives a shift to the SM Higgs mass m_h in Eq. (1.18). However, the SM has no prediction for the Higgs mass, because λ as a free parameter is not connected to any other known observable than the Higgs mass and the Higgs self-couplings. Thus, the shift to the Higgs mass can be considered as unphysical, since one can compensate it by choosing $\lambda \rightarrow \lambda - \frac{15 c_6 v^2}{4 m_{BSM}^2}$.

A top-down approach may connect λ (and thus m_h) to other parts of the Lagrangian, giving the possibility to falsify the model because λ is already fixed. In addition, this can also happen through threshold corrections which are not suppressed by v/m_{BSM} but non-decoupling terms.

Supposed that the fundamental theory is renormalizable, it follows from the decoupling theorem, that the higher dimensional operators become unimportant at a certain scale. The question arises, at which scale the v/m_{BSM} terms are no longer relevant for a precise Higgs mass calculation. The impact of dimension six terms, compared to ordinary threshold corrections (not suppressed by the heavy scale), on the Higgs mass in a matching of the SM to the MSSM was studied in Ref. [35]. It was found that for $500 \text{ GeV} < m_{BSM} < 1000 \text{ GeV}$, a two-loop matching of c_6 yields corrections on m_h in the sub-GeV range, which rapidly drop for $m_{BSM} > 1 \text{ TeV}$. Since the focus of this thesis is set on BSM scenarios with $m_{BSM} \geq 1 \text{ TeV}$, we will neglect all v/m_{BSM} contributions during the matching. This is in agreement with setting

$$p^2 = m_{SM\text{particle}}^2 \propto v^2 \rightarrow \epsilon_{match}^2 \rightarrow 0 \quad (1.32)$$

all SM particles on-shell and massless during the matching procedure. The artificial parameter ϵ_{match} is later used to isolate IR divergences. In analogy to the argumentation in Section 1.1.1, all IR divergent parts $\propto \log \frac{\epsilon_{match}}{Q_{match}}$ must cancel in the matching condition. After carefully isolating all IR terms, one can also set them to zero without computing and canceling them against the corresponding diagrams in the EFT.

1.3. The Minimal Supersymmetric Standard Model

The Minimal Supersymmetric Standard Model (MSSM) is often motivated to stabilize a rather light Higgs mass [36] required for EWSB in the presence of heavy UV-physics, at latest playing a role at the scale of quantum gravity $m_{\text{PLANCK}} \approx 10^{18} \text{ GeV}$. However, it can also provide solutions for other problems like a Dark Matter (DM) candidate or unification of the gauge couplings in a grand unified theory (GUT). In addition, local supersymmetry (SUSY) is a popular link between gauge theories and gravity and sets directions for reducing the variety of soft-SUSY-breaking possibilities. Thus, even if the Higgs mass may again appear *unnatural* in case of a large SUSY breaking scale $m_{\text{SUSY}} \gg m_Z$, there are good reasons for continuing to study *quasi-natural* or even *unnatural* SUSY [9]. There are also attempts to recover naturalness in the heavy SUSY scenario with a relaxion mechanism [37].

Since there is a broad literature on SUSY introductions available [38–41], we will only focus on the notations and conventions used in this thesis to describe the MSSM at tree-level.

Since supersymmetry requires

$$n_B = n_F \quad (1.33)$$

i.e. the bosonic and fermionic degrees of freedom (d.o.f.) to match, it is a common notation to write fermion and boson fields with the same quantum numbers as a single superfield, denoted by a hat, which fulfills Eq. (1.33). The chiral superfield $\hat{\Phi}$ then carries a complex spin 0 scalar boson Φ as well as a two component WEYL spinor Ψ . Likewise, the vector superfield \hat{A} is composed out of a real spin 1 boson A_μ and a spinor λ .

When constructing the most general gauge- and SUSY invariant interactions, a very useful object, the *superpotential* \mathcal{W} , is introduced. It is a holomorphic function of the superfields, has mass dimension 3 and is invariant under the gauge group transformations. Additional discrete symmetries of the superpotential may be introduced in order to account for experimental observations.

With a given set of chiral (vector) superfields $\hat{\Phi}_{1,\dots,n}$ ($\hat{A}_{1,\dots,m}$) and a set of gauge group generators $T_{1,\dots,m}$ with gauge couplings $g_{1,\dots,m}$ (here $1, \dots, m$ are not the gauge indices but just a counting index for the different groups), the scalar potential of the Lagrangian is derived from the superpotential $\mathcal{W}(\hat{\Phi}_n)$ as follows [38]

$$\begin{aligned} V(\Phi_{1,\dots,n}, \Psi_{1,\dots,n}, \lambda_{1,\dots,m}) = & \underbrace{\mathcal{W}_i^* \mathcal{W}^i}_{\text{F-Terms}} + \underbrace{\frac{1}{2} g_a^2 \left(\Phi^{i*} T_{ij}^a \Phi^j \right)^2}_{\text{D-Terms}} \\ & + \underbrace{\frac{1}{2} \left(\mathcal{W}^{ij} \Psi_i \Psi_j + \text{h.c.} \right) + \sqrt{2} g_a \left((\Phi^{i*} T_{ij}^a \Psi^j) \lambda_a + \text{h.c.} \right)}_{\text{YUKAWA couplings and fermion masses}}, \end{aligned} \quad (1.34)$$

where summation over repeated indices is implicit and

$$\mathcal{W}^{i_1, \dots, i_n} = \frac{\delta^n \mathcal{W}}{\delta \Phi_{i_1} \dots \delta \Phi_{i_n}} \quad (1.35)$$

is the functional derivative of the super potential w.r.t. the scalar components. The *D-terms* as well as the *F-terms* are a consequence of elementary auxiliary fields necessary for the requirement of Eq. (1.33) for off-shell fields.

Since we did not introduce the superfields along with the superspace, we do not have the formalism at hand to explain the supersymmetric construction of terms involving space time derivatives (i.e. kinetic terms) from the KÄHLER potential [42]. For our purpose it is enough to mention that the construction of gauge invariant kinetic terms, as described in Section 1.2.1, is indeed also supersymmetric.

1.3.1. Particle Content

Since the model should at least contain all SM fields, it is natural to start with G_{SM} , built upon the SM notation in Table 1.3. The corresponding SUSY partners are usually denoted by the same symbols as their SM partners, supplemented with an additional tilde. For instance, the superpartners of the quarks q are called squarks \tilde{q} . A complete list of all vector and chiral superfields is given in Table 1.4

Because \mathcal{W} needs to be holomorphic, YUKAWA interactions with a single Higgs doublet like those in the SM Eq. (1.12) are not possible. One Higgs doublet $H_u = (H_u^+, H_u^0)^T$ is only able to give masses to the up-type quarks but not to the down type quarks and leptons because of their iso-spin and hypercharge. Furthermore, the appearance of gauge anomalies due to the Higgs superpartners (higgsinos) forces the introduction of a second Higgs doublet $H_d = (H_d^0, H_d^-)^T$ with opposite hypercharge. In order to forbid lepton-flavour-violating

Super field	$s = 1$	$s = 1/2$	SM Gauge Group
\hat{B}	B	\tilde{B}	$U(1)$
\hat{W}	W	\tilde{W}	$SU(2)$
\hat{g}	g	\tilde{g}	$SU(3)$

Super field	$s = 1/2$	$s = 0$	Generations	$U(1) \otimes SU(2) \otimes SU(3)$
\hat{H}_u	\tilde{H}_u	H_u	1	$(\frac{1}{2}, \mathbf{2}, \mathbf{1})$
\hat{H}_d	\tilde{H}_d	H_d	1	$(-\frac{1}{2}, \mathbf{2}, \mathbf{1})$
\hat{q}	q	\tilde{q}	3	$(\frac{1}{6}, \mathbf{2}, \mathbf{3})$
\hat{l}	l	\tilde{l}	3	$(-\frac{1}{2}, \mathbf{2}, \mathbf{1})$
\hat{d}	\bar{d}	\tilde{d}^*	3	$(\frac{1}{3}, \mathbf{1}, \bar{\mathbf{3}})$
\hat{u}	\bar{u}	\tilde{u}^*	3	$(-\frac{2}{3}, \mathbf{1}, \bar{\mathbf{3}})$
\hat{e}	\bar{e}	\tilde{e}^*	3	$(1, \mathbf{1}, \mathbf{1})$

Table 1.4.: Vector- and chiral superfields with spin in the Minimal Supersymmetric Standard model (MSSM). The superpartners have the same names as their SM counterparts with the exception that (i) fermions have an appended "ino" (ii) scalars have a prepended "s".

terms in the resulting Lagrangian, a discrete symmetry, called R -parity, is introduced,

$$\begin{aligned}
 R\Phi &= +1\Phi && \text{if } \Phi \text{ is a SM particle} \\
 R\Phi &= -1\Phi && \text{if } \Phi \text{ is a SUSY partner of a SM particle}
 \end{aligned}
 \tag{1.36}$$

from which follows that the lightest SUSY particle (LSP) is stable and thus a possible dark matter candidate.

With all necessary ingredients at hand, the most general superpotential reads

$$\mathcal{W}_{\text{MSSM}} = -Y_l \hat{l} \cdot \hat{H}_d \hat{e} + Y_u \hat{q} \cdot \hat{H}_u \hat{u} - Y_d \hat{q} \cdot \hat{H}_d \hat{d} + \mu \hat{H}_u \cdot \hat{H}_d,
 \tag{1.37}$$

where μ is a mass parameter and $\hat{H}_u \cdot \hat{H}_d = \hat{H}_u^+ \hat{H}_d^- - \hat{H}_u^0 \hat{H}_d^0$ is a symplectic product invariant under $SU(2)$. We consider a CP-conserving MSSM and thus assume μ , as well as all other MSSM parameters, to be real.

1.3.2. The MSSM Lagrangian

Before applying Eq. (1.34) to the MSSM superpotential, we briefly want to discuss the breaking of SUSY. If we consider SUSY as an effective theory which is completed at latest at the PLANCK scale, it must be broken by parameters of mass dimension equal or greater than one in order to accommodate a mass hierarchy between the SM, SUSY and a yet unknown *theory of everything* (or some other intermediate theory in-between). Instead of giving specific scenarios of SUSY breaking, a common strategy is to parametrize all possible ways of soft-SUSY-breaking (i.e. breaking through parameters with mass dimension greater or equal to one) which are allowed by the symmetries of the superpotential. In case of the MSSM, the soft-SUSY-breaking Lagrangian reads

$$\begin{aligned}
 \mathcal{L}_{\text{soft}} = & B_\mu (H_u \cdot H_d + h.c.) \\
 & + T_l \tilde{l} \cdot H_d \tilde{e}^* + T_d \tilde{q} \cdot H_d \tilde{d}^* + T_u \tilde{q} \cdot H_u \tilde{u}^* \\
 & + m_{H_d}^2 |H_d|^2 + m_{H_u}^2 |H_u|^2 + \mathbf{m}_q^2 |\tilde{q}|^2 + \mathbf{m}_l^2 |\tilde{l}|^2 \\
 & + \mathbf{m}_d^2 |\tilde{d}|^2 + \mathbf{m}_u^2 |\tilde{u}|^2 + \mathbf{m}_e^2 |\tilde{e}|^2 \\
 & - \frac{M_1}{2} \tilde{B} \tilde{B} - \frac{M_2}{2} \tilde{W} \tilde{W} - \frac{M_3}{2} \tilde{g} \tilde{g},
 \end{aligned} \tag{1.38}$$

where B_μ is the soft bilinear term of the μ -term and has mass dimension two. Likewise, the second line in Eq. (1.38) contains soft terms for the trilinear YUKAWA terms of the scalar superpartners (sleptons and squarks). The third and fourth lines are the soft scalar mass terms which, in case of H_u and H_d , are also needed to realize EWSB. The T_i (\mathbf{m}_i) are complex (hermitian) 3x3 matrices in the generation space. The last line contains soft mass terms for the gauge boson superpartners bino (M_1), wino (M_2) and gluino (M_3). For a better readability, we refrain from the use of tildes in the soft mass parameters.

The soft parameters T_i and \mathbf{m}_i are strongly constrained by the absence of lepton-flavour-violating (LFV) processes. Since LFV is not of relevance for this thesis we parametrize for simplicity

$$\begin{aligned}
 T_n &= Y_n A_n, \quad n = l, d, u \\
 (\mathbf{m}_k)_{ij} &= \delta_{ij} m_{k_i}, \quad k = l, d, u, e
 \end{aligned} \tag{1.39}$$

and always assume flavour diagonal YUKAWA matrices. Thus, the stop coupling A_t is the most important soft breaking coupling of sfermions to the Higgs bosons due to the contribution of $Y_t \approx 1$.

After the breaking of SUSY we use the first line of Eq. (1.34) to construct the MSSM scalar

Higgs potential

$$\begin{aligned}
 V_{\text{MSSM}}^{\text{scalar}}(H_u, H_d) = & \underbrace{\left(\mu^2 + m_{H_d}^2 \right) |H_d|^2 + \left(\mu^2 + m_{H_u}^2 \right) |H_u|^2}_{\text{F-terms and soft masses}} + \underbrace{B_\mu (H_u \cdot H_d + \text{h.c.})}_{\text{soft bilinear term}} \\
 & + \underbrace{\frac{1}{8} (g_1^2 + g_2^2) \left(|H_u|^4 + |H_d|^4 - |H_u|^2 |H_d|^2 \right) + \frac{g_2^2}{2} |H_u^\dagger H_d|^2}_{\text{D-terms}}.
 \end{aligned} \tag{1.40}$$

From the F-terms and $\mu^2 > 0$, the necessity of $m_{H_{u,d}}^2$ for successful EWSB can be seen. As expected, the D-terms connect the quartic Higgs couplings with the SM gauge sector. We do not show the F- and D-terms for the sfermions as they are not discussed further. The YUKAWA sector which does not concern sfermion interactions reads

$$\begin{aligned}
 \mathcal{L}_{\text{MSSM}}^{\text{YUKAWA}} = & Y_d q \cdot H_d^\dagger \bar{d}_R - Y_u q \cdot H_u \bar{u}_R - Y_e l \cdot H_u \bar{e}_R \\
 & - \frac{g_2}{\sqrt{2}} \tilde{H}_u \cdot H_u^\dagger \tilde{W} - \frac{g_1}{\sqrt{2}} \tilde{H}_u \cdot H_u^\dagger \tilde{B} \\
 & - \frac{g_2}{\sqrt{2}} \tilde{H}_d \cdot H_d^\dagger \tilde{W} - \frac{g_1}{\sqrt{2}} \tilde{H}_d \cdot H_d^\dagger \tilde{B} \\
 & - \mu \tilde{H}_u \cdot \tilde{H}_d \\
 & + \text{h.c.} ,
 \end{aligned} \tag{1.41}$$

where the first line is the supersymmetric version for quark and lepton YUKAWA couplings. The second and third line describe higgsino-gaugino-Higgs interactions which are governed by SM gauge couplings. The fourth line is actually no YUKAWA coupling in the ordinary sense. However, as we come to the singlet extension of the MSSM, it will be useful for comparison to include it in this place.

1.3.3. Electroweak Symmetry Breaking in the MSSM

Assuming that the condition for EWSB [38]

$$B_\mu^2 > \left(\mu^2 + m_{H_u}^2 \right) \left(\mu^2 + m_{H_d}^2 \right) \tag{1.42}$$

is fulfilled, both Higgs boson fields acquire VEVs

$$\begin{aligned}
 \langle H_u \rangle &= \left(\frac{v_u}{\sqrt{2}}, 0 \right)^T \text{ and} \\
 \langle H_d \rangle &= \left(0, \frac{v_d}{\sqrt{2}} \right)^T ,
 \end{aligned} \tag{1.43}$$

which are usually connected by the definition of the mixing angle β

$$\tan \beta = \frac{v_u}{v_d} \tag{1.44}$$

such that $v_u^2 + v_d^2 = v^2$ is the Standard Model VEV. To shorten the notation, we introduce the abbreviations

$$\tan \beta \equiv t_\beta \quad \sin \beta \equiv s_\beta \quad \cos \beta \equiv c_\beta . \quad (1.45)$$

The minimum of the potential reads

$$\begin{aligned} \langle V_{\text{MSSM}}^{\text{scalar}} \rangle = & \left(\mu^2 + m_{H_d}^2 \right) v_d^2 + \left(\mu^2 + m_{H_u}^2 \right) v_u^2 + 2 B_\mu v_d v_u \\ & + \frac{1}{8} \left(g_1^2 + g_2^2 \right) \left(v_u^2 - v_d^2 \right)^2 \end{aligned} \quad (1.46)$$

from which we can extract conditions for the soft mass parameters by applying the tadpole conditions $\partial \langle V \rangle / \partial v_i|_{i=u,d} = 0$ for each Higgs VEV,

$$\begin{aligned} m_{H_d}^2 = & B_\mu t_\beta - \frac{1}{2} m_Z^2 c_{2\beta} - \mu^2 , \\ m_{H_u}^2 = & B_\mu t_\beta^{-1} + \frac{1}{2} m_Z^2 c_{2\beta} - \mu^2 , \end{aligned} \quad (1.47)$$

where the definition of the tree-level Z boson mass Eq. (1.22) has been used.

1.3.4. Tree-Level Masses and Mixing Matrices

In the following sections, we give expressions for the mass matrices in the gauge basis at tree-level in unitary gauge. The diagonalization of the mass matrices is performed in Chapters 3 and 4 where different approximations are applied.

1.3.4.1. Neutral and Charged Higgs States

After EWSB, five physical Higgs bosons mix to two CP-even h, H , one CP-odd A and a pair of charged scalar bosons H^\pm . It was shown in Ref. [38], that β can diagonalize the CP-even, CP-odd and charged Higgs boson mass matrices simultaneously if the spectrum contains only one light CP-even Higgs boson ("decoupling limit"). Thus, we will refrain from the definition of further mixing angles for the moment. Using the tadpole conditions Eq. (1.47) we get the symmetric CP-even (CP-odd) Higgs boson mass matrix \mathbf{m}_H^2 (\mathbf{m}_A^2) as well as the mass matrix $\mathbf{m}_{H^\pm}^2$ of the charged one in unitary gauge

$$\begin{aligned} \mathbf{m}_H^2 = & Z_H \begin{pmatrix} B_\mu t_\beta + m_Z^2 c_\beta^2 & -B_\mu - m_Z^2 \frac{s_{2\beta}}{2} \\ & B_\mu t_\beta^{-1} + m_Z^2 s_\beta^2 \end{pmatrix} Z_H^T , \\ \mathbf{m}_A^2 = & B_\mu Z_A \begin{pmatrix} t_\beta & 1 \\ & t_\beta^{-1} \end{pmatrix} Z_A^T \quad \text{and} \quad (1.48) \\ \mathbf{m}_{H^\pm}^2 = & Z_P \begin{pmatrix} B_\mu t_\beta + m_W^2 s_\beta^2 & B_\mu + m_W^2 \frac{s_{2\beta}}{2} \\ & B_\mu t_\beta^{-1} + m_W^2 c_\beta^2 \end{pmatrix} Z_P^T , \end{aligned}$$

where the Z_i rotate the Higgs states into the mass basis and diagonalize the squared mass matrices. In this rather simple form one can see that for very large B_μ all mass matrices are degenerate

$$\mathbf{m}_H^2, \mathbf{m}_{H^\pm}^2 \xrightarrow{v^2 \rightarrow 0} \mathbf{m}_A^2. \quad (1.49)$$

Because $\det(\mathbf{m}_A) = 0$, there is at least one massless CP-odd scalar which is the pseudo GOLSTONE boson of the Z boson. If we instead expand the eigenvalues of \mathbf{m}_H^2 to the first non-vanishing order in m_Z^2 , we get

$$m_h^2 \approx m_Z^2 \cos^2 2\beta, \quad (1.50)$$

which is at least $\approx (34 \text{ GeV})^2$ below the experimental value of m_h^2 . Hence, large higher-order corrections to Eq. (1.50) are needed if the MSSM is supposed accommodate the value of the observed Higgs boson mass. The leading stop and top contributions to the lightest Higgs mass for degenerate stop masses m_{SUSY}^2 and $A_t = 0$ reads

$$\delta m_h^2 \propto + \frac{1}{\pi^2} \frac{m_t^4(m_{SUSY})}{v^2} \log \frac{m_{SUSY}^2}{m_t^2(m_{SUSY})}, \quad (1.51)$$

where m_t is the top mass evaluated at the SUSY scale. The larger the stop mass, the larger the shift on m_h^2 making the MSSM more realistic. However, at the same time the large logarithm starts to amplify the uncertainty which is introduced through the running of m_t to m_{SUSY} (or any other scale) in a truncated perturbative series. Thus, the theoretical uncertainty in the Higgs mass prediction increases with too large stop masses.

1.3.4.2. Neutralinos and Charginos

All neutral (charged) SUSY fermions mix after EWSB to the neutralinos χ_i^0 (charginos χ_i^\pm), except the gluino which is the only fermionic color octet,

$$\begin{aligned} (\tilde{B}, \tilde{W}_3, \tilde{H}_u, \tilde{H}_d)^T &\rightarrow N (\chi_1^0, \dots, \chi_4^0)^T, \\ (\tilde{W}^+, \tilde{H}_u^+)^T &\rightarrow V (\chi_1^+, \chi_2^+)^T, \\ (\tilde{W}^-, \tilde{H}_d^-)^T &\rightarrow U (\chi_1^-, \chi_2^-)^T, \end{aligned} \quad (1.52)$$

where N , U and V are unitary transformations to diagonalize the mass matrices through a singular value decomposition,

$$\mathbf{m}_{\chi^0} = N^* \begin{pmatrix} M_1 & 0 & -\frac{vg_1}{2}c_\beta & \frac{vg_1}{2}s_\beta \\ & M_2 & \frac{vg_2}{2}c_\beta & -\frac{vg_2}{2}s_\beta \\ & & 0 & -\mu \\ & & & 0 \end{pmatrix} N^\dagger, \quad \mathbf{m}_{\chi^\pm} = U^* \begin{pmatrix} M_2 & \frac{vg_2}{\sqrt{2}}s_\beta \\ \frac{vg_2}{\sqrt{2}}c_\beta & \mu \end{pmatrix} V^\dagger. \quad (1.53)$$

The squared eigenvalues $m_{\chi_{1,2}^\pm}^2$ of the chargino mass matrices \mathbf{m}_{χ^\pm} are doubly degenerate such that

$$V\mathbf{m}_{\chi^+}^\dagger\mathbf{m}_{\chi^+}V^\dagger = U^*\mathbf{m}_{\chi^+}\mathbf{m}_{\chi^+}^\dagger U^T = \text{diag}\left(m_{\chi_1^\pm}^2, m_{\chi_1^\pm}^2\right) \quad (1.54)$$

The indexing of the states indicates their mass ordering

$$\begin{aligned} |m_{\chi_1^0}| &< \dots < |m_{\chi_4^0}|, \\ |m_{\chi_1^\pm}| &< |m_{\chi_2^\pm}|. \end{aligned} \quad (1.55)$$

1.3.4.3. Squark and Slepton Masses

Although we did not show the full Lagrangian for the scalar superpartners of the quarks and leptons, we can give their mass matrices in a limit important for our calculation. The focus of this thesis is set on scenarios where the sfermions are heavy enough to be integrated out. This means that the soft-SUSY-breaking mass parameters must be much larger than v . Thus, all sfermion mass matrices are already diagonal due to the requirement of minimal flavour violation (MFV) Eq. (1.39) and determined by the soft-SUSY-breaking mass matrices. Assuming universal soft-SUSY-breaking masses leads then to a degenerate sfermion spectrum.

From the discussion of the decoupling theorem in Section 1.1.2 it follows, that including terms which are proportional to v in the mass matrix would lead to contributions that are suppressed by $(v/m_{\text{sfermion}})^2$ in the matching conditions, which are not of relevance if the sfermion masses are well above 1 TeV. This assumption is kept in all following chapters of this thesis.

1.3.5. SUSY Breaking and UV Completions

In 1967 it was shown, that it is not possible to embed space time symmetries and internal symmetries into one set of commuting generators rather than writing them as a direct product of both [43]. With the introduction of SUSY and the anti-commuting SUSY-algebra into QFT, one possible loophole from this theorem was found [44]. Making it possible to embed interactions of gravity in QFT, local SUSY is one of the most popular ways to suggest boundary conditions of soft-SUSY-breaking parameters. Without referring to a specific model we want to mention that gravity-mediated SUSY breaking models (SUGRA) often predict universal soft-SUSY-breaking parameters at the PLANCK scale. If we consider SUSY to be broken near the GUT scale, the RGE running of the soft-SUSY-breaking parameters may be neglected and thus universal soft parameters are one possible choice to reduce the parameters space.

1.4. The Next-To Minimal Supersymmetric Standard Model

The MSSM has two major theoretical issues,

- (i) the appearance of the artificial mass parameter μ in the superpotential is not connected to the SUSY breaking scale, but determined by some heavy UV theory so that one would expect $\mu \gg m_{\text{soft}}$,
- (ii) the tree-level Higgs mass is too small, so that large higher-order corrections (i.e. large stop masses) are necessary,

which lead to the proposal of various extensions. There are many ways of going beyond the MSSM with an extra gauge singlet. We restrict ourself to the CP-conserving and scale-invariant superpotential, which leads to a \mathbb{Z}_3 -invariant scalar potential, as described in Ref. [45] which is called the *Next-To-Minimal Supersymmetric Standard Model* (NMSSM). All chiral superfield components have the same charge $e^{\frac{2\pi i}{3}}$ under the \mathbb{Z}_3 .

1.4.1. Particle Content

The additional chiral superfield \hat{S} is a singlet under the gauge group G_{SM} but charged under a global \mathbb{Z}_3 symmetry. Concerning the field content, we use the notation in Table 1.4 from the MSSM and append Table 1.5.

Super field	$s = 1/2$	$s = 0$	Generations	$U(1) \otimes SU(2) \otimes SU(3)$
\hat{S}	\tilde{S}	S	1	$(0, \mathbf{1}, \mathbf{1})$

Table 1.5.: The additional degrees of freedom in the Next-To Minimal Supersymmetric Standard model (NMSSM) compared to the MSSM.

The scale-invariant superpotential and the \mathbb{Z}_3 -invariant soft breaking part are also based on their MSSM counter parts. The idea is to replace the μ parameter with the VEV of the singlet naturally connecting it to the soft-SUSY-breaking scale through the tadpole conditions of the singlet. Thus, we can reuse the MSSM superpotential by setting $\mu = 0$ and add all singlet terms allowed by our restrictions. In the same manner we also set the soft bilinear term $B_\mu = 0$. Hence, the NMSSM superpotential and its soft terms read

$$\begin{aligned} \mathcal{W}_{\text{NMSSM}} &= \mathcal{W}_{\text{MSSM}}|_{\mu=0} + \lambda \hat{S} \hat{H}_u \cdot \hat{H}_d + \frac{\kappa}{3} \hat{S}^3, \\ \mathcal{L}_{\text{NMSSM}}^{\text{soft}} &= \mathcal{L}_{\text{MSSM}}^{\text{soft}}|_{B_\mu=0} - \left(\frac{T_\kappa}{3} S^3 + T_\lambda S H_u \cdot H_d + \text{h.c.} \right) - m_S^2 |S|^2, \end{aligned} \quad (1.56)$$

where the bilinear and its soft term are restored once the singlet obtains a VEV

$$\langle S \rangle = \frac{v_S}{\sqrt{2}}. \quad (1.57)$$

A soft singlino mass term is forbidden by the \mathbb{Z}_3 symmetry. The YUKAWA-like terms can also be expressed in terms of the MSSM YUKAWAS with vanishing μ and additional singlet interactions

$$\mathcal{L}_{\text{NMSSM}}^{\text{YUKAWA}} = \mathcal{L}_{\text{MSSM}}^{\text{YUKAWA}}|_{\mu=0} - \lambda S \tilde{H}_u \cdot \tilde{H}_d - \kappa \tilde{S} \tilde{S} S + \lambda \tilde{S} \left(\tilde{H}_u \cdot H_d + \tilde{H}_d \cdot H_u \right) \text{h.c.}, \quad (1.58)$$

which is also manifestly \mathbb{Z}_3 invariant.

1.4.2. Tree-Level Masses and Mixing Matrices

In the following sections, we will proceed as in the MSSM. The connection between the μ parameter and v_s as well as other soft breaking terms was already mentioned in the previous section. In order to get expressions that are comparable to the MSSM, we introduce the abbreviations

$$\begin{aligned}\mu_{\text{eff}} &= \frac{v_s \lambda}{\sqrt{2}} \quad \text{and} \\ B_{\mu}^{\text{eff}} &= \frac{v_s}{2} \left(v_s \kappa \lambda + \sqrt{2} T_{\lambda} \right).\end{aligned}\tag{1.59}$$

1.4.2.1. Tadpole Equations

There is one additional vacuum condition from the complex scalar singlet. Solving all conditions w.r.t. the squared soft mass parameters yields

$$\begin{aligned}m_{H_d}^2 &= B_{\mu}^{\text{eff}} t_{\beta} - m_Z^2 \frac{c_{2\beta}}{2} - \frac{v^2 \lambda^2}{2} s_{\beta}^2 - \mu_{\text{eff}}^2, \\ m_{H_u}^2 &= B_{\mu}^{\text{eff}} t_{\beta}^{-1} + m_Z^2 \frac{c_{2\beta}}{2} - \frac{v^2 \lambda^2}{2} c_{\beta}^2 - \mu_{\text{eff}}^2,\end{aligned}\tag{1.60}$$

$$m_S^2 = B_{\mu}^{\text{eff}} \frac{v^2 s_{2\beta}}{v_s^2} + v^2 \kappa \lambda s_{2\beta} - \frac{v^2 \lambda^2}{2} - \frac{v_s T_{\kappa}}{\sqrt{2}} - v_s^2 \kappa^2,\tag{1.61}$$

where the λ^2 term in the conditions for v_u and v_d is due to F-term contributions of the singlet. Apart from that, the first two conditions are of the same form as the tadpole conditions in Eq. (1.47) of the MSSM. The singlet tadpole condition for $v \rightarrow 0$ and $T_{\kappa} \approx m_S$ yields $v_s \approx \mathcal{O}(m_S)$ naturally connecting the singlet VEV (and thus μ_{eff}) to the SUSY breaking scale.

1.4.2.2. Higgs States

There are two additional d.o.f. in the Higgs sector, due to the complex singlet, appending one extra dimension to the MSSM CP-even/odd mass matrices. However, similarly to the tadpoles, the upper left 2x2 matrices are comparable to the MSSM while the CP-even and

charged Higgs masses have additional F-term contributions

$$\begin{aligned}
\mathbf{m}_H^2 &= \begin{pmatrix} B_\mu^{\text{eff}} t_\beta + m_Z^2 c_\beta^2 & -B_\mu^{\text{eff}} - (m_Z^2 - v^2 \lambda^2) \frac{s_{2\beta}}{2} & \lambda v v_s (\lambda c_\beta - \kappa s_\beta) - \frac{v T_\lambda s_\beta}{\sqrt{2}} \\ & B_\mu^{\text{eff}} t_\beta^{-1} + m_Z^2 s_\beta^2 & -\lambda v v_s (\lambda c_\beta - \kappa s_\beta) - \frac{v T_\lambda s_\beta}{\sqrt{2}} \\ & & 2v_s^2 \kappa^2 + \frac{v_s T_\kappa}{\sqrt{2}} + \frac{v^2 T_\lambda s_{2\beta}}{v_s 2\sqrt{2}} \end{pmatrix} \\
\mathbf{m}_A^2 &= \begin{pmatrix} B_\mu^{\text{eff}} t_\beta & B_\mu^{\text{eff}} & \frac{v T_\lambda}{\sqrt{2}} s_\beta - \kappa \lambda v v_s s_\beta \\ & B_\mu^{\text{eff}} t_\beta^{-1} & \frac{v T_\lambda}{\sqrt{2}} c_\beta - \kappa \lambda v v_s s_\beta \\ & & v^2 \kappa \lambda s_{2\beta} + \frac{v^2 T_\lambda s_{2\beta}}{v_s 2\sqrt{2}} - \frac{3v_s T_\kappa}{\sqrt{2}} \end{pmatrix} \quad (1.62) \\
\mathbf{m}_{H_\pm}^2 &= \begin{pmatrix} B_\mu^{\text{eff}} t_\beta + \left(m_W^2 - \frac{v^2 \lambda^2}{2}\right) s_\beta^2 - \frac{v^2 \lambda^2}{2} & B_\mu^{\text{eff}} + \frac{1}{2} m_W^2 s_{2\beta} - \frac{v^2 \lambda^2}{2} \\ & B_\mu^{\text{eff}} t_\beta^{-1} + \left(m_W^2 - \frac{v^2 \lambda^2}{2}\right) c_\beta^2 \end{pmatrix}
\end{aligned}$$

Imposing not too large mixing with the new singlet components, the lightest CP-even mass eigenvalue of the 2x2 sub-matrix in the limit $v \ll v_s, T_\lambda$ reads

$$m_h \approx m_Z^2 \cos^2 2\beta + v^2 \lambda^2 \sin^2 2\beta, \quad (1.63)$$

which is able to reach the experimental value of m_h at tree level, if $\tan \beta$ is not too large, and allows for small higher-order corrections compared to the MSSM.

1.4.2.3. Neutralinos and Charginos

Similar to the scalar sector, the fermion sector of the MSSM gets modified by effective μ -terms and an additional two-component WEYL spinor leading to five neutralinos compared to four in the MSSM. Because of its singlet nature, the singlino can mix with the two higgsinos but not with the gauginos,

$$\mathbf{m}_{\chi_0} = N^* \begin{pmatrix} M_1 & 0 & -\frac{v g_1}{2} c_\beta & \frac{v g_1}{2} s_\beta & 0 \\ & M_2 & \frac{v g_2}{2} c_\beta & -\frac{v g_2}{2} s_\beta & 0 \\ & & 0 & -\mu_{\text{eff}} & -\frac{v \lambda}{\sqrt{2}} s_\beta \\ & & & 0 & -\frac{v \lambda}{\sqrt{2}} c_\beta \\ & & & & \sqrt{2} v_s \kappa \end{pmatrix} N^\dagger \quad (1.64)$$

$$\mathbf{m}_{\chi_\pm} = U^* \begin{pmatrix} M_2 & \frac{v g_2}{\sqrt{2}} s_\beta \\ \frac{v g_2}{\sqrt{2}} c_\beta & \mu_{\text{eff}} \end{pmatrix} V^\dagger. \quad (1.65)$$

The neutralino mass matrix implies that for $v_s < M_{1,2}, v$ and $\kappa < \lambda$ a singlet-like LSP particle can be possible. Whether scenarios with a singlet-like LSP can predict the measured relic density of DM is studied in Chapter 3.

1.5. Supersymmetry without Natural Scalars

It was already mentioned that one of the major motivations for weak-scale SUSY is that it can solve the *hierarchy problem*, which says that scalar masses are not protected by ordinary internal symmetries but receive large quantum corrections pushing them the scale of new physics. However, the Higgs boson mass $m_h \approx \mathcal{O}(125 \text{ GeV})$ is required to be small, e.g. in order to restore unitarity in the SM, while new physics is at latest expected to appear at the PLANCK scale $m_{\text{PLANCK}} \approx 10^{18} \text{ GeV}$. Thus, the counter term of the SM Higgs boson mass must be fine-tuned to a precision of about $\mathcal{O}(m_{\text{PLANCK}}^2/m_h^2) \approx 10^{32}$. This large cancellation is interpreted as a sign for a hidden approximate symmetry, which is responsible for the smallness of the SM Higgs boson mass. Low-scale SUSY is a possible candidate for such a symmetry which does not only address the question of naturalness in the scalar sector, but for instance also of dark matter or gauge coupling unification. However, the observation of a non-zero but small cosmological constant $\Lambda_{\text{CC}} \approx 10^{-48} \text{ GeV}^4$ [2, 46] is neither addressed in the MSSM nor in most of its extensions. As an example, SUGRA predicts the soft-SUSY-breaking scale m_{SUSY} to be generated by the VEV $\langle F \rangle$ of an auxiliary field in a yet unspecified sector due to gravitational effects

$$m_{\text{SUSY}} \approx \frac{\langle F \rangle^2}{m_{\text{PLANCK}}}, \quad (1.66)$$

assuming that it is possible to describe the entire space-time including gravity within the SUSY framework. Thus, SUSY with $m_{\text{SUSY}} \lesssim 1 \text{ TeV}$ predicts a vacuum energy of roughly $\Lambda_{\text{UV}}^{\text{cutoff}} \approx \langle F \rangle^2 \approx \mathcal{O}(10^{12} \text{ GeV})$ which is much larger than the observed $\sqrt{\Lambda_{\text{CC}}}$. Hence, even if weak-scale SUSY solves the hierarchy problem, it does not solve the *cosmological constant problem* [47] which concerns a constant term in the superpotential fine-tuned to $\mathcal{O}(\langle F \rangle^4/\Lambda_{\text{CC}}) \approx 10^{96}$ orders of magnitude. Therefore, even weak-scale SUSY would be fine tuned (indeed also the SM itself is fine-tuned to ≈ 50 digits by the same arguments).

Relaxing the requirement of naturalness, alternative approaches involving selection principles [48] were developed to explain the smallness of the cosmological constant. In the presence of e.g. a landscape of many different possible vacua, it is just a logical consequence that human life is only realized in those solutions which stabilize the electroweak scale. Thus, naturalness in the ordinary sense may not be extended to the scalar sector even in the supersymmetric case. However, fermion masses *are* protected by chiral symmetries since loop corrections to masses enter only in such a way, that they disappear in the symmetry-restoring limit of vanishing masses. Hence, the use of anthropic principles in the scalar sector does not imply that 'T HOOFT's principle of naturalness [49] is no longer applicable, but may only be applied to the fermionic sector where it turns out to be a very predictive and successful tool.

One consequence of a fine-tuned Higgs bosons mass for supersymmetric theories is, that superpartner masses must no longer be at the TeV-scale. In this case, one may ask about the further significance of SUSY for particle physics phenomenology because its major motivation, the solution of the big hierarchy problem, would become obsolete. Nevertheless, SUSY can still be a very predictive framework even with a fine-tuned scalar sector as it is shown in chapters 3 and 4.

However, the presence of a large SUSY breaking scale m_{SUSY} introduces a hierarchy between the SM and the BSM sector such that EFT techniques described in the previous sections become appropriate. The technical subtleties arising when supersymmetric theories are to be matched are reviewed in the next section.

1.6. Higher-Order Threshold Corrections in Supersymmetric Models

Higher order corrections in supersymmetric theories require a special treatment. We have already seen that scalar couplings as well as masses are no free parameters anymore, but are connected to the gauge and YUKAWA sector. Thus, for a consistent perturbative expansion one needs to take into account, that higher-order corrections in the gauge sector are transmitted to the scalar sector through the D-terms. Furthermore, it is of fundamental importance that the mathematical treatment of UV divergences in higher-order corrections does not break SUSY.

In the following, we briefly discuss how these two aspects can be accounted for in a diagrammatic calculation at the one-loop order.

1.6.1. Dimensional Regularization and Dimensional Reduction

When higher-order corrections to a scalar coupling are computed, diagrams with internal vector bosons carrying a LORENTZ index may be involved. These diagrams are potentially UV divergent. A common way to deal with the divergences is to regularize them in a gauge covariant way, called *dimensional regularization* (DREG). The strategy is to compute the diagrams in $D = 4 - 2\epsilon$ space-time dimensions which allows for an analytical continuation of the expressions and an isolation of the divergences in a power series of $1/\epsilon$. In a *minimal subtraction* ($\overline{\text{MS}}$) renormalization scheme, all UV divergent parts $\Delta_{\overline{\text{MS}}}$ with an additional constant part

$$\Delta_{\overline{\text{MS}}} = \frac{1}{\epsilon} - \gamma_E + \log 4\pi, \quad (1.67)$$

where γ_E is the EULER-MASCHERONI constant, are absorbed into the corresponding counter terms. As a consequence of DREG the B boson, for instance, now has D d.o.f. while the bino \tilde{B} still has four d.o.f. Hence, SUSY is broken when applying DREG because $n_B = n_F$ is violated.

A way to overcome this problem is given by *dimensional reduction* (DRED) where all four-momenta are treated in D dimensions while the vector fields are still four dimensional. It was shown in Ref. [50], that DRED is indeed equivalent to DREG up to finite terms appearing in the $\overline{\text{DR}}$ scheme counter terms of the DRED computation. Thus, if

a non-supersymmetric model, conventionally computed in $\overline{\text{MS}}$, is to be matched to a supersymmetric model including higher-order corrections, one needs to account for the conversion from $\overline{\text{MS}}$ to $\overline{\text{DR}}$.

The computation of one-loop amplitudes in DREG as well as DRED (actually constrained differential renormalization which is equivalent to DRED at one loop) is fully automatized in the computer program FORMCALC [28], which we use to compute the difference of the two schemes.

1.6.2. Threshold Corrections to Gauge Couplings

From the tree-level relation Eq. (1.50) of the lightest Higgs boson mass in the MSSM,

$$m_h^2 \approx \frac{v^2}{4} (g_1^2 + g_2^2) \cos^2 2\beta, \quad (1.68)$$

which has its origin in supersymmetric D-terms, it can be seen that one-loop corrections to the gauge couplings $g_{1,2}$ also enter the one-loop Higgs boson mass. For a generic spectrum generator, it is thus important to be able to compute the threshold corrections to any gauge coupling in general gauge theories, even if it is only intended to match the scalar sectors at higher orders.

Generic expressions for one-loop threshold corrections to gauge couplings g_{EFT} in spontaneously broken gauge theories were first computed in Refs. [51] and [52],

$$g_{\text{EFT}}(Q_{\text{match}}) = g(Q_{\text{match}}) \left(1 + \frac{g^2(Q_{\text{match}})}{192\pi^2} \sum_f C_f T_f^{(3)} T_f^{(2)} S_f I_f^r \log \frac{M_f^2}{Q_{\text{match}}^2} \right), \quad (1.69)$$

where the sum runs over all heavy fields f with masses M_f . The factors C_f , S_f , $T_f^{(2)}$ and $T_f^{(3)}$ account for reversed propagator lines (charge factor), spin, iso-spin and the color factor of the heavy field running in the loop,

$$C_f = \begin{cases} 2 & , f \text{ charged} \\ 1 & , f \text{ neutral} \end{cases} \quad T_f^{(N)} = \text{Dim}_r SU(N)$$

$$S_f = \begin{cases} 1 & , s = 0 \\ 4 & , s = 1/2 \\ 2^{1/2} & , s = 1 \end{cases} \quad I_f^r = \begin{cases} \text{DYNKIN index of the field } f \\ \text{transforming under the repr-} \\ \text{esentation } r \text{ of the gauge group} \end{cases}. \quad (1.70)$$

1.7. Effective Higgs Masses in Supersymmetric Models

1.7.1. General Overview

This section puts the aim of this thesis, a generic matching between two arbitrary scalar sectors, into the context of the literature already available on the topic of effective Higgs

mass calculations.

A comprehensive summary of SUSY spectrum generators as well as dedicated studies on Higgs mass computations is given in Ref. [53]. Although the publication of this summary was only two years ago, there were many developments in the field of EFT Higgs mass calculation. Computer programs, which were originally based on pure fixed-order calculations, such as FEYNHIGGS [54–56], FLEXIBLESUSY [6, 57, 58] or SARAHS/SPHENO [12, 59], are nowadays able to compute the lightest Higgs mass in an effective SM, if all other SUSY particles (except one Higgs boson) are heavy. This scenario is also called *high-scale SUSY*. Although different renormalization schemes as well as computational techniques are involved, there is a good agreement [59] between new implementations of e.g. effective Higgs mass calculations in SARAHS/SPHENO and results of SUSYHD [60], which is a dedicated tool for high-scale SUSY scenarios.

A quantitative comparison between the spectrum generators SARAHS/SPHENO, FLEXIBLESUSY, FEYNHIGGS and SUSYHD computing the lightest MSSM Higgs mass in an effective SM was made in Ref. [59] and is shown in Fig. 1.6a. The plot shows the Higgs mass prediction m_h as a function of the matching scale m_{SUSY} at which the SUSY partners are integrated out. There is a good agreement over many orders of magnitude between the different approaches. One major difference between SUSYHD and the other codes is, that it does not account for v^2/m_{SUSY}^2 suppressed terms. These terms become most important for $m_{SUSY} < 0.5$ TeV, where the brown SUSYHD curve starts to differ significantly from the other codes. The red-dotted line shows the fixed-order calculation of SARAHS, which does not rely on EFT techniques. The fixed-order result, incorporating the v^2/m_{SUSY}^2 terms, seems to be complementary and starts to differ from the EFT approach if $m_{SUSY} > 0.5$ TeV. This leads to the question how the theoretical uncertainties in both approaches behave. The uncertainties on the Higgs mass prediction in a fixed-order and a comparable EFT calculation are studied in Ref. [6] and are shown in Fig. 1.6b. The red band shows the uncertainty of a three-loop fixed-order calculation, rapidly increasing as m_{SUSY} approaches the TeV scale. The grey band shows the uncertainty of an EFT calculation at two-loop order which is again complementary to the conventional approach. The authors of Ref. [6] found that both bands have the same width at the scale $m_{SUSY}^{\text{equal}} \approx 1.2$ TeV.

The influence of higher-order QCD corrections in the EFT framework also has been improved in dedicated studies [9, 35]. Recently, four-loop order contributions $\mathcal{O}(\alpha_s^2 \alpha_t^2)$ have been studied [57] which influence the Higgs mass prediction in the sub-GeV range. In studies which go beyond one-loop, the higher-order corrections decrease with the matching scale and are negligibly small if $m_{SUSY} > 10^5$ TeV.

Furthermore, EFTs which go beyond the SM as a low-energy theory are very popular because they have a rich phenomenology. Matchings of the MSSM to a two Higgs doublet model (2HDM) were performed in Refs. [8, 61] and has been implemented in FeynHiggs [54]. Split SUSY, where the fermionic superpartners are kept in the EFT taking the weaker bounds on electroweakinos into account, was first proposed in 2003 [62] while the Split MSSM was phenomenologically studied in Refs. [7, 35]. However, studies involving EFT techniques which go beyond the MSSM such as Refs. [10, 63–65] are rare and often do not

consider higher-order corrections.

This offers the possibility to test the new implementation, which was developed within this thesis, against results available in the literature. Moreover, we can now address open questions which were hard to answer without the availability of a generic spectrum generator being able to perform generic matchings in the scalar sector. This is the topic of Chapters 3 and 4.

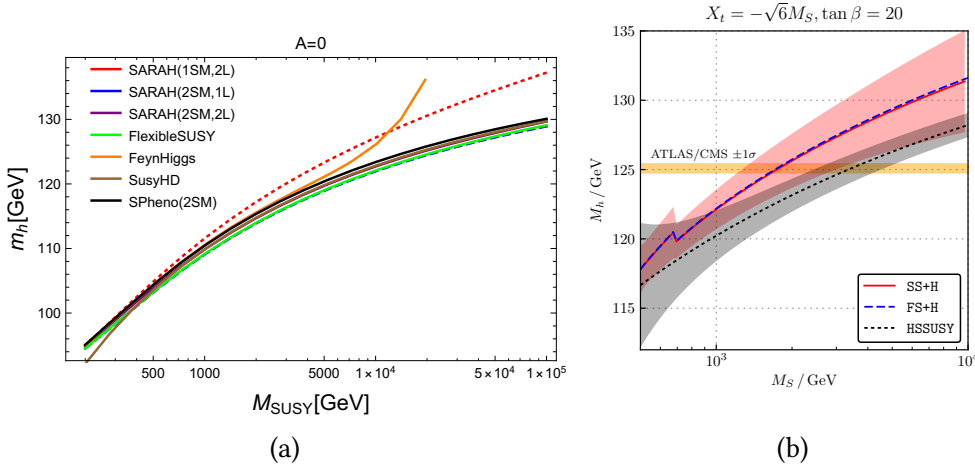


Figure 1.6.: (a) Comparison of the Higgs mass prediction from the MSSM matching to an effective SM between various computer codes as well as one fixed-order calculation (red-dotted line). (b) Uncertainty estimate on the Higgs mass prediction in a fixed-order calculation at three-loop order and an EFT calculation at two-loop order. The grey/red band represents the uncertainty of the EFT/fixed-order calculation. The computer codes in the legend are: SS: SOFTSUSY (fixed-order), FS: FLEXIBLESUSY (fixed-order), +H: HIMALAYA, HSSUSY: FLEXIBLESUSY (EFT).

1.7.2. Status Quo in SARAH/SPheno

Although SARAH was introduced as a generic spectrum generator, able to calculate the mass spectrum for any renormalizable Lagrangian, an EFT calculation for m_h was so far only possible for an effective SM. If there are further light Higgs states present, the EFT routines were not used, leading to less precise predictions of scalar masses. The following paragraph gives details on the EFT Higgs mass strategy used so far and how it is modified in order to be able to perform a generic matching.

The SPHENO FORTRAN code generated by SARAH is using an iterative procedure shown in Fig. 1.7 in order to obtain an effective Higgs mass. First, all Lagrangian parameters are extracted from measured observables at the scale m_Z using one-loop relations in an $\overline{\text{MS}}$ scheme. Second, an RGE running using SM RGEs is employed up to the matching scale Q_{match} where all parameters are translated into a $\overline{\text{DR}}$ scheme. Third, a *pole-mass* matching to the BSM Higgs pole-mass prediction is performed from which the effective quartic

coupling $\overline{\lambda}_{SM}^{\text{MS}}(Q_{\text{match}})$ is extracted (this procedure is explained in the next paragraph). Fourth, all parameters, including the new effective coupling, are run down to the top mass m_t where the one-/two-loop corrected mass spectrum is calculated within the SM. If the mass spectrum significantly differs from the previous iteration, a new iteration starts by running to m_Z and proceeds with step two.

The reason why this procedure cannot be extended to a non-SM EFT (where the additional Lagrangian parameters would be user input) is due to the used pole-mass matching instead of a direct matching of the quartic coupling

$$\begin{aligned} \left(m_h^{\text{BSM,pole}}(Q_{\text{match}})\right)^2 &= \left(m_h^{\text{SM,pole}}(Q_{\text{match}})\right)^2 \\ &= \left(m_h^{\text{SM,Tree}}(Q_{\text{match}})\right)^2 + \Pi_h^{\text{SM}}(Q_{\text{match}}) \\ \Rightarrow v_{\text{SM}}^2 \lambda_{\text{SM}} &= \left(m_h^{\text{BSM,pole}}\right)^2 - \Pi_h^{\text{SM}}, \end{aligned} \quad (1.71)$$

where the tree-level relation Eq. (1.12) has been used. In favour of better readability, the dependence of all parameters on the matching scale in the last line has been omitted. $m_h^{\text{BSM,pole}}(Q_{\text{match}})$ is the one-/two-loop Higgs mass in the BSM model whereas Π_h^{SM} are the one-/two-loop corrections in the SM calculated using the effective potential. However, an extended Higgs sector often has much more scalar couplings than masses, making it impossible to invert the tree-level relations without introducing mixing angles. For instance, a CP-conserving 2HDM of type II has five quartic couplings, but only four Higgs boson mass parameters. Thus, one also needs to take the matching of the mixing angle into account, which is not straight-forward to do in a pole-mass matching.

The next chapter is discussing the matching of scalar couplings at the one-loop order which is replacing the pole-mass matching. With this replacement, the procedure in Fig. 1.7 can be applied to EFTs beyond the SM.

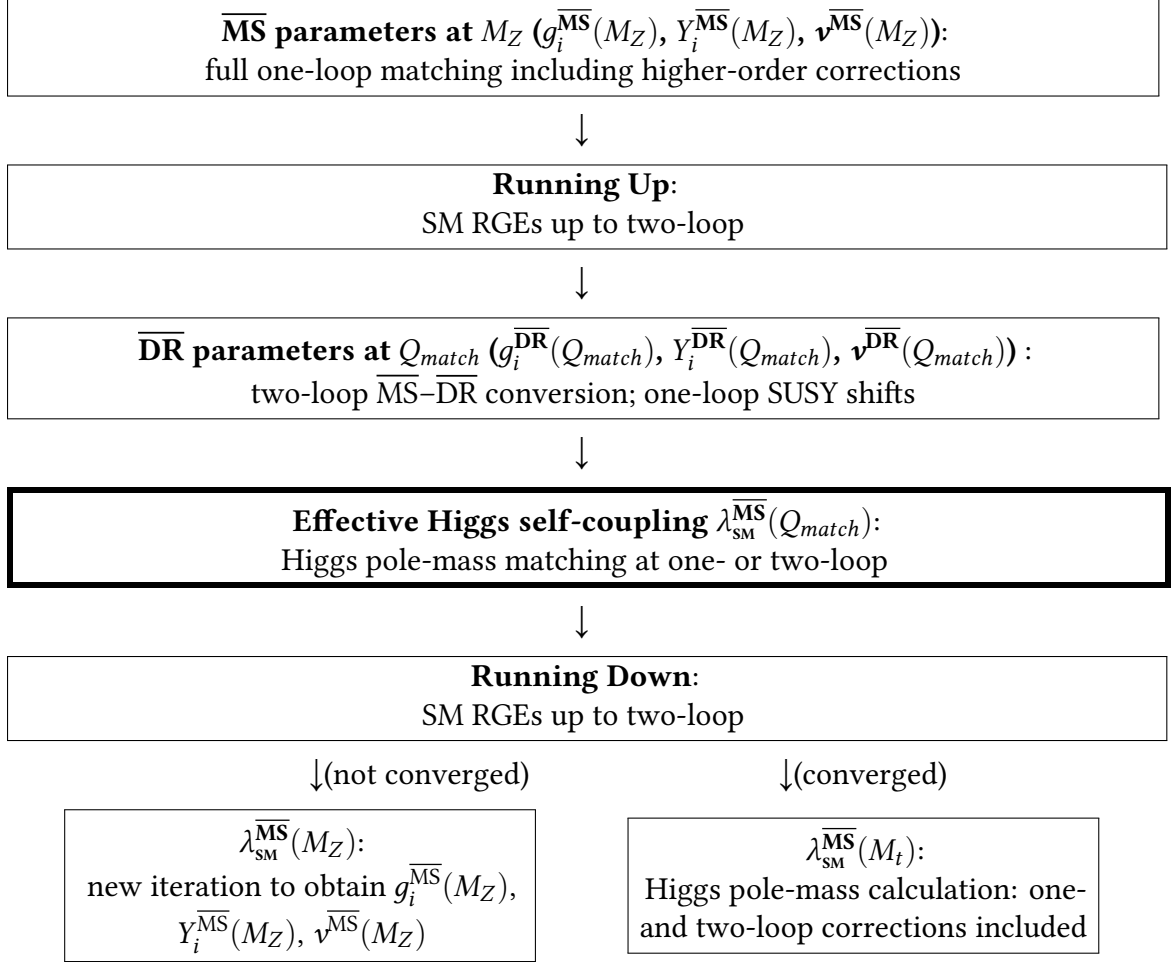


Figure 1.7.: Effective SM Higgs boson mass calculation in SARAH/SPHENO [59]. The replacement of the pole-mass matching (highlighted box) through a direct matching of the scalar coupling(s) is one issue addressed in this thesis.

2. Scalar Matching Conditions at Next-to Leading Order

In the previous chapter, the theoretical ingredients necessary for the matching of two scalar theories were discussed. This chapter reviews the technical details required for a one-loop calculation of generic scalar amplitudes in the limit of vanishing external momenta. In addition, the separation of local and non-local contributions for all possible light and heavy field insertions is discussed. As mentioned in the introduction, only the local contributions enter threshold corrections after matching conditions have been applied. Hence, the separation of scales has to be done only once for each loop integral. In a specific (model-dependent) calculation of threshold corrections, one can then restrict oneself to the use of the modified loop functions that contain the local parts only.

In order to verify that the separation of scales has been done correctly, both sides of the matching condition (the EFT and the full theory part) are investigated separately in a toy model, to show that all non-local terms indeed cancel. Finally, the implementation of the technical aspects in SARAH is discussed.

2.1. Topologies and Generic Diagrams and their Amplitudes

In this thesis, we distinguish between four types of FEYNMAN-like diagrams which are based on the FEYNARTS notation:

1. *Topologies*

Neither the statistical nature (spin=0,1,1/2) nor the mass (light or heavy i.e. zero or non-zero) are specified. Since the focus is on the matching of scalar sectors, external fields are always light scalars denoted by dashed lines.

2. *Generic Diagrams*

The spin of all fields is specified but not their mass hierarchies. This is still a model-independent graph.

3. *Generic Amplitudes*

The spins determine the LORENTZ structure of the diagram. Thus, all necessary information is given to compute a model-independent expression of the diagram. All couplings and masses are yet unspecified.

4. *Insertions*

These are FEYNMAN diagrams in the ordinary sense. All couplings and masses take

the form governed by a given model. The summation over generation and group indices is also performed here.

In order to support a large class of BSM models for the computation of threshold corrections, all possible diagrams of the first three types as well as the expressions for the generic amplitudes need to be known. Because this thesis computes threshold corrections to renormalizable operators, only those diagrams that connect 2, 3 or 4 external lines at leading and next-to-leading order are needed. From the requirement of renormalizability it follows further that internal vertices cannot connect more than 4 lines. At tree level, only singly connected internal vertices (i.e. no closed internal lines) are required while at one-loop level exactly one closed internal line and optional singly connected internal vertices (leading to 1PR topologies) must be present.

The graphical notation for the topologies is as follows. Vertices, denoted by a black filled dot, represent generic couplings that can have any form allowed by renormalizability and LORENTZ invariance. External scalar legs are drawn with a dashed line while internal straight lines are reserved for all possible field-types (vector, fermion or scalar) and mass insertions. The external legs can be charged or neutral and do not necessarily have the same field insertions amongst the different legs.

The notation used to describe the topologies within this thesis and the implementation in SARAH is described in Fig. 2.1. Topologies are denoted by a string with a length between two and five characters. The first letter specifies whether it is a tree-level (T), self-energy (S), WFR (W) or ordinary one-loop diagram (blank). The next letter gives information about the involved loop integrals (which are defined later in Eq. (2.6)) followed by three numbers specifying the number of external legs (2,3 or 4), whether it is a 1PI (1) or 1PR (2) diagram and a counting index. A complete list of all tree-level and one-loop topology diagrams is given in Appendix A.1, while this section discusses only an excerpt of this list.

2.1.1. Generic Tree-Level Graphs

The two-point function is necessary for the matching of scalar sectors that involve no Higgs bosons i.e. scalars that do not develop a VEV. In this case the scalar masses and couplings are independent parameters and have to be matched separately. At tree level, the two-point topology T2 has two external lines singly connected by a dot. This accounts for squared diagonal and off-diagonal mass terms.

Since there is only one three-point topology (T3) at tree level, shown in Fig. 2.2 (a), the trilinear couplings in a tree-level matching can also directly be determined by comparing the two Lagrangians.

Furthermore, there are two tree-level topologies with four external scalars, shown in Fig. 2.2 (b) and (c). The first one is a local quartic coupling which could for example be given by supersymmetric D-terms and/or F-terms while the second has one internal propagator, necessarily heavy and of bosonic nature. Thus, fermions can only enter one-loop and higher-order corrections but not the tree-level matching. The tree-level contribution of

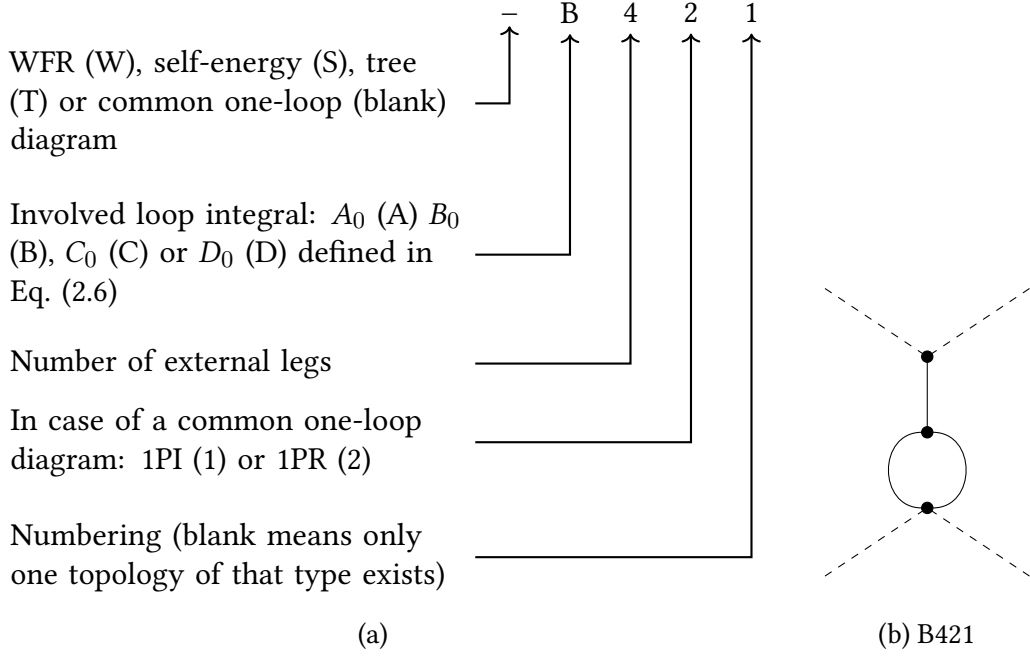


Figure 2.1.: Notation on topologies shown in Appendix A.1. The example expression explained in (a) corresponds to the topology shown in (b).

the corresponding generic amplitude is always of the form $\delta\lambda^{\text{Tree}} \propto T_1 T_2 / m_H^2$, with trilinear couplings T_i of mass dimension one and a heavy mass $m_H^2 \gg p^2$. In case of a heavy vector, the amplitude is proportional to the external momentum which vanishes in the approximation $p^2 \rightarrow 0$. Thus, only heavy scalar bosons can contribute at tree level to the generic scalar amplitudes.

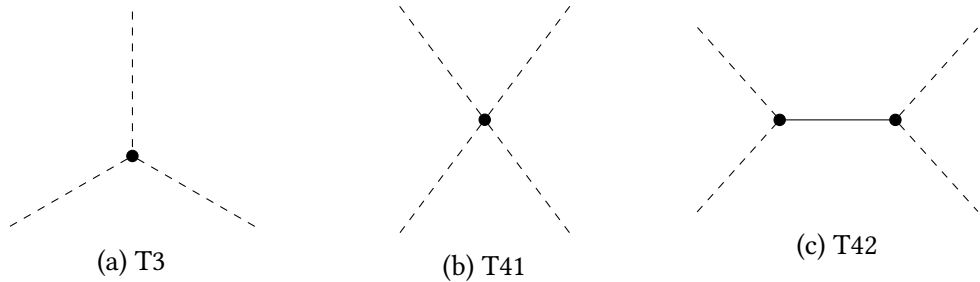


Figure 2.2.: Tree-level graphs with 3 and 4 external scalars. The straight line can be a heavy scalar or a heavy vector boson.

2.1.2. Generic One-Loop Graphs

There are a large number of generic one-loop diagrams and non-zero generic amplitudes (i.e. generic amplitudes that are not linear in p^2), see Table 2.1. Thus, only an excerpt of topologies, shown in Fig. 2.3, is discussed. Also the discussion of possible generic amplitudes is restricted to diagrams with either only heavy fermions or heavy scalars,

2. Scalar Matching Conditions at Next-to Leading Order

External Scalars	Topologies	Generic Diagrams	Non-zero Amplitudes
2	2	6 (7)	6 (7)
3	4	14 (15)	14 (15)
4	12	51 (60)	44 (49)

Table 2.1.: Counting of the different possible diagram types for 2, 3 and 4 external scalars. The numbers in brackets include diagrams with ghost fields.

to describe the overall scaling behaviour of their contributions. A full list of one-loop topologies is given in Appendix A.1.

Since we work always in the limit of massless SM gauge bosons at the matching scale i.e. $v_{\text{SM}} \rightarrow 0$, the SM ghost fields do not contribute to the threshold corrections. However, in the context of extended gauge theories it might be necessary to also compute loops that involve ghost fields of heavy vector bosons. Thus, we also count the number of diagrams and non-zero amplitudes including ghosts given in brackets in Table 2.1.

2.1.2.1. Two-Point Function

At the one-loop order, two two-point topologies, shown in Fig. 2.3, involving either a quartic (a) or two trilinear couplings (b) exist. The difference between generic two-point amplitudes of heavy scalars and fermions is due to the different mass dimensions of the couplings and the additional topology (A2), available for scalars only, involving the quartic coupling. The generic amplitude scales as

$$[\mathcal{M}_{1 \rightarrow 1}^{\text{scalar}}] = [\text{mass}]^2 = \begin{cases} [\text{YUKAWA coupling}]^2 \cdot [\text{loop mass}]^2 & , \text{heavy fermion} \\ [\text{quartic coupling}]^2 \cdot [\text{loop mass}]^2 \\ + [\text{trilinear coupling}]^2 & , \text{heavy scalar} \end{cases} . \quad (2.1)$$

Thus, YUKAWA couplings with heavy fermions will always lead to a fine-tuned squared mass parameter, as the new contributions must be canceled against other parameters in the potential in order to keep the external scalar light. When heavy scalars are integrated out, large fine-tuning appears only if there is a quartic coupling to the light fields or if a large trilinear coupling is present. However, in theories with spontaneous symmetry breaking, this fine-tuning is often *hidden* in the tadpole equations.

2.1.2.2. Three-Point Function

Four three-point one-loop topologies exist. The scaling of generic three-point amplitudes with fermions/scalars is again determined by dimensional arguments. For instance, the C3 (triangle) topology shown in Fig. 2.3 (c) scales as

$$[\mathcal{M}_{2 \rightarrow 1}^{\text{scalar}}] = [\text{mass}] = \begin{cases} [\text{YUKAWA coupling}]^3 \cdot [\text{loop mass}] & , \text{heavy fermion} \\ \frac{[\text{trilinear coupling}]^3}{[\text{loop mass}]^2} & , \text{heavy scalar} \end{cases} . \quad (2.2)$$

The scalar contribution decouples if the trilinear coupling is not connected to the scalar masses while the fermion contributions behave similar to the two-point function.

2.1.2.3. Four-Point Function

Fig. A.7 shows the 12 one-loop topologies that involve 4 external scalars out of which 4 (WA41, WA42, WB41 and WB42) are wave-function renormalization diagrams and two (SB4 and SA4) account for self-energies. The D4 (box) topology, shown in Fig. 2.3 (d), is discussed in more detail. Since the four point function is dimensionless, the scaling behaviour of the box topology is given by

$$[\mathcal{M}_{2 \rightarrow 2}^{\text{scalar}}] = [1] = \begin{cases} [\text{YUKAWA coupling}]^4 \cdot & , \text{heavy fermion} \\ \frac{[\text{trilinear coupling}]^4}{[\text{loop mass}]^4} & , \text{heavy scalar} \end{cases} . \quad (2.3)$$

Thus, scalars behave similar to the three-point function while the impact of heavy fermions is less critical, as their masses can only contribute in ratios of heavy masses.

From the dimensional arguments given above one can specify two types of operators. The *important* operators have mass dimension 2 or 3, which will be fine-tuned if either a YUKAWA coupling to heavy fermions or a quartic coupling of the light scalars to heavy ones exists. The *marginal* operators have dimension four and dimensionless couplings. They are either suppressed by some heavy mass or at least a loop factor.

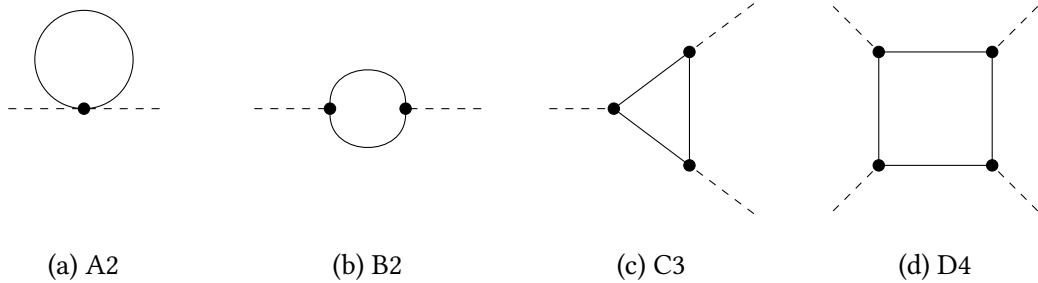


Figure 2.3.: Excerpt of the topology list given in Appendix A.1.

2.2. Loop Functions with vanishing External Momenta

All diagrams are computed with vanishing external momenta, which significantly simplifies the evaluation of the involved loop integrals. With the definition of the common prefactor

$$\kappa_D = \frac{(2\pi Q)^{4-D}}{i\pi^2} \quad (2.4)$$

and the integrand

$$I_n = \prod_{i=1}^n (q^2 - m_i^2)^{-1} , \quad (2.5)$$

2. Scalar Matching Conditions at Next-to Leading Order

all necessary loop functions reduce to

$$\begin{aligned}
A_0(m_1^2) &= \kappa_D \int d^D q I_1 , \\
B_0(m_1^2, m_2^2) &= \kappa_D \int d^D q I_2 , \\
C_0(m_1^2, m_2^2, m_3^2) &= \kappa_D \int d^D q I_3 , \\
D_0(m_1^2, m_2^2, m_3^2, m_4^2) &= \kappa_D \int d^D q I_4 ,
\end{aligned} \tag{2.6}$$

where we have omitted all momenta in the arguments of the function definitions. As already mentioned, loops containing light and heavy fields are crucial for the decoupling. Our calculation assumes that all light fields have a negligible mass m_L as well as external momenta are small compared to the large matching scale $p^2, m_L^2 \equiv \epsilon_{match}^2 \rightarrow 0$. For instance, a $C_0(0, m^2, m^2)$ function appears in scalar triangle topologies and corresponds to one light and two heavy loop-field insertions.

Using $\epsilon_{match}^2 \rightarrow 0$ is an unphysical assumption when only light fields appear in non-local parts of the calculation, yielding apparent divergences

$$\begin{aligned}
\Delta_{p^2} &\equiv \lim_{\epsilon_{match}^2 \rightarrow 0} \log \frac{\epsilon_{match}^2}{Q_{match}^2}, \\
\Delta_D &\equiv \lim_{p^2, m_L^2 \rightarrow 0} \frac{1}{p^2 - m_L^2},
\end{aligned} \tag{2.7}$$

which are supposed to cancel in the matching condition (the D stands for "denominator" divergence, while the Δ_p^2 marks non-local p^2 dependent logarithmic divergences). In the following, the UV-finite parts of the loop integrals are given, whereas the divergent parts $\propto \Delta_{\overline{\text{MS}}}$ can be found in Ref. [66]. The tadpole integral A_0 [67] vanishes for a vanishing argument

$$A_0(m^2) = m^2 \left(1 - \log \frac{m^2}{Q_{match}^2} \right) , \tag{2.8}$$

$$A_0(0) = 0 , \tag{2.9}$$

where Q_{match} is the renormalization scale at which the matching takes place. Before proceeding with the analytical expressions for the B_0 integral, consider the two-point graph in Fig. 2.4 (a) with one heavy (double solid line) and one light (dashed line) propagator (the external fields are omitted as they do not play a role in this discussion). The naive picture of an EFT tells us that we can deform the graph in such a way that the heavy propagator shrinks to one point. The result of this operation, shown in Fig. 2.4 (c), corresponds to a loop with one light propagator. This graphical interpretation shows the interplay between the B_0 and the A_0 integral. Since the light loop is connected to the UV behaviour *not* entering the WILSON coefficient, there must be a second contribution denoted by the effective vertex in Fig. 2.4 (b) corresponding to the local (p^2 -independent) part of the two-point diagram. Thus, the separation of the different scales connects a loop function with integrand I_n to a loop function with integrand I_m with $m < n$.

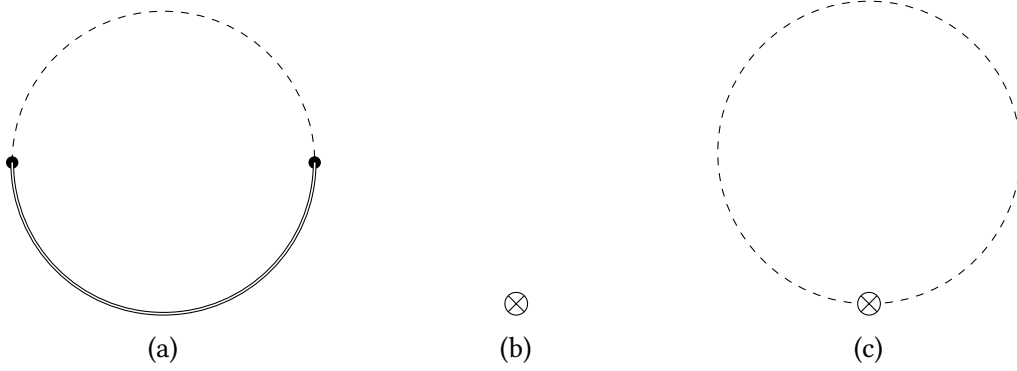


Figure 2.4.: The two-point function with a heavy and a light insertion (a) splits for vanishing external momenta into two pieces: (b) a local part $\propto A_0(m^2)$ and (c) a p^2 dependent part $\propto A_0(\epsilon_{match}^2) = 0$.

Furthermore, the deformation in Fig. 2.4 is obviously symmetric in the propagators. Thus, one can already guess the form of the B_0 with vanishing external momenta

$$B_0(m_1^2, m_2^2) = \frac{A_0(m_1^2) - A_0(m_2^2)}{m_1^2 - m_2^2}, \quad (2.10)$$

$$B_0(m^2, m^2) = -\log \frac{m^2}{Q_{match}^2} \xrightarrow{m^2 \rightarrow 0} -\Delta_{p^2}, \quad (2.11)$$

$$(2.12)$$

which is identical to the solution found in Ref. [68] by using partial differentiation and the method of partial fraction. The analytical correspondence to Fig. 2.4 is then

$$B_0(m^2, 0) = \underbrace{\frac{A_0(m^2)}{m^2}}_{p^2\text{-independent}} - \lim_{\epsilon_{match}^2 \rightarrow 0} \underbrace{\frac{A_0(\epsilon_{match}^2)}{m^2}}_{p^2\text{-dependent}}, \quad (2.13)$$

where in this case the p^2 -dependent part vanishes. This is not the case for all higher loop integrals as their p^2 dependent parts correspond to non-local contributions (i.e. light propagators connecting different points in momentum space).

In the same manner, the three-point function C_0 is connected to the two-point function, like the B_0 is connected to the A_0 for vanishing external momenta

$$C_0(m_1^2, m_2^2, m_3^2) = \frac{B_0(m_1^2, m_3^2) - B_0(m_2^2, m_3^2)}{m_1^2 - m_2^2}. \quad (2.14)$$

Inserting one heavy and two light fields, i.e. consider $C_0(m^2, 0, 0)$, shrinks the heavy propagator to a point connecting the three-point function to two-point integrals $B_0(0, 0)$ and $B_0(m_1, 0)$ as shown in fig Fig. 2.5. The local part in Fig. 2.5 (b) corresponds to the finite terms $\propto B_0(m^2, 0)/m^2$ in Eq. (2.14) while the two-point topology corresponds to the

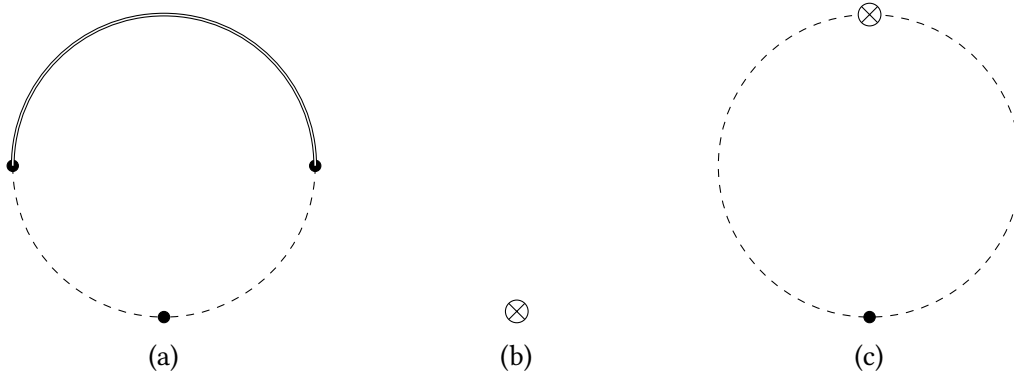


Figure 2.5.: The three point function with a heavy and two light insertion (a) splits for vanishing external momenta into two pieces: (b) a local part $\propto 1/m_{heavy}^2$ and (c) a non-local part proportional to Δ_{p^2} .

term $B_0(0, 0) \propto \Delta_{p^2}$. Thus we expect that non-local terms from triangle-diagrams like C4 (c.f. Fig. A.7 (a)) cancel in the matching condition against B_0 diagrams, like B4 (c.f. Fig. A.7 (d)), from within the EFT.

A different way of understanding that the non-local parts $\propto B_0(0, 0)$ cannot contribute is by taking the limit $\epsilon_{match} \rightarrow 0$ before performing the loop integration

$$B_0(0, 0) = \kappa_D \int d^D q \frac{1}{(q^2)^2} = 0, \quad (2.15)$$

which vanishes because it is a scale-less integral. However, this viewpoint makes it impossible to cross-check if the IR-divergent parts of two theories cancel in the matching condition. In addition, also 1PR diagrams involving light propagators $\propto \Delta_D$ must cancel in the matching condition. This happens in the most trivial way within a tree-level matching, where the scales are already separated and diagrams with light propagators directly cancel against their EFT counterparts.

The four-point function D_0 behaves very similar, except that there are many possibilities to connect it to the C_0 , B_0 and A_0 integrals by choosing different mass limits. The general case with four different masses is

$$D_0(m_1^2, m_2^2, m_3^2, m_4^2) = \frac{1}{m_1^2 - m_2^2} \left(C_0(m_1^2, m_3^2, m_4^2) - C_0(m_2^2, m_3^2, m_4^2) \right). \quad (2.16)$$

The expressions of the loop functions for arbitrary masses given in Eqs. (2.10), (2.14) and (2.16) are not suitable for the implementation into a computer program because of the apparent poles in certain mass limits (e.g. all masses being equal). The analytical limits of all possible mass combinations are given in Appendix A.2.

We have shown that, for $p^2 \rightarrow 0$, it is sufficient to solve only the A_0 integral analytically and from there on use the fact that physical scales get separated into local and non-local parts by re-writing scalar integrals of higher orders in terms of the lower-order ones (where the order denotes the integrand I_n). However, in the calculation of diagonal

WFR constants, also the derivatives of loop functions w.r.t to their external momentum appear. In the one-loop case, the derivatives of the A_0 and B_0 are sufficient. The A_0 does not depend on the external momentum and thus the derivative vanishes while the derivative of the B_0 [66] is given by

$$\partial_{p^2} A_0 = 0, \quad (2.17)$$

$$\begin{aligned} \partial B_0(m_1^2, m_2^2) &\equiv \kappa_D \partial_p^2 \int d^D q \left((q+p)^2 - m_2^2 \right)^{-1} \left(q^2 - m_1^2 \right)^{-1} \Big|_{p^2 \rightarrow 0} \\ &= \frac{1}{2(m_1^2 - m_2^2)^2} \left(m_1^2 + m_2^2 + \frac{2m_1^2 m_2^2 \log \frac{m_2^2}{m_1^2}}{m_1^2 - m_2^2} \right), \end{aligned} \quad (2.18)$$

Since we use FORMCALC for the generation of generic amplitudes, all tensor integrals are already decomposed into scalar integrals using the PASSARINO-VELTMAN (PaV) reduction algorithm [69].

2.3. A Toy-Model with Two Real Singlets

In this section the matching of a toy-model with two real singlet scalar fields to a usual ϕ^4 -theory with one light singlet is discussed. The purpose of this calculation is to demonstrate the cancellation of all IR contributions in the matching condition, which will be ignored in the automatized calculations (i.e. we set $\Delta_{p^2} = \Delta_D = 0$).

The most general renormalizable potential for two real singlets ϕ_1 and ϕ_2 reads

$$\begin{aligned} V_{\text{FULL}} &= \frac{1}{2} m_1^2 \phi_1^2 + \frac{\lambda_1}{4!} \phi_1^4 + \frac{1}{2} m_2^2 \phi_2^2 + \frac{\lambda_2}{4!} \phi_2^4 \\ &\quad + \frac{\lambda_{12}}{4} \phi_1^2 \phi_2^2 + \frac{\kappa_2}{3!} \phi_2^3 + \frac{\kappa_{112}}{2} \phi_1^2 \phi_2, \end{aligned} \quad (2.19)$$

with a large mass splitting $m_1 \ll m_2$ and ϕ_1 being charged under a \mathbb{Z}_2 symmetry $\phi_1 \rightarrow -\phi_1$. Our aim is to determine the parameters of the low-energy Lagrangian

$$V_{\text{EFT}} = \frac{1}{2} m_{\text{EFT}}^2 \phi^2 + \frac{\lambda_{\text{EFT}}}{4!} \phi^4 \quad (2.20)$$

in terms of the UV-parameters of V_{FULL} at the one-loop level. Further, we want to show that, using effective tree-level couplings in the EFT, all IR contributions appearing in the one-loop matching condition cancel.

2.3.1. Tree-Level Matching

The tree-level threshold corrections to λ_{EFT} are due to heavy ϕ_2 propagators in the T42 topology shown in Fig. 2.2c. For the quartic coupling we find

$$\lambda_{\text{EFT}}^{(0)} = \lambda_1 - \frac{3\kappa_{112}^2}{m_2^2}, \quad (2.21)$$

while the mass parameter can be identified with $m_{\text{EFT}}^{(0)} = m_1$. The FEYNMAN rules for the effective couplings will again be drawn by a crossed dot.

2.3.2. One-Loop Amplitudes

The \mathbb{Z}_2 symmetry of ϕ_1 protects the generation of a trilinear coupling κ_1^{EFT} to all orders in perturbation theory. The one-loop quartic coupling $\lambda_{\text{EFT}}^{(1)}$ receives corrections through box diagrams (D4), triangle diagrams (C41 and C42) and various B_0 diagrams (B41, B421, B422, SA4 and SB4). All other contributions are absent because of the \mathbb{Z}_2 symmetry. Furthermore, no additional wave function renormalization contributions to ϕ exist,

$$\phi = \phi_1 \left(1 - \frac{1}{2} \partial_{p^2} \prod_{1 \rightarrow 1} - \frac{1}{m_1^2 - m_2^2} \prod_{2 \rightarrow 1} \right) \Big|_{p^2 \rightarrow 0} = \phi_1, \quad (2.22)$$

where $\prod_{1 \rightarrow 1} = 0$ is the diagonal self-energy contribution. The off-diagonal contribution $\prod_{2 \rightarrow 1} = 0$ is also protected by the discrete symmetry to all orders. The reason for a vanishing diagonal WFR is the absence of a linear coupling $\phi_1^2 \phi_2$ which would get rise to the derivative of a B_4 topology. However, the only WFR diagrams that can be drawn have a tadpole integral on the external legs (A_4 topology) which has a vanishing derivative at the one-loop order.

The one-loop part of the $\phi_1 \phi_1 \rightarrow \phi_1 \phi_1$ amplitude in the full theory for $p^2, m_1^2 \rightarrow 0$ reads

$$\begin{aligned} -i(4\pi)^2 \mathcal{M}_{\text{FULL}}^{(1)} = & \frac{3}{2} \left[\lambda_1^2 B_0(0, 0) + \lambda_{12}^2 B_0(m_2^2, m_2^2) \right. \\ & + 4\kappa_{112}^2 \lambda_{12} C_0(m_2^2, m_2^2, 0) + 4\kappa_{112}^2 \lambda_1 C_0(m_2^2, 0, 0) \\ & \left. + 4\kappa_{112}^4 D_0(m_2^2, m_2^2, 0, 0) \right] \\ & - \frac{3}{m_2^2} \left[4\kappa_{112}^2 \lambda_{12} B_0(m_2^2, 0) + \kappa_2 \kappa_{112} \lambda_{12} B_0(m_2^2, m_2^2) \right. \\ & + 2\kappa_2 \kappa_{112}^3 C_0(m_2^2, m_2^2, 0) + 2\kappa_{112}^4 C_0(m_2^2, 0, 0) \\ & \left. + \kappa_{112}^2 \lambda_1 B_0(0, 0) \right] \\ & + \frac{3}{2m_2^4} \left[\kappa_{112}^2 \lambda_2 A_0(m_2^2) + \kappa_2^2 \kappa_{112}^2 B_0(m_2^2, m_2^2) \right. \\ & \left. + A_0(0) \kappa_{112}^2 \lambda_{12} + \kappa_{112}^4 B_0(0, 0) \right], \end{aligned} \quad (2.23)$$

where no analytical expressions or relations between the loop integrals have been used so far. The $B_0(0, 0)$ terms correspond to diagrams with light loops only, i.e. the diagrams (c)-(e) in Fig. 2.6. The C_0 and D_0 integrals with more than one light field, drawn in Fig. 2.6 (f)-(h), need to be separated into local and non-local terms

$$\begin{aligned}
 C_0(m_2^2, 0, 0) &= -\frac{B_0(m_2^2, 0)}{m_2^2} - \frac{B_0(0, 0)}{m_2^2}, \\
 D_0(m_2^2, m_2^2, 0, 0) &= -\frac{B_0(m_2^2, 0) + 1}{m_2^4} + \frac{B_0(0, 0)}{m_2^2}.
 \end{aligned} \tag{2.24}$$

Further separation is not needed as the non-local terms in $B_0(m_2^2, 0)|_{\text{non-local}} \propto A_0(0) = 0$ vanish. Using the relations in Eq. (2.24), all non-local IR contributions are reflected in the $B_0(0, 0) \propto \Delta_{p^2}$ terms. Thus, we can write the one-loop amplitude as

$$\mathcal{M}_{\text{FULL}}^{(1)} = \left[\mathcal{M}_{\text{FULL}}^{(1)} \right]_{\text{UV}} + \left[\mathcal{M}_{\text{FULL}}^{(1)} \right]_{\text{IR}}, \tag{2.25}$$

where the IR part includes all non-local Δ_{p^2} terms while the UV part contains the local terms including the finite pieces of Eq. (2.24). Simplifying the IR part yields

$$-i(4\pi)^2 \left[\mathcal{M}_{\text{FULL}}^{(1)} \right]_{\text{IR}} = \frac{3}{2} \left(\lambda_1^2 - \frac{3\kappa_{112}^2}{m_2^2} \right)^2 B_0(0, 0). \tag{2.26}$$

The $\phi\phi \rightarrow \phi\phi$ one-loop amplitude in the EFT is given by the diagram in Fig. 2.6 (b). Using the tree-level relation in Eq. (2.21) for the effective tree-level vertices shows that

$$\begin{aligned}
 -i(4\pi)^2 \mathcal{M}_{\text{EFT}}^{(1)} &= \frac{3}{2} \left(\lambda_{\text{EFT}}^{(0)} \right)^2 B_0(0, 0) \\
 &= \frac{3}{2} \left(\lambda_1 - \frac{3\kappa_{112}^2}{m_2^2} \right)^2 B_0(0, 0) \\
 &= -i(4\pi)^2 \left[\mathcal{M}_{\text{FULL}}^{(1)} \right]_{\text{IR}},
 \end{aligned} \tag{2.27}$$

i.e. the IR contributions of the full theory and the EFT are identical. Thus, we can impose the matching condition for the one-loop amplitude

$$\mathcal{M}_{\text{FULL}}|_{p^2 \rightarrow 0} \equiv \mathcal{M}_{\text{EFT}}|_{p^2 \rightarrow 0}, \tag{2.28}$$

where $\left[\mathcal{M}_{\text{FULL}}^{(1)} \right]_{\text{IR}}$ and $\left[\mathcal{M}_{\text{EFT}}^{(1)} \right]_{\text{IR}}$ cancel such that the effective one-loop coupling is given by the UV terms of the full model

$$\delta\lambda_{\text{EFT}}^{(1)} = -i \left[\mathcal{M}_{\text{FULL}}^{(1)} \right]_{\text{UV}}. \tag{2.29}$$

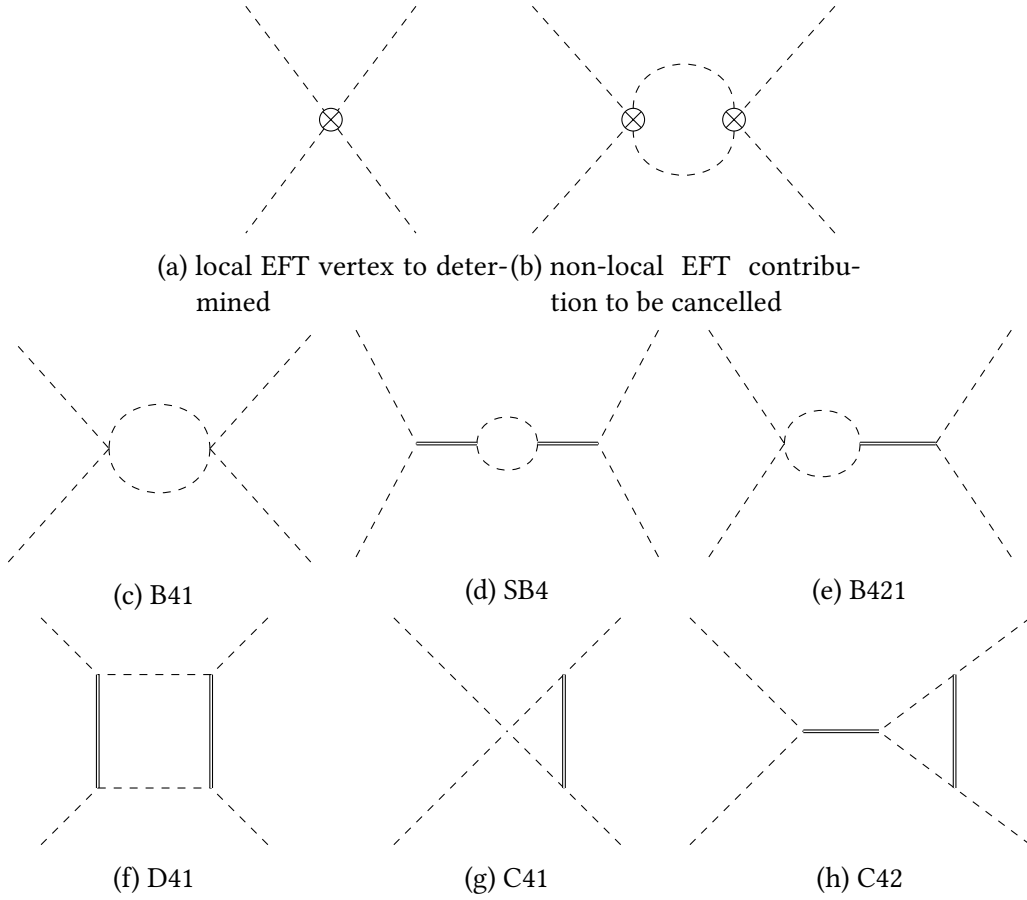


Figure 2.6.: All IR-divergent diagrams appearing in the matching condition. The first row are diagrams of the EFT amplitude. The second row contains diagrams in the full theory with light loops, only while the third row contains diagrams with mixed loops. Heavy fields are denoted by a double line. Crossed diagrams are not drawn but included in the calculation.

For completeness we give the final result of the one-loop matched quartic coupling

$$\begin{aligned}
 (4\pi)^2 \delta\lambda_{\text{EFT}}^{(1)} &= \frac{\kappa_{112}^2}{2m_2^2} (14\lambda_1 + 3\lambda_2 - 18\lambda_{12}) - \frac{\kappa_{112}^3}{m_2^4} (7\kappa_{112} - 2\kappa_2) \\
 &\quad - \frac{3\kappa_{112}}{2m_2^2} \left(\kappa_{112}^2 (5\lambda_1 + \lambda_2 - 8\lambda_{12}) - 2\kappa_2 \lambda_{12} \right) \log \frac{m_2^2}{Q_{\text{match}}^2} \\
 &\quad - \frac{3\kappa_{112}^2}{2m_2^2} \left(\kappa_2^2 - 8\kappa_{112}^2 \right) \log \frac{m_2^2}{Q_{\text{match}}^2} \\
 &\quad - \frac{3\lambda_{12}^2}{2} \log \frac{m_2^2}{Q_{\text{match}}^2}.
 \end{aligned} \tag{2.30}$$

2.3.2.1. Matching of the Mass Parameter

In addition, the mass parameter m_{EFT} has to be matched, since V_{FULL} is an ordinary scalar theory, without spontaneous symmetry breaking. The only non-local contribution is a diagram of the type A2 with a vanishing massless tadpole integral $A_0(0)$. Thus, we can express the mass parameter m_{EFT}^2 in terms of the full one-loop amplitude

$$\begin{aligned} (4\pi)^2 \delta m_{\text{EFT}}^{2(1)} &= \frac{\lambda_1}{2} A_0(0) + \frac{\lambda_{12}}{2} A_0(m_2^2) + \kappa_{112}^2 B_0(m_2^2, 0) \\ &= \frac{1}{2} \left(\lambda_{12} m_2^2 + 2\kappa_{112}^2 \right) \left(1 - \log \frac{m_2^2}{Q_{\text{match}}^2} \right). \end{aligned} \quad (2.31)$$

2.4. Implementation in SARAH/SPHENO

This section describes the implementation of the technical aspects from the previous sections in the spectrum generator SARAH.

The flow of information, when the matching routines are called, is drawn in Fig. 2.7. The generation of topologies, generic diagrams and generic amplitudes is done with FEYNARTS and FORMCALC using the generic model file `LORENTZ.gen` which does not contain any model dependent information but only all possible LORENTZ structures and renormalizable couplings. The topologies as well as generic amplitudes and their $\overline{\text{MS}} - \overline{\text{DR}}$ conversion factors are extracted in a SARAH readable format and saved into SARAH's source code. This procedure is shown in the yellow box in Fig. 2.7 and has already been performed such that there is no direct dependence on FEYNARTS/FORMCALC during the program call.

Before performing a matching, two SARAH model files for the UV and EFT model need to be chosen. Also the correspondence between an amplitude in the UV model and an effective coupling in the EFT model must be provided as input. After the UV model has been initialized, this information is given as a *boundary condition* for the EFT model at the matching scale and is used to compute the (correctly normalized) amplitudes in the UV model. Furthermore, various assumptions and parametrisations can be defined (i.e. replacements of $\overline{\text{DR}}$ parameters through $\overline{\text{MS}}$ definitions or which VEVs shall be neglected at the matching scale). When initializing the matching routines, this information is used to diagonalize the mass spectrum analytically. If the automatic mass diagonalization fails, one can use the numerical FORTRAN routines which are not part of this thesis.

After the matching routines were successfully initialized, all possible field insertions for the generic topologies are generated, couplings and masses are determined and inserted into the generic amplitudes provided by FORMCALC. The modified loop functions (without IR parts) from Appendix A.2 are inserted after the summation over all generation and group indices has been performed. If the tree-level contribution contains gauge couplings, Eq. (1.69) is used to calculate one-loop contributions to the coupling originating from gauge coupling thresholds.

Finally, an analytical expression is given which can optionally be incorporated into the SPHENO output of the EFT model. The generated FORTRAN code operates as described in Fig. 1.7 where the pole-mass matching is replaced with the analytical expressions of the

effective couplings.

A comprehensive manual of SARAH's matching interface is provided in Appendix A.3.

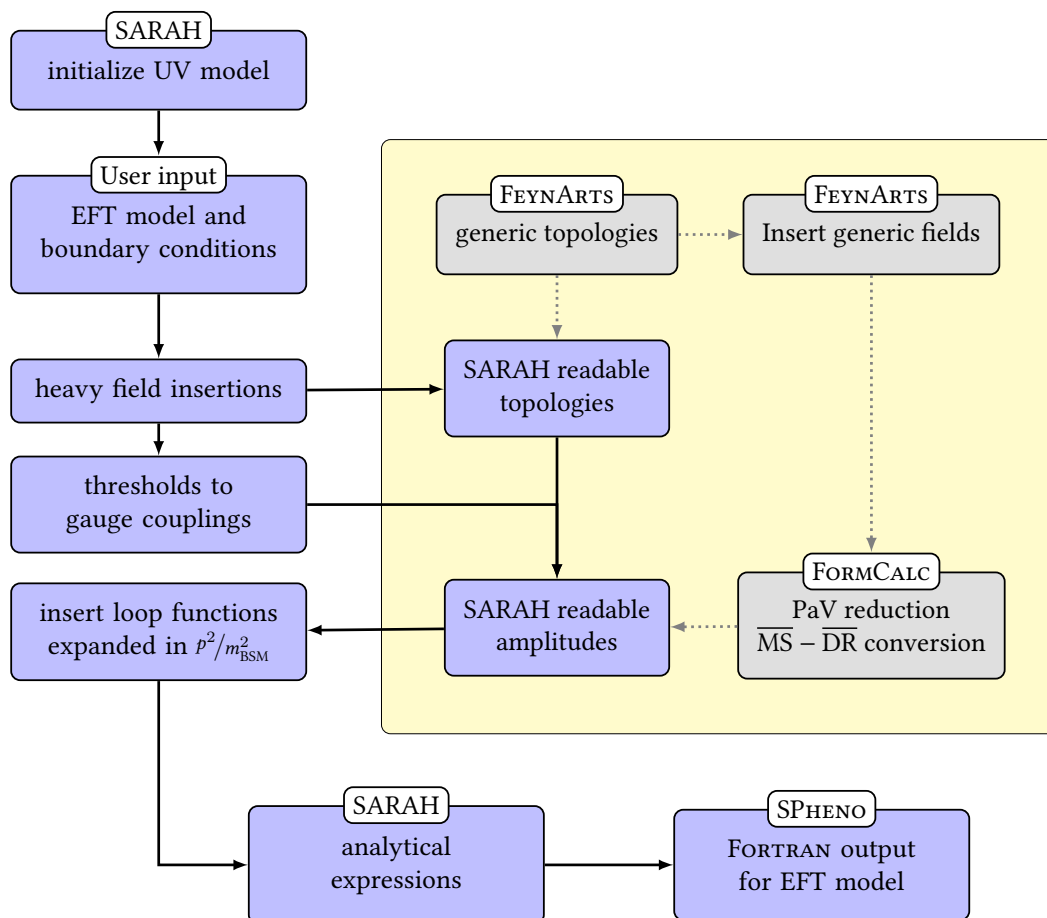


Figure 2.7.: Flow of information when invoking the matching interface from a UV-model. The operations with the grey dotted arrows were done once and do not need to be repeated with the downloadable version of SARAH. All black straight arrows carry model-dependent informations.

3. Validation: High-Scale Supersymmetry

The following chapters apply the new SARAH/SPHENO implementation of EFT Higgs boson mass determinations on two different kinds of EFT models. The first one includes *high-scale SUSY* scenarios where all SUSY partners are integrated out at the matching scale, leading either to an effective SM or an effective 2HDM, depending on the mass hierarchy in the Higgs boson sector. The second scenario is *split SUSY*, which additionally includes all fermionic super partners in the EFT while only the scalar fields are integrated out. The complexity of the EFT Lagrangian will increase with each of the following chapters. The numerical scans in all chapters are using an one-loop matching, one-loop RGE running and one-loop mass calculations at the electroweak scale.

3.1. High-Scale MSSM: an Overview

The MSSM is one of the most precisely studied BSM theories for SUSY scales not too far away from the electroweak scale. Thus, it is natural to begin a high-scale BSM scenario by applying the new implementation on the MSSM. This has successfully been done in the literature [6, 9, 35, 59, 70]. The tree-level matching of the quartic coupling,

$$\lambda_{\text{EFT}}(m_{\text{SUSY}}) = \frac{1}{4} (g_1^2 + g_2^2) \cos^2 2\beta, \quad (3.1)$$

shows, that only two MSSM parameters have an influence on the effective tree-level Higgs boson mass $m_h^{\text{EFT}} \approx \lambda_{\text{EFT}}(m_Z) v^2$. These are the mixing angle β and m_{SUSY} , which enters through the running of λ_{EFT} from m_Z to m_{SUSY} using SM RGEs. In particular, β is not an input parameter of the SM but completely determined at the UV scale. Thus, the choice of the renormalization scheme for β is ambiguous, as one can always compensate finite counter terms $\delta\beta$ by choosing an appropriate input value of β at the matching scale. We adopt the renormalization scheme of Ref. [9] and choose the finite part of the mixing angle counter term to cancel the off-diagonal external leg contributions to the SM-like Higgs boson at vanishing external momenta

$$\delta\beta^{\text{finite}} = -\frac{1}{m_A^2} \prod_{A \rightarrow h} (0), \quad (3.2)$$

where A denotes the heavy Higgs boson doublet with degenerate components in the $v \rightarrow 0$ limit as shown in Eq. (1.49). This choice is not only motivated by the significant simplification of the higher-order threshold corrections to the quartic coupling, but also because the definition of $\tan\beta$ through the VEV ratio becomes ill defined at the matching scale where $v_u, v_d \approx 0$ is assumed [70]. However, the choice of Eq. (3.2) introduces a scale

dependence on β above the matching scale, which enters higher-order calculations in the full theory. With the new extension of SARAH, it is in principle also possible to choose a scale-independent (i.e. $\overline{\text{MS}}$) scheme for β and optionally include the off-diagonal WFR contributions into the threshold corrections. For the comparison with the literature we do not take this possibility into account.

The one-loop corrections to Eq. (3.1) are listed in Ref. [9] in all detail for non-degenerate SUSY particles. Thus, we refrain from listing them here again but only mention that the new SARAH version is able to reproduce their analytical results with the input file `MSSM/Matching_HighScaleSUSY.m` provided with the new release.

The precise experimental and theoretical value of m_h reduces the analysis of the BSM sector to a two-dimensional problem in the (m_{SUSY}, β) -space at tree level, while at the one-loop order all soft parameters discussed in Section 1.3 enter the threshold corrections through heavy particles in the loops. Gluinos are the only exception which start to contribute at the two-loop order. The leading one-loop contributions are due to heavy stops and scale with powers of the stop mixing parameter

$$\hat{X}_t \equiv \frac{X_t}{\sqrt{m_{q_3} m_{u_3}}}, \quad X_t \equiv A_t - \mu \tan^{-1} \beta \quad (3.3)$$

and are maximal for $\hat{X}_t = \sqrt{6}$. By choosing a degenerate spectrum of heavy masses i.e. $m_A = \mu = m_{q_i} = m_{u_i} = m_{e_i} = m_{l_i} = m_{SUSY}$, the parameter A_t can be fixed for a maximal/minimal stop contribution reducing the parameter space again down to two dimensions. It was shown in Ref. [9], that a high-scale MSSM can reproduce the measured value of m_h within the range of $10^4 \text{ GeV} \lesssim m_{SUSY} \lesssim 10^{10} \text{ GeV}$, which is in contrast to the findings in Ref. [70] where the authors assumed very large non-degeneracies between the SUSY fields to amplify the threshold corrections. However, large mass hierarchies within the SUSY spectrum again raise the uncertainties of the Higgs boson mass predictions which was not considered in Ref. [70]. Thus, concerning the MSSM, soft-SUSY-breaking coinciding with the GUT scale is ruled out in the more precise scenario of degenerate masses. Using the SARAH input file `MSSM/SimpleHighScaleSUSY.m`, contained in the new version, the matching routines perform the MSSM \rightarrow SM matching assuming a degenerate mass spectrum. The numerical results of a scan in the $(m_{SUSY} - \tan \beta)$ -space are shown in Fig. 3.1. The red area marks points with $m_h = 125 \pm 4 \text{ GeV}$ and is always below the upper limit of 10^{10} GeV found in Ref. [9] for a non-degenerate mass spectrum. The blue and green bands mark the $\pm 2 \text{ GeV}$ and $\pm 1 \text{ GeV}$ regions. In Fig. 3.1 it is also shown that for $\tan \beta > 5$, high-scale SUSY above 10^5 GeV is not possible in the MSSM.

Because of the running of the SM quartic coupling [71], rather small or even negative values for $\lambda_{SM}^{\text{EFT}}(m_{SUSY})$ are needed for large matching scales in order reproduce the correct Higgs boson mass. Since g_1 and g_2 grow with the running from the SM to the matching scale while $\lambda_{SM}^{\text{EFT}}$ grows with the running from the matching scale to the SM scale, the correct matching scale which reproduces the observed Higgs boson mass rapidly drops with increasing t_β as the D-terms always have a positive contribution. This picture dramatically changes as one proceeds with the high-scale NMSSM, which is discussed in the next

section.

Since we always combine the one-loop matching with a one-loop RGE running, our upper bound on m_{SUSY} with a degenerate spectrum accidentally coincides with the upper bound of Ref. [9] which used a non-degenerate spectrum (larger stop contributions) but a three-loop RGE running which shifts the running of λ_{SM}^{EFT} towards negative values (larger matching scale). Thus, in the MSSM, the N³LO RGE-running seems to accidentally compensate larger threshold corrections due to non-degenerate scenarios.

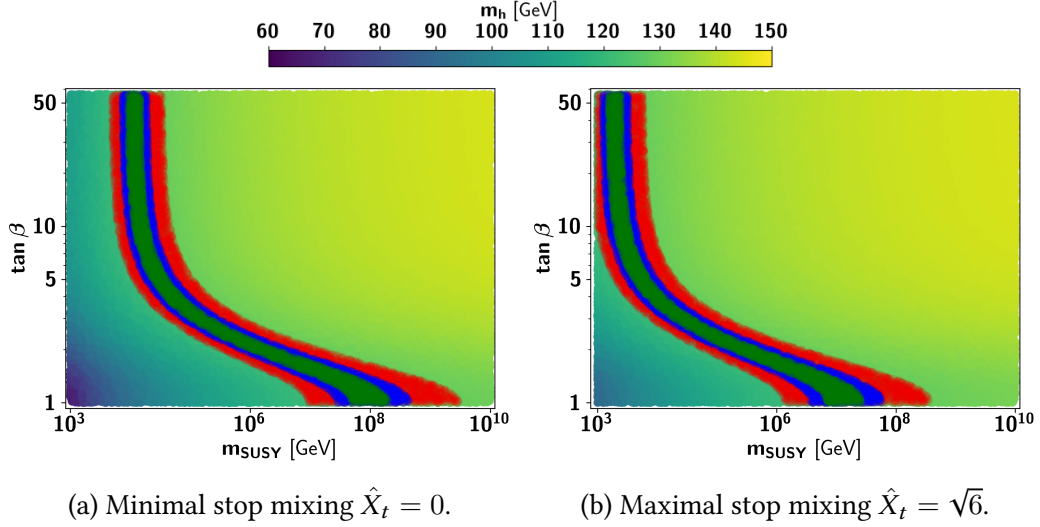


Figure 3.1.: The Higgs boson mass prediction m_h as a function of $\tan \beta$ and m_{SUSY} in the degenerate high-scale MSSM for minimal (a) and maximal (b) stop mixing. The red/blue/green bands are points with $m_h = 125 \pm 4/2/1$ GeV.

3.2. Non-Minimal SUSY: Matching the NMSSM to the SM

In this section, the \mathbb{Z}_3 symmetric NMSSM, described in Section 1.4, is matched to the SM by computing the one-loop threshold corrections to the quartic coupling of the SM-like Higgs boson. The *singlet decoupling parametrization* is introduced, which connects the NMSSM to the MSSM and allows to take the continuous limit from the NMSSM to the MSSM. The limit is taken within a 3 dimensional parameter scan, showing the new features introduced by the singlet extension. Furthermore, comparisons between leading order and next-to-leading order threshold corrections and their impact on the Higgs boson mass predictions are made.

In contrast to the MSSM, the NMSSM explicitly connects the μ -parameter to the soft-SUSY-breaking scale, c.f. Section 1.4.2.1. Thus, if the soft singlet mass m_S and the soft sfermion masses are generated in the hidden sector by the same mechanism at m_{SUSY} , the NMSSM is a valid candidate for a high scale SUSY scenario. In this case not only heavy sfermions, a heavy Higgs boson doublet and heavy electroweakinos enter the threshold

corrections of the quartic SM Higgs boson self-coupling, but also a heavy singlet and a heavy singlino.

3.2.1. Tree-Level Mass Spectrum at the Matching Scale

Before the threshold corrections are studied, the mass spectrum at the matching scale m_{SUSY} is calculated. Since every field which is not part of the SM Lagrangian is integrated out, we chose all dimensionful parameters of the NMSSM to be of the order of the matching scale $T_\kappa, T_\lambda, v_s \approx \mathcal{O}(m_{SUSY})$. With the assumption of a vanishing SM VEV $v \ll m_{SUSY}$, all SM fields are treated as massless at the matching scale.

3.2.1.1. Heavy Higgs Bosons

Using $v \rightarrow 0$ in the Higgs boson mass matrices Eq. (1.62) yields block diagonal matrices where all mixing components with the singlet vanish. The upper left 2x2 matrices (i.e. the H_u, H_d components) are diagonalized by $\tan \beta$ which rotates H_u and H_d into a basis of one heavy (A) and one light (H) Higgs doublet

$$\begin{pmatrix} H \\ A \end{pmatrix} = \begin{pmatrix} c_\beta & s_\beta \\ -s_\beta & c_\beta \end{pmatrix} \begin{pmatrix} -\epsilon H_d^* \\ H_u \end{pmatrix}, \quad (3.4)$$

while the singlet is already in the mass basis. The non-zero eigenvalues of the CP-even Higgs boson mass matrix read

$$m_A^2 = \frac{1 + t_\beta^2}{2t_\beta^2} v_s \left(v_s \kappa \lambda + \sqrt{2} T_\lambda \right) = \frac{1 + t_\beta^2}{t_\beta} B_\mu^{\text{eff}}, \quad (3.5)$$

$$m_S^2 = 2v_s^2 \kappa^2 + \frac{v_s T_\kappa}{2}, \quad (3.6)$$

where the definition of the effective soft bilinear parameter from Eq. (1.59) was used. Similarly, the CP-odd Higgs boson mass matrix has two non-zero eigenvalues. As already mentioned in Section 1.3.4, the state associated with the doublets is degenerate with the CP-even and the charged Higgs boson mass m_A^2 .

The mass of the CP-odd state associated with the complex singlet can be read off from the mass matrix with vanishing SM VEV,

$$m_{A_s}^2 = -\frac{3v_s T_\kappa}{\sqrt{2}}. \quad (3.7)$$

In the following we choose $v_s > 0$ and $T_\kappa < 0$ to ensure a positive squared mass parameter of the CP-odd state. From the CP-even singlet mass it then follows that $0 > T_\kappa > -4v_s \kappa$.

3.2.1.2. Neutralinos and Charginos

The chargino mass matrix is diagonal in the limit $v \rightarrow 0$ so that the tree-level mass and interaction eigenstates coincide and the rotation matrices are just the unit matrix,

$$\mathbf{m}_{\chi^\pm} = \text{diag} \left(M_2, \frac{v_s \lambda}{\sqrt{2}} \right), \quad (3.8)$$

whereas the neutralino mass matrix in Eq. (1.64) still has two off-diagonal elements originating from the $\mu_{\text{eff}} H_u \cdot H_d$ -term. The rotation into the mass basis is performed by a unitary transformation \tilde{U} for the higgsino fields

$$N = \begin{pmatrix} \mathbb{1}_{2 \times 2} & & \\ & \tilde{U} & \\ & & 1 \end{pmatrix}, \quad \tilde{U} = \begin{pmatrix} \frac{i}{\sqrt{2}} & \frac{i}{\sqrt{2}} \\ -\frac{1}{\sqrt{2}} & \frac{1}{\sqrt{2}} \end{pmatrix}, \quad (3.9)$$

while all other fields are already mass eigenstates. The neutralino masses are then given by

$$\mathbf{m}\chi^0 = \text{diag} \left(M_1, M_2, \frac{v_s \lambda}{\sqrt{2}}, \frac{v_s \lambda}{\sqrt{2}}, \sqrt{2} v_s \kappa \right). \quad (3.10)$$

In order to decouple all neutralinos, we also require $M_1, M_2 \approx \mathcal{O}(m_{SUSY})$.

3.2.2. Matching to the SM

With the masses and mixing matrices at hand, the quartic coupling of the lightest Higgs boson is calculated at the one-loop order

$$\begin{aligned} \lambda_{\text{SM}}^{\text{EFT}} &= \lambda_{\text{NMSSM}} \Big|_{v^2, p^2 \ll m_{SUSY}^2} \\ &= \underbrace{\frac{1}{4} (g_1^2 + g_2^2) \cos^2 2\beta}_{\text{MSSM D-terms}} \\ &\quad + \underbrace{\frac{\lambda}{2} \sin^2 2\beta}_{\text{singlet F-terms}} \\ &\quad - \underbrace{\frac{3 \left(\sin 2\beta \left(\sqrt{2} T_\lambda + 2\kappa \lambda v_s \right) - 2\lambda^2 v_s \right)^2}{8 m_s^2}}_{\text{singlet s/t/u-channel exchange}} \\ &\quad + \delta\lambda_{\text{EFT}}^{(1)}, \end{aligned} \quad (3.11)$$

where the first line are D-terms as in the MSSM, the second line are singlet F-terms and the third line is generated by tree-level diagrams involving an internal singlet which is integrated out (i.e. a T42 topology). The one-loop contributions to the quartic coupling in the fourth line are rather lengthy but can easily be reproduced with SARAH using the input file `NMSSM/SimpleHighScaleSUSY.m` for the matching routines included in the new release. The leading stop contributions of order $\mathcal{O}(Y_t^4)$ to $\delta\lambda_{\text{EFT}}^{(1)}$ are comparable to the MSSM. Using the effective μ -parameter $\mu_{\text{eff}} = \lambda v_s / \sqrt{2}$, given in Eq. (1.59), we define the effective stop mixing parameter $X_t^{\text{eff}} = A_t - \mu_{\text{eff}} t_\beta^{-1}$. The leading one-loop contributions from stops degenerate in mass m_{stop} are

$$\delta\lambda_{\text{EFT}}^{(1)} \supset -\frac{Y_t^4}{32\pi^2} \hat{X}_t^{\text{eff}, 2} \left(\hat{X}_t^{\text{eff}, 2} - 12 \right) - \frac{3Y_t^4}{8\pi^2} \log \frac{Q_{\text{match}}^2}{m_{\text{stop}}^2}, \quad (3.12)$$

which are maximized for $\hat{X}_t^{\text{eff}} = \pm\sqrt{6}$ ("maximal stop mixing") and minimized for $\hat{X}_t^{\text{eff}} = 0$ ("minimal stop mixing").

3.2.3. The Singlet Decoupling Parametrisation

The following section studies the impact of the singlet extension onto the Higgs boson mass prediction in the high-scale scenario. Although the NMSSM introduces two new superpotential parameters κ, λ and three dimensionful parameters v_s, T_λ and T_κ (m_S^2 can be traded for the other three by using the tadpole equation Eq. (1.60)), the high scale scenario can again be reduced to a problem with only a few dimensions. The physical reason for this is that the high-scale scenario requires all non-SM states to live at the scale $\propto m_{SUSY}$ constraining most of the parameters to be within certain regions. The assumption, that no further hierarchies are present between the non-SM fields, can be realized by using a parametrization that connects all soft and dimensionless parameters with only one dimensionless parameter and m_{SUSY} . The mass hierarchy is then controlled by these two parameters only. We introduce one possible parametrization and compare the effects of the full NLO corrections with partial corrections that are already available in the literature.

Being independent of the singlet sector we always use a degenerate sfermion and gaugino spectrum $m_{sfermions} = M_1 = M_2 = m_{SUSY}$.

The NMSSM introduction in Section 1.4 pointed out, that the NMSSM reproduces all MSSM couplings when relating the singlet VEV and λ with the MSSM μ parameter as well as defining an effective bilinear term B_μ^{eff} . Taking these relations as input, the NMSSM can be divided into an MSSM-like sector with effective parameters and a singlet sector. Thus, the limit $\lambda, \kappa, T_\lambda, T_\kappa \rightarrow 0$, does not influence the MSSM sector, while it turns off all couplings that concern the singlet and thus recovers the MSSM with effective μ and B_μ -terms. Because the singlet can effectively be decoupled from all interactions, we call this the *decoupling parametrization* (not to be confused with the meaning of the decoupling theorem).

In addition, demanding a degenerate mass spectrum at m_{SUSY} yields the conditions

$$\begin{aligned} v_s &= \frac{\sqrt{2} \mu_{\text{eff}}}{\lambda} = \frac{\sqrt{2} m_{SUSY}}{\lambda}, \\ B_{\mu_{\text{eff}}} &= \frac{v_s}{2} \left(v_s \kappa \lambda + \sqrt{2} T_\lambda \right) \\ &= \frac{t_\beta}{1 + t_\beta^2} m_A^2 = \frac{t_\beta}{1 + t_\beta^2} m_{SUSY}, \end{aligned} \tag{3.13}$$

which need to be fulfilled to ensure that the neutralinos and the heavy doublet have a mass of m_{SUSY} . Similarly the conditions

$$\begin{aligned} T_\lambda &= \frac{m_{SUSY}}{2} \lambda (\sin 2\beta - 1), \\ \kappa &= \frac{\lambda}{2}, \\ T_\kappa &= -\frac{\lambda}{3} m_{SUSY}, \end{aligned} \quad (3.14)$$

lead to a singlino mass $m_{\tilde{s}} = m_{SUSY}$ and singlet masses $m_{A_s} = m_{SUSY}$ and $m_s = \sqrt{3/2} m_{SUSY}$. In fact, it is not possible to have all masses degenerate within this parametrization.

3.2.4. Numerical Analysis

Using the decoupling parametrization and the requirement of degenerate masses, only λ , $\tan \beta$ and m_{SUSY} are not fixed (while A_t is chosen to maximize/minimize the MSSM-like stop contributions). Thus, taking the limit $\lambda \rightarrow 0$ is enough to recover a high-scale MSSM scenario as it can be seen in Fig. 3.2 which compares the N/MSSM Higgs boson mass predictions as a function of the matching scale for various values of λ at $t_\beta = 4$. The figure also shows that at fixed t_β , the NMSSM matching scale which reproduces the measured Higgs boson mass can be many orders of magnitude larger than in the MSSM.

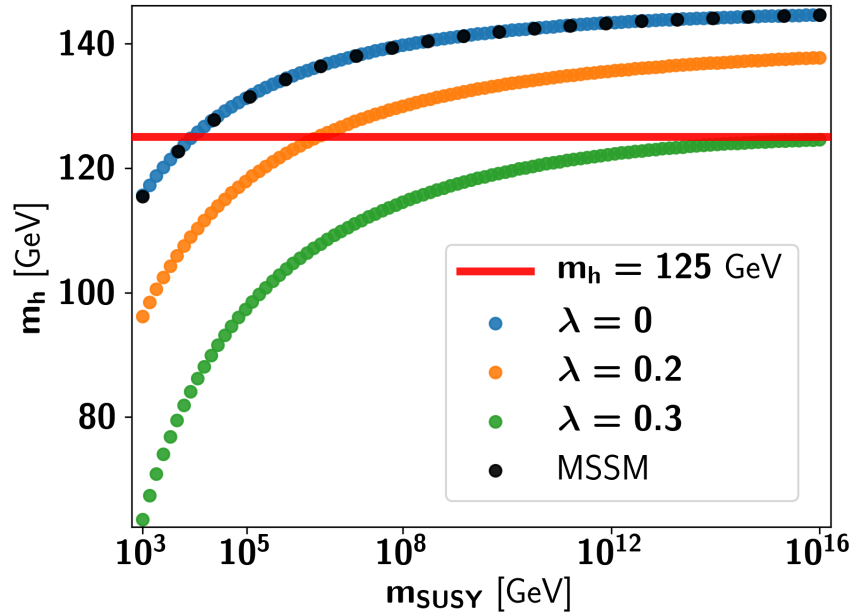


Figure 3.2.: Prediction of the effective SM Higgs boson mass as a function of the matching scale in the MSSM and the NMSSM for $\lambda = \{0, 0.2, 0.3\}$ and $\tan \beta = 4$ using the decoupling parametrization defined in Eqs. (3.13) and (3.14).

Using the effective parameters from Eq. (3.13) in the tree-level matching condition shows

that the singlet s/t/u-channel contributions to (3.11) are only λ^2 dependent because all quartic terms are proportional to $v_s^2 \lambda^4 \propto \mu_{\text{eff}}^2 \lambda^2$. The MSSM-like D-terms vanish for $t_\beta = 1$, such that the effective SM quartic becomes negative

$$\lambda_{\text{SM}}^{\text{EFT}}(t_\beta = 1) \approx -\frac{\lambda^2}{4}, \quad (3.15)$$

enabling the possibility of GUT-scale soft-SUSY breaking. For larger t_β , the D-terms become important while the singlet F-terms are suppressed and the value of $\lambda_{\text{SM}}^{\text{EFT}}$ at the matching scale again strongly depends on the values of the gauge couplings at the matching scale

$$\lambda_{\text{SM}}^{\text{EFT}}(t_\beta \rightarrow \infty) \approx \frac{1}{4} (g_1^2 + g_2^2) - 3\lambda^2(1 - t_\beta^{-1}) + \mathcal{O}(t_\beta^{-2}). \quad (3.16)$$

Thus, for low values of t_β , the correct matching scale should be rather high as the (negative) NMSSM contributions are dominant while large values of t_β look more MSSM-like i.e. small values of λ are required.

We performed numerical scans in the $(\lambda, \tan \beta, m_{\text{SUSY}})$ -space and chose A_t to minimize or maximize the leading NLO stop contributions while requiring a Higgs boson mass of $m_h = 125 \pm 2 \text{ GeV}$. The results are shown in contour plots in Figs. 3.3a and 3.3b. The qualitative correlations are as described above. The dark blue area, corresponding to the MSSM limit $\lambda \rightarrow 0$, has the same shape as the pure MSSM prediction in Fig. 3.1. However, for $\lambda > 0$, all possible values of $\tan \beta$ and $m_{\text{SUSY}} > m_{\text{SUSY}}^{\text{MSSM}}$ are allowed by the Higgs boson mass constraint. Another remarkable result is, that λ cannot be larger than ≈ 0.65 below the GUT scale.

Higher-order matching conditions for the MSSM to an effective SM have been well known for a long time. Thus, it is straightforward to partially compute NMSSM matching conditions by using the following recipe:

1. Take the general expressions of the one-loop threshold corrections for $\lambda_{\text{SM}}^{\text{EFT}}$ computed in the MSSM,
2. make use of the NMSSM decoupling parametrization in Eq. (3.13) i.e. write $\mu = \mu_{\text{eff}}(v_s, \lambda)$ and $B_\mu = B_\mu^{\text{eff}}(\lambda, \kappa, v_s, T_\kappa)$,
3. add the tree-level contributions from the NMSSM given in Eq. (3.11).

Using this method, partially NMSSM higher-order corrections are computed in Ref. [10]. However, contributions from the heavy singlet at NLO are missing. For instance B4 topologies, which involve a heavy singlet loop and two $hhSS$ -couplings or D4 (box) topologies involving singlinos and higgsinos shown in Fig. 3.4, are not accounted for. Since the full NMSSM^{NLO} results are now available, we can compare them against an MSSM^{NLO} calculation where the singlet tree-level contributions have been added. In the following, the approximate calculation is called *mMSSM* approach for *modified MSSM*. The difference $m_h^{\text{NMSSM}} - m_h^{\text{mMSSM}}$ in the Higgs boson mass prediction between the two approaches is shown in Figs. 3.3c and 3.3d. In particular, the difference is maximized for large values of λ , i.e. matchings near the GUT scale. This is due to the special choice of parametrization, as all

other singlet-couplings and soft-breaking parameters scale with λ (see Eqs. (3.13) and (3.14)). Depending on the choice of minimal/maximal stop mixing, the difference between the two approaches can be up to 2 GeV. The maximum difference Δm between the NMSSM and the mMSSM prediction also scales with the stop contributions since $\Delta m^{A_i^{min}} < \Delta m^{A_i^{max}}$. This is consistent with the findings from the NMSSM scans in Figs. 3.3a and 3.3b, that maximal stop mixing allows for larger values of λ and thus also leads to larger deviations from the mMSSM calculation.

In summary, the mMSSM approach, to re-use known MSSM threshold corrections in the NMSSM with a decoupling parametrization, is a good estimate of higher-order corrections which introduces a new systematic uncertainty of a few hundred MeV for $m_{SUSY} < 10^8$ GeV and minimal stop mixing. However, in GUT scale SUSY breaking scenarios, which were one motivation for introducing the high-scale NMSSM, this uncertainty can be up to 2 GeV for $\tan \beta < 5$. If maximal stop mixing is considered, the additional Higgs boson mass uncertainty is at least ≈ 1 GeV for $\lambda > 0.3$ and any value of $\tan \beta$.

3.3. High-Scale MSSM with Low m_A : Matching to a 2HDM

The high-scale NMSSM is an interesting framework which shows that non-minimal SUSY without naturalness could be realized even at the GUT scale. Using the decoupling parametrisation it also yields the possibility to verify the new implementation of the SARAH matching routines by comparing numerical results with the well-known MSSM results in the MSSM-limit $\lambda \rightarrow 0$, as we did in the previous section. However, this does not test the correct operation of the routines on extended Higgs sectors, since the high-scale NMSSM only leaves the SM Higgs boson in the EFT. For the purpose of validating the new implementation, a matching of the MSSM to a 2HDM is performed as the NLO threshold corrections have been well known for a long time [8, 61, 72, 73] and give another possibility to compare the automatically generated results of SARAH against the literature.

From a phenomenological point of view, the matching to a 2HDM is interesting because it gives hints about how a general 2HDM can experimentally be distinguished from an MSSM-like 2HDM, even if only the MSSM Higgs boson sector is measured while all other MSSM fields are out of experimental reach. This idea is also supplemented in the *hMSSM* approach [74], where the Higgs sector is only described by $m_A < 500$ GeV and $\tan \beta$ while the size of radiative corrections is determined by $m_h \approx 125$ GeV, which is considered as an input. However, the *hMSSM* does not involve a proper matching of the scalar sectors but only solves the fixed-order NLO result for a 125 GeV Higgs boson mass with the result of $m_{SUSY} \gtrsim 1$ TeV for small values of $\tan \beta$. Unfortunately, the (one-loop) fixed order result is already starting to become untrustworthy in this mass range because large logarithms are not accounted for. Thus, the *hMSSM* is well suited for moderate values of $m_{SUSY} \lesssim 1$ TeV i.e. larger values of $\tan \beta$. Consequently, Ref. [8] found deviations between the *hMSSM* and the EFT prediction in the heavy Higgs boson mass which can be 10 GeV large for small values of $\tan \beta < 5$. In this region, large values of m_{SUSY} are required by the input of the light SM Higgs boson mass.

Another example, which shows that the EFT matching has to be done properly by considering all mass hierarchies, is given by the recent developments in the computer program FEYNHIGGS [75] which previously was not able to compute the light Higgs boson mass in the effective 2HDM. Including the effects of an intermediate effective 2HDM, the authors of Ref. [75] found differences of $\mathcal{O}(10 \text{ GeV})$ in the Higgs boson mass prediction compared to previous versions of FEYNHIGGS.

However, the focus of this section is on the validation of the analytical results rather than a phenomenological study. Thus, we will only introduce all technical informations necessary for the matching procedure.

3.3.1. The Low-Energy Lagrangian

The most general renormalizable CP-conserving scalar potential for two Higgs boson doublets H_1 and H_2 [76, 77] reads,

$$\begin{aligned}
 V_{2\text{HDM}} = & m_1^2 |H_1|^2 + \lambda_1 |H_1|^4 + m_2^2 |H_2|^2 + \lambda_2 |H_2|^4 \\
 & + \lambda_3 |H_1|^2 |H_2|^2 + \lambda_4 \left| H_2^\dagger H_1 \right|^2 \\
 & + \left[m_{12}^2 H_1^\dagger H_2 + \frac{1}{2} \lambda_5 \left(H_2^\dagger H_1 \right)^2 \right. \\
 & \left. + \left(\lambda_6 |H_1|^2 + \lambda_7 |H_2|^2 \right) \left(H_1^\dagger H_2 \right) + \text{h.c.} \right],
 \end{aligned} \tag{3.17}$$

where both doublets have hypercharge +1. In order to make a connection to the MSSM Higgs sector, we identify the doublets of the general 2HDM with those of the MSSM by flipping the hypercharge and iso-spin of H_d

$$\begin{aligned}
 H_1 & \rightarrow -\epsilon H_d^*, \\
 H_2 & \rightarrow H_u.
 \end{aligned} \tag{3.18}$$

However, this choice is not unique as there is no preferred basis of Higgs doublets in a general 2HDM, i.e. one could also interchange H_1 and H_2 in Eq. (3.18) (or take any linear combination of both). With the choice made in Eq. (3.18), one can simultaneously apply a rotation into the mass basis on (H_1, H_2) and $(H_u, -\epsilon H_d^*)$ so that the tree-level mixing angle $\tan \beta$ of the MSSM coincides with the EFT.

Replacing the general 2HDM fields with their MSSM counter parts yields the potential

$$\begin{aligned}
 V_{2\text{HDM}} = & m_1^2 H_d^\dagger H_d + \lambda_1 \left| H_d^\dagger H_d \right|^2 + m_2^2 H_u^\dagger H_u + \lambda_2 \left| H_u^\dagger H_u \right|^2 \\
 & + \lambda_3 |H_d|^2 |H_u|^2 - \lambda_4 \left| H_d^\dagger H_u \right|^2 \\
 & + \left[-m_{12}^2 H_d \cdot H_u + \frac{1}{2} \lambda_5 \left(H_d^\dagger H_u \right)^2 \right. \\
 & \left. - \left(\lambda_6 |H_d|^2 + \lambda_7 |H_u|^2 \right) \left(H_d \cdot H_u \right) + \text{h.c.} \right],
 \end{aligned} \tag{3.19}$$

which shall be expressed in terms of the MSSM potential Eq. (1.40) at tree- and one-loop level.

3.3.2. Tree-Level Matching

The tree-level matching can in principle be performed by comparing the tree-level Lagrangian derived in this section and the scalar potential derived in the MSSM introduction in Eq. (1.40). However, in order to make the transition to the one-loop matching trivial, all necessary tree-level MSSM amplitudes are computed instead and are matched to the Lagrangian parameters of the 2HDM. Thus, at one-loop order, one just has to replace the corresponding tree-level amplitudes by their one-loop counterparts.

The matching is performed using tree-level mass eigenstates. However, since $v_u, v_d \rightarrow 0$, the mass and gauge eigenstates do coincide and we can write

$$H_2 = H_u = \frac{1}{\sqrt{2}} \begin{pmatrix} H + iA \\ H^+ \end{pmatrix}, \quad H_1 = -\epsilon H_d^* = \frac{1}{\sqrt{2}} \begin{pmatrix} h + iG^0 \\ -G^+ \end{pmatrix}, \quad (3.20)$$

because the CP-even, CP-odd and charged Higgs rotation matrices are unit matrices in this limit. All other mass and rotation matrices for the electroweakinos and sfermions are as in the high-scale scenario of the previous sections.

The effective couplings are then given by the amplitudes shown in Fig. 3.5, where the field normalizations, permutation factors and different sign conventions compared to the MSSM have been considered as well. The resulting quartic couplings read

$$\lambda_1 = \frac{1}{8} (g_1^2 + g_2^2), \quad (3.21)$$

$$\lambda_2 = \lambda_1, \quad (3.22)$$

$$\lambda_3 = \frac{1}{4} (g_1^2 - g_2^2), \quad (3.23)$$

$$\lambda_4 = -\frac{1}{2} g_2^2, \quad (3.24)$$

$$\lambda_5 = \lambda_6 = \lambda_7 = 0, \quad (3.25)$$

while all mass parameters are given by

$$m_{12}^2 = -B_\mu, \quad (3.26)$$

$$m_1^2 = \mu^2 + m_{H_d}^2, \quad (3.27)$$

$$m_2^2 = \mu^2 + m_{H_u}^2. \quad (3.28)$$

As in the MSSM, m_1^2 and m_2^2 can be traded for the quartic couplings through the use of tadpole equations. The parameter m_{12}^2 is given by the mass of the CP-odd state $m_A^2 \propto B_\mu$. Since the CP-odd Higgs boson mass is also responsible for the doublet mixing, the renormalization of the mixing angle is connected to whether threshold corrections to m_{12}^2 have to be considered as well. The scheme dependent choice of $\tan \beta$ in Eq. (3.2), for example, already accounts for those threshold corrections above the scale m_A . Thus, m_A^2 is interpreted as an input parameter at the matching scale, since it is given by the bi-linear soft-SUSY-breaking term.

Furthermore, different possible renormalization schemes for v_u, v_d and $\tan \beta$ are e.g. discussed in Ref. [61].

3.3.3. One-Loop Matching

The matching is performed by computing the amplitudes in Fig. 3.5 at the one-loop order with vanishing external momenta and $v_u, v_d \rightarrow 0$. Since $B_\mu \propto m_A^2 < 1 \text{ TeV}$, also the bi-linear coupling is set to zero at the matching scale m_{SUSY} .

Using SARAH's matching routines as described in Appendix A.3.1.3 together with the included input file `MSSM/Matching_THDMI1.m`, the full one-loop threshold corrections are computed. Comparisons with the expressions originating from heavy sfermions given in Refs. [8, 72] yield identical results if the different normalizations are taken into account and their chosen degree of mass degeneracy in the stop sector is considered. The contributions from non-degenerate electroweakinos were computed in Ref. [61] and are also identical to our findings.

In summary, the new SARAH matching routines have been validated using three comparisons with results available in the literature, one of them with an extended Higgs boson sector. In addition, the correct separation of local and non-local contributions has been shown using a simple toy-model.

Thus, we are able to apply the routines on untested scenarios. The next chapter discusses the first dedicated application of SARAH's new matching routines on a model with an extended scalar sector. A phenomenological study of the model including Higgs boson and dark matter searches as well as low-energy constraints is performed.

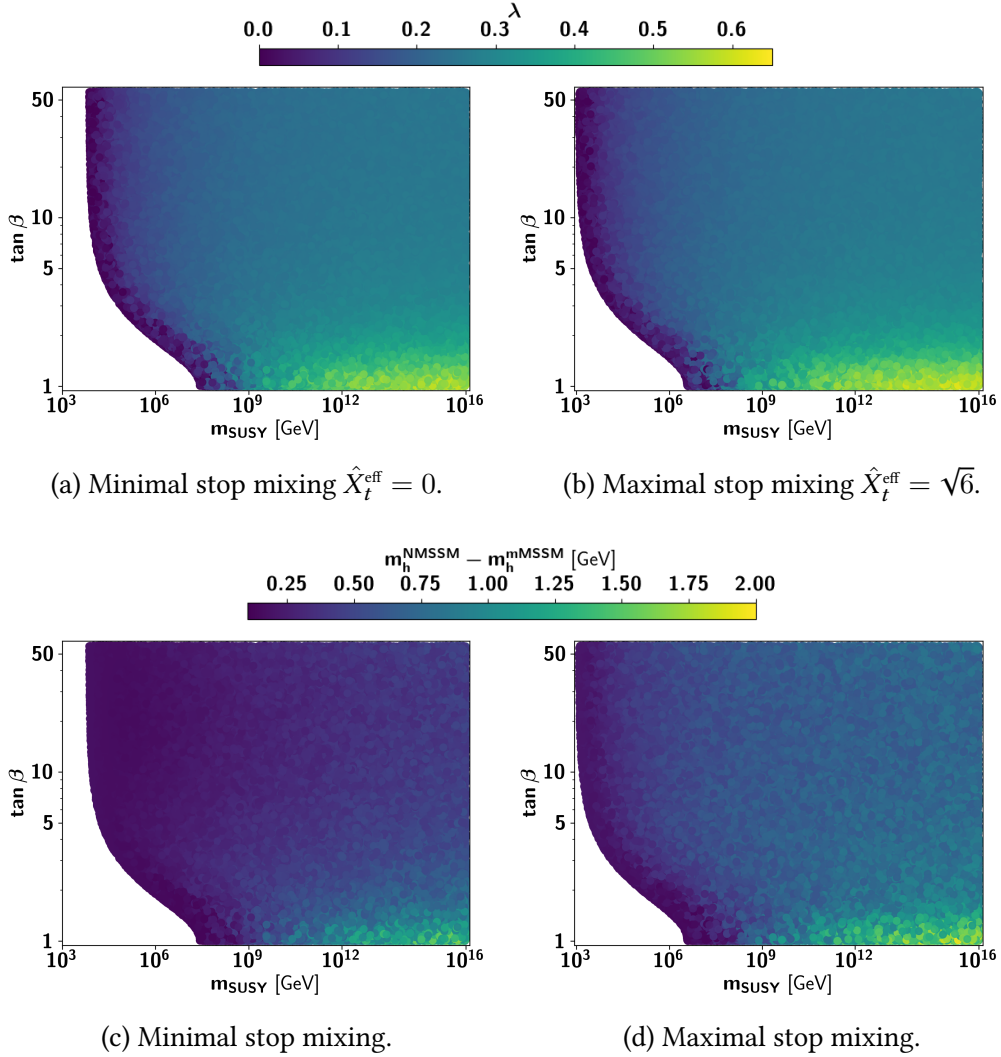


Figure 3.3.: NMSSM parameter points for a degenerate mass spectrum in the decoupling parametrization which fulfill $m_h = 125 \pm 2$ GeV. (a)/(b) are for minimal/maximal stop mixing. Figures (c)/(d) compare the NLO Higgs boson mass prediction of the high-scale NMSSM m_h^{NMSSM} with the modified MSSM prediction m_h^{mMSSM} (i.e. MSSM NLO thresholds plus tree-level singlet contributions).

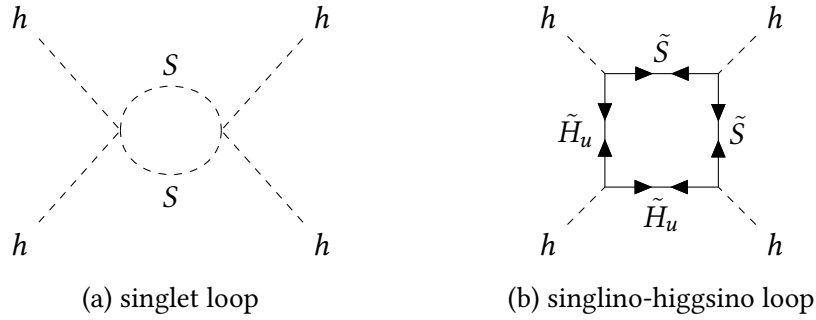


Figure 3.4.: Excerpt of diagrams not accounted for in the calculation of threshold corrections in Ref. [10] where only MSSM-like contributions are included. The double-arrow denotes MAJORANA fermions.

$$\begin{aligned}
 \lambda_1 &= -\frac{4!}{\sqrt{2}^4} \begin{array}{c} h \quad h \\ \diagdown \quad \diagup \\ \otimes \\ \diagup \quad \diagdown \\ h \quad h \end{array} &
 \lambda_2 &= -\frac{4!}{\sqrt{2}^4} \begin{array}{c} H \quad H \\ \diagdown \quad \diagup \\ \otimes \\ \diagup \quad \diagdown \\ H \quad H \end{array} &
 \lambda_3 &= -\frac{2!2!}{\sqrt{2}^4} \begin{array}{c} h \quad h \\ \diagdown \quad \diagup \\ \otimes \\ \diagup \quad \diagdown \\ H^+ \quad H^- \end{array} \\
 \lambda_4 &= \frac{2!2!}{\sqrt{2}^4} \left(\begin{array}{c} h \quad H \\ \diagdown \quad \diagup \\ \otimes \\ \diagup \quad \diagdown \\ G^+ \quad H^- \end{array} + i \begin{array}{c} h \quad A \\ \diagdown \quad \diagup \\ \otimes \\ \diagup \quad \diagdown \\ G^- \quad H^{+-} \end{array} \right) &
 \lambda_6 &= -\frac{2 \cdot 2!}{\sqrt{2}^4} \begin{array}{c} h \quad H \\ \diagdown \quad \diagup \\ \otimes \\ \diagup \quad \diagdown \\ G^+ \quad G^- \end{array} \\
 \lambda_5 &= \frac{2!2!}{\sqrt{2}^4} \left(\begin{array}{c} h \quad H \\ \diagdown \quad \diagup \\ \otimes \\ \diagup \quad \diagdown \\ G^+ \quad H^- \end{array} - i \begin{array}{c} h \quad A \\ \diagdown \quad \diagup \\ \otimes \\ \diagup \quad \diagdown \\ G^- \quad H^+ \end{array} \right) &
 \lambda_7 &= -\frac{2 \cdot 2!}{\sqrt{2}^4} \begin{array}{c} h \quad H \\ \diagdown \quad \diagup \\ \otimes \\ \diagup \quad \diagdown \\ H^+ \quad H^- \end{array}
 \end{aligned}$$

Figure 3.5.: Matching conditions for quartic couplings expressed in terms of effective amplitudes in the unbroken SU(2) phase where the components of the mass eigenstates h , H , H^\pm , G^\pm , A and G^0 coincide with the components of the gauge doublets H_d and H_u .

4. Application: Split Supersymmetry

The following chapter studies the NMSSM with a large mass hierarchy which does not separate SM fields from all non-SM fields, as in the high-scale SUSY scenario, but assumes that only scalar superpartners of the SM fermions as well as one Higgs doublet are decoupled.

In the previous chapter we argued that the NMSSM may be more suited for a high-scale SUSY scenario because it intrinsically connects the μ parameter to the (large) SUSY breaking scale without specifying the hidden sector responsible for SUSY breaking. In case of the MSSM, further assumptions on the hidden sector are necessary for $\mu \propto m_{SUSY}$. If this is not the case, μ as well as all soft fermion masses can be protected by an approximate global $U(1)$ symmetry which is a remnant of the discrete R symmetry $R[\hat{H}_u \cdot \hat{H}_d] = 0$ [78]. Thus, it is also possible that supersymmetric fermions are light while only the scalars are decoupled (except at least one light Higgs boson). Likewise, the effective μ parameter in the NMSSM can only be protected by taking further assumptions of the SUSY breaking pattern into account which separate the soft singlet mass term (and thus $v_s \propto \mu_{\text{eff}}$) from all other soft terms. This idea will be explained in more detail in the next section.

These aspects emerged in *split SUSY* scenarios where the experimental constraints on the squark masses [79, 80] are taken as a guidance for multi-TeV or even heavier scalar soft-SUSY-breaking parameters. However, due to the weaker bounds on uncolored fermion masses [81, 82], fermionic SUSY particles can still be light. Thus, split SUSY as an intermediate EFT, consisting of the typical SUSY spectrum with the heavy scalars being integrated out, is an economic way to account for experimental constraints and to give precise predictions at the same time. In contrast to high-scale SUSY, the split scenario still benefits from the additional light fermions. They enter not only predictions of low-energy observables, but also contribute to the RGE running which can improve unification of the SM gauge couplings g_1, g_2 and g_3 near the GUT scale. In Fig. 4.1 the running of the SM gauge couplings is compared between the MSSM (a) and the split MSSM (b) using two-loop RGEs generated with SARAH. Due to the missing scalars, the prediction of the unified gauge coupling strength in the split MSSM is smaller. In the specific example shown here, where no sfermion threshold corrections have been considered, i.e. $m_{\text{sfermion}} > m_{\text{GUT}}$, unification is even more precise. The quality of unification is determined by $\delta = |1 - g_3/g_{1,2}|$ evaluated at the scale where g_1 and g_2 are unified. We find $\delta_{\text{MSSM}}/\delta_{\text{split MSSM}} \approx 4.5$. Furthermore, stable fermions with masses of about one TeV and couplings to SM-fields comparable with the strength of the weak interaction, i.e. Weakly Interacting Massive Particles (WIMPs), are known to be able to reproduce the observed relic density $\Omega h^2 \approx 0.12$ of dark matter particles. Electroweakinos can fulfill these conditions and also evade predictions for direct detection (DD) searches of DM scattering cross-sections with heavy

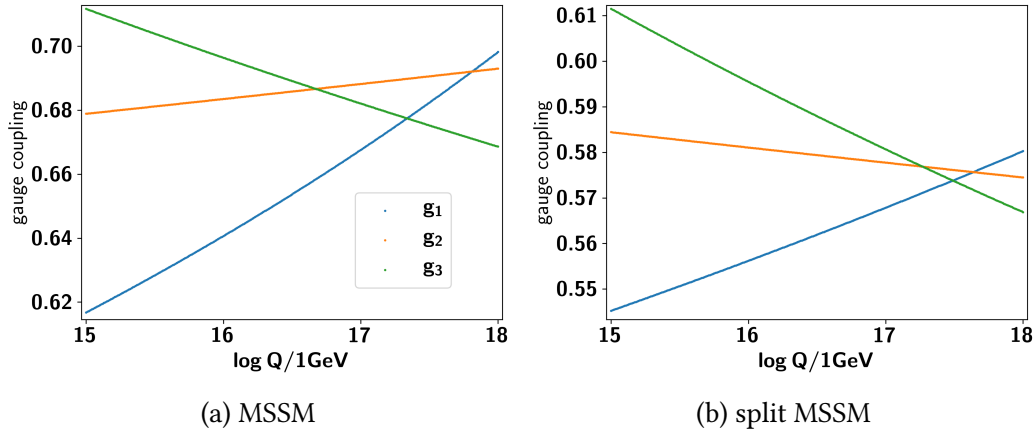


Figure 4.1.: The two-loop RGE running of the SM gauge couplings g_1 , g_2 and g_3 in the MSSM and the split MSSM near the GUT scale. The RGEs have been calculated by SARAH. The running starts at 3 TeV using the inputs: $g_1 = 0.45$, $g_2 = 0.63$ and $g_3 = 1.04$. The area of the enclosed triangle in (b) is about ≈ 16 times smaller compared to (a).

nuclei [83].

In addition, interesting collider signatures are predicted by split SUSY scenarios. Due to the missing colored scalars, the relatively light gluino can only decay through higher dimensional operators of the form $\tilde{g}q\bar{q}\chi_0$ suppressed by the soft-SUSY-breaking scale. Thus a large gluino lifetime and associated displaced vertices are typical signatures of split SUSY [7, 84, 85] and are part of recent experimental searches [5].

However, the major motivations for the NMSSM given in Section 1.4 are also valid for split SUSY scenarios if the singlet VEV is not associated with the SUSY breaking scale responsible for the heavy sfermions but with an approximate symmetry which is a good symmetry even after SUSY is broken. Furthermore, the NMSSM provides an additional dark matter candidate, the singlino, which has the possibility to annihilate into a singlet through resonant s -channel diagrams at tree-level. This process would be important during the thermal freeze-out, providing a mechanism to reduce the relic abundance which is often too large in the MSSM. These aspects are e.g. studied in Ref. [86] for the natural SUSY case at fixed-order.

4.1. Non-Minimal Split SUSY: The Split NMSSM

The most general singlet extended split SUSY scenario was already considered in Refs. [64, 65, 87] with the focus on strongly first order electroweak phase transitions taking the SM Higgs boson mass constraint into account using a one-loop matching which extended the existing split MSSM corrections.

The focus of this section is on singlino dominated dark matter within the context of the split NMSSM and the interplay with the scalar sector at low energies. Thus, the simplest singlet-extended SUSY model described in Section 1.4 is considered as UV-model. The

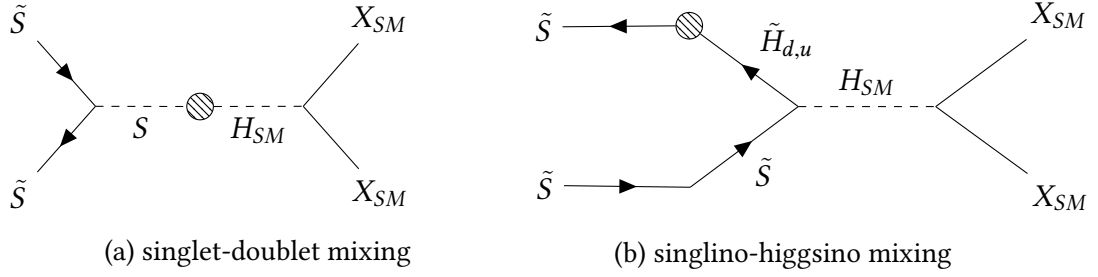


Figure 4.2.: Possible processes during the thermal freeze-out. The SM particles X_{SM} will decay further while the singlino \tilde{S} , if it is the LSP, contributes to the relic density. The blob indicates the mixing between the singlet and the doublet and the singlino with the higgsinos, respectively. Similar diagrams with non-resonant t/u-channel exchange exist as well.

scalar singlet must be light enough to be able to mix with the SM-like Higgs in order to serve as a possible mediator between the singlino and SM fields as indicated by the blob in Fig. 4.2a. Furthermore, the singlino mass $\propto v_s$ requires the singlet VEV also to be at or below the TeV-scale. However, this predicts that the effective μ -term and thus the higgsino masses are at the TeV-scale, too. Hence, the singlino can also couple to the SM-like Higgs boson through mixing with the higgsinos as shown in Fig. 4.2b. Thus, the minimal EFT content is the SM extended with a complex singlet S , a singlino \tilde{S} , two neutral and two charged higgsinos \tilde{H}_u, \tilde{H}_d . The three gauginos \tilde{W}, \tilde{B} and \tilde{g} are also kept in the EFT because of a symmetry argument given later.

The following sections elaborate this principle idea of the two models at the UV and IR further and give analytical expressions for mass matrices suitable at their corresponding energy scales. A one-loop matching of the scalar sector as well as a tree-level matching of the YUKAWA sector is performed using the matching routines described in Section 2.4. The loop-corrected spectrum generated by SPHENO is then used to study the possibility of singlino dominated dark matter.

4.1.1. The NMSSM at m_{SUSY}

The CP-conserving NMSSM introduced in Section 1.4 is assumed at the matching scale. The superpotential and the soft breaking terms are

$$\mathcal{W}_{\text{NMSSM}} = \mathcal{W}_{\text{MSSM}}|_{\mu=0} + \lambda \hat{S} \hat{H}_u \cdot \hat{H}_d + \frac{\kappa}{3} \hat{S}^3, \quad (4.1)$$

$$V_{\text{NMSSM}}^{\text{soft}} = V_{\text{MSSM}}^{\text{soft}}|_{B_\mu=0} + \frac{T_\kappa}{3} S^3 + T_\lambda S H_u \cdot H_d + m_S^2 |S|^2 + B_\mu H_u \cdot H_d$$

where the soft breaking potential $V_{\text{NMSSM}}^{\text{soft}}$ contains an additional MSSM-like bilinear soft term B_μ . Because the singlet is supposed to be light i.e. $v_s \ll m_{SUSY}$, the separation into one heavy and one light Higgs doublet through a large singlet VEV $B_\mu^{\text{eff}} \propto v_s^2$ is no longer possible in the \mathbb{Z}_3 -symmetric NMSSM. The solution to this problem is the additional

bilinear term $B_\mu \approx \mathcal{O}(m_{SUSY}^2)$ which is an additional source of mass for the heavy doublet. A motivation for Eq. (4.1), including the large B_μ -term, is given in Ref. [88] and is based on a discrete R symmetry which forbids operators with couplings of dimension $[mass]^1$ but allows for those of dimension $[mass]^2$ except for the singlet superfield.

Thus, it follows from the arguments given in the introduction to the decoupling theorem in Section 1.1.2, that all R -invariant operators have couplings $\mathcal{O}(m_{SUSY}^2)$ while the soft R -symmetry breaking terms are protected and assumed to be of order $\mathcal{O}(m_t) \ll m_{SUSY}$ such that the symmetry is restored in the limit of vanishing soft parameters.

Thus, the linear R -breaking parameters v_s , $M_{1,2,3}$ and $A_{u,d,e}$ are input of the EFT at the TeV scale and negligible at the large matching scale. This is analogous to the $v \rightarrow 0$ approximation in the high-scale SUSY scenario and effectively excludes higher dimensional operators suppressed by v_s/m_{SUSY} from the calculation of scalar masses.

The singlet, the charginos and neutralinos are then treated as massless at the matching scale $\propto m_{SUSY}$. Using modified loop functions in the calculation of threshold corrections will account for the separation of mass scales and the cancellation of IR divergences introduced through this approximation, as it was shown in the toy-model example in Section 2.3.

Because all dimension three operators (i.e. trilinear scalar couplings and fermion mass terms) are protected by an R -symmetry, sources of masses at the matching scale are present in the scalar sector only

$$B_\mu, m_{l_i}^2, m_{e_i}^2, m_{q_i}^2, m_{d_i}^2 \text{ and } m_{u_i}^2 \propto m_{SUSY}^2 \gg m_t^2. \quad (4.2)$$

Thus, threshold corrections at the matching scale appear only from the heavy doublet as well as from sfermions. In particular, the stop mixing parameter $\hat{X}_t \propto A_t/m_{SUSY}$ is suppressed by the large SUSY breaking scale m_{SUSY} and vanishes in the R -symmetry restoring limit. Thus, as we set $A_t = 0$, the leading stop contributions from Eq. (3.12) are not present in the split SUSY scenario.

4.1.2. Parameter Counting

Assuming all heavy scalars to be degenerate in mass m_{SUSY} , eleven free NMSSM input parameters remain

$$\tan \beta, \lambda, \kappa, M_{1,2,3}, v_s, T_\lambda, T_\kappa, B_\mu, m_{SUSY}. \quad (4.3)$$

The mixing angle $\tan \beta$ plays the same role as in the high-scale NMSSM and rotates H_u, H_d into the SM Higgs basis $H = \cos \beta H_d - \sin \beta \epsilon H_u^*$.

B_μ is connected to the heavy Higgs boson mass and also eliminated in favour of a degenerate mass spectrum.

$$B_\mu = \frac{\tan \beta}{1 + \tan^2 \beta} m_{SUSY}^2. \quad (4.4)$$

Overall, there are 10 free parameters in the degenerate case, out of which the six parameters $\tan \beta, v_s, T_\lambda, T_\kappa, \lambda$ and κ affect couplings of the scalar sector.

4.1.3. The Split NMSSM at m_t

The following section discusses the low-energy EFT of the split NMSSM with a large B_μ introduced in the previous section and performs the tree-level matching of the scalar as well as fermion sector.

4.1.3.1. Scalar Sector

The scalar potential in the gauge basis reads

$$\begin{aligned}
 V(H, S) = & m_H^2 HH^\dagger + \frac{\lambda_H}{2} |HH^\dagger|^2 \\
 & + m_S^2 SS^* + \frac{\lambda_S}{2} |SS^*|^2 \\
 & + \lambda_{SH} SS^* HH^\dagger \\
 & + (\kappa_{SH} SHH^\dagger + \kappa_S SSS + \text{h.c.}),
 \end{aligned} \tag{4.5}$$

where the quartic and trilinear couplings κ_i and λ_i shall be expressed in terms of their NMSSM counterparts at the matching scale. The squared mass parameters m_H^2 and m_S^2 can again be eliminated by the use of tadpole equations. Comparing Eq. (4.5) with the tree-level potential of the NMSSM, after rotating it into a basis of one light and one heavy doublet, yields the tree-level matching conditions valid at the scale $Q_{match} \propto m_{SUSY}$

$$\begin{aligned}
 \lambda_H = & \frac{1}{4}(g_2^2 + g_1^2) \cos^2 2\beta + \frac{1}{2}\lambda^2 \sin^2 2\beta, \\
 \lambda_S = & 2\kappa^2, \\
 \lambda_{SH} = & \lambda^2 - 2\kappa\lambda \frac{t_\beta}{1+t_\beta^2} - \frac{T_\lambda^2}{m_{SUSY}^2} \left(\frac{t_\beta^2 - 1}{t_\beta^2 + 1} \right)^2, \\
 \kappa_S = & \frac{1}{3}T_\kappa, \\
 \kappa_{SH} = & -T_\lambda \frac{t_\beta}{1+t_\beta^2},
 \end{aligned} \tag{4.6}$$

which shall be extended by higher-order contributions. Remarkably, the quartic singlet-doublet coupling λ_{SH} is the only coupling which has additional m_{SUSY}^{-2} suppressed contributions (which do not scale with a VEV) from integrating out the heavy Higgs bosons. Thus, λ_{SH} is very sensitive to Higgs boson masses that are of similar order as T_λ .

An important aspect of the trilinear couplings is, that they have dimension mass and thus are sensitive to UV cut-offs $\propto m_{SUSY}$. In particular, the contributions of heavy fermions to the trilinear couplings, do not decouple but scale with the mass of the heavy fermions in the loop, as it was shown in the dimensional analysis of the generic amplitudes in Section 2.1. In order to have a stable vacuum, all trilinear couplings and the light singlet mass should be of similar order. Thus, large cancellations between the tree-level parameters of the trilinear couplings and their loop-corrections are necessary. However, the trilinear couplings in the NMSSM are protected through a discrete R symmetry. Consequently, also

the parameters of the EFT κ_{SH} and κ_S cannot receive such corrections since all fermions are light.

After EWSB, the real singlet as well as the real part of the light doublet component mix to two CP-even scalars h and S . The 2x2 CP-even scalar mass matrix reads

$$\mathbf{m}_H^2 = \begin{pmatrix} m_{11}^2 & m_{12}^2 \\ m_{12}^2 & m_{22}^2 \end{pmatrix} = \begin{pmatrix} \lambda_H v^2 & \sqrt{2} v \kappa_{SH} + v v_s \lambda_{SH} \\ \sqrt{2} v \kappa_{SH} + v v_s \lambda_{SH} & -\frac{v^2 \kappa_{SH}}{2 v_s} + \frac{3 v_s \kappa_S}{\sqrt{2}} + v_s^2 \lambda_S \end{pmatrix}, \quad (4.7)$$

which can be diagonalized analytically using an orthogonal field transformation $Z_H(\theta)$. The eigenvalues of the matrix in Eq. (4.7),

$$m_{h,S}^2 = \frac{1}{2} \left(m_{11}^2 \pm m_{22}^2 + \sqrt{(m_{11}^2 - m_{22}^2)^2 + 4m_{12}^4} \right), \quad (4.8)$$

are related through the mixing angle θ

$$\tan 2\theta = 2 \frac{m_{12}^2}{m_{11}^2 - m_{22}^2} = \frac{4 v v_s (\sqrt{2} \kappa_{SH} + v_s \lambda_{SH})}{v^2 (\sqrt{2} \kappa_{SH} + 2 v_s \lambda_H) - v_s^2 (3 \sqrt{2} \kappa_S + 2 v_s \lambda_S)}, \quad (4.9)$$

such that for a small singlet VEV $v_s \ll v$ one obtains $\tan \theta \propto \frac{v_s}{v}$. The imaginary part of the singlet corresponds to a pseudoscalar after EWSB with the mass

$$m_A^2 = -\frac{9 v_s^2 \kappa_S + v^2 \kappa_{SH}}{\sqrt{2} v_s}, \quad (4.10)$$

while the remaining degrees of freedom from the doublet act as GOLDSTONE bosons to give rise of vector boson masses as discussed in Section 1.2.

4.1.3.2. Running in the Gauge Basis

In the previous section it was shown that the imaginary part of the singlet leads to a CP-odd pseudoscalar which does not mix with any other fields. Furthermore, the imaginary part of S does not take part in the κ_{SH} -interaction because of the hermicity of the Lagrangian and the assumed CP-conservation. As a consequence, the beta functions of the CP-even/odd singlets in the electroweak basis differ by a term $\propto \kappa_{SH}^2$ because the CP-odd field S_i (i.e. A in the mass basis) does not couple linearly to the Higgs doublet.

In order to account for this difference in the gauge basis, where the singlet CP-even and CP-odd components have the same mass parameter $m_S^2 SS^*$, the usual splitting into CP-even/odd components is performed before EWSB

$$S = \frac{1}{\sqrt{2}} (S_r + iS_i), \quad \langle S_r \rangle = v_s, \quad (4.11)$$

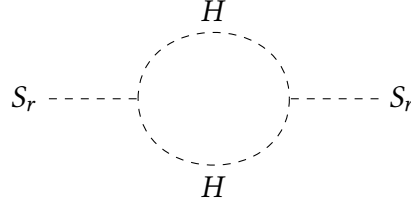


Figure 4.3.: One-loop contribution to the singlet propagator involving two internal doublets. Only the real component of the singlet is affected, leading to an additional contribution of the beta function of the scalar CP-even states.

which equivalently describes a CP-conserving model with two real singlets

$$\begin{aligned}
 V(H, S) &\equiv V(H, S_i, S_r) \\
 &= m_H^2 HH^\dagger + \frac{\lambda_H}{2} (HH^\dagger)^2 \\
 &+ \frac{m_{S_r}^2}{2} S_r S_r + \frac{\lambda_{S_r}}{8} (S_r S_r)^2 + \frac{m_{S_i}^2}{2} S_i S_i + \frac{\lambda_{S_i}}{8} (S_i S_i)^2 \\
 &+ \frac{\lambda_{S_{ri}}}{4} S_r S_r S_i S_i + \frac{\lambda_{SH_r}}{2} S_r S_r HH^\dagger + \frac{\lambda_{SH_i}}{2} S_i S_i HH^\dagger \\
 &+ \sqrt{2} \kappa_{SH_r} S_r HH^\dagger + \frac{1}{\sqrt{2}} \kappa_{S_r} S_r S_r S_r - \frac{3}{\sqrt{2}} \kappa_{S_{ri}} S_r S_i S_i
 \end{aligned} \tag{4.12}$$

with additional boundary conditions at the matching scale

$$\begin{aligned}
 \kappa_{SH} &\equiv \kappa_{SH_r} , \\
 \kappa_S &\equiv \kappa_{S_r} = \kappa_{S_{ri}} , \\
 \lambda_S &\equiv \lambda_{S_{ri}} = \lambda_{S_i} = \lambda_{S_r} , \\
 \lambda_{SH} &\equiv \lambda_{SH_r} = \lambda_{SH_i} , \\
 m_S^2 &\equiv m_{S_r}^2 = m_{S_i}^2 .
 \end{aligned} \tag{4.13}$$

Note that the S_i field does indeed not couple through κ_{SH} terms as it drops out once the hermitian conjugate is added. The additional contribution to the beta function of the scalar CP-even states due to the κ_{SH_r} coupling is shown in Fig. 4.3. In contrast to the S_i -propagator, the S_r -propagator receives a one-loop contribution with two internal doublets. The quartic couplings are not influenced by this effect because their beta functions are identical i.e. the CP-even and CP-odd components are coupled quadratically in the same way because $V(S_r, S_i)$ is assumed to be CP-conserving.

The numerical effect of the different beta functions on the running of the mass parameters is shown in Fig. 4.4a, where the absolute difference between the mass parameters $m_{S_r}^2$ and $m_{S_i}^2$ of the real and imaginary singlet component is shown. The parameters are computed at the top mass scale and drawn as functions of the scale at which they were matched to the NMSSM using SPHENO (as described in the next section). The analogue is shown for the trilinear singlet self-coupling κ_S separated into κ_{S_r} and $\kappa_{S_{ri}}$ in Fig. 4.4b, which also receives different contributions at the one-loop order.

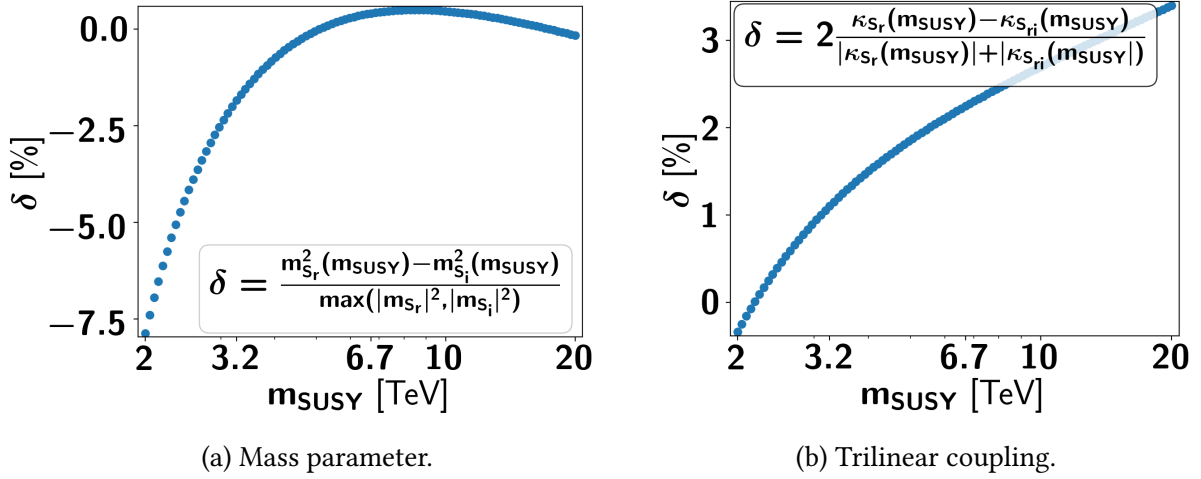


Figure 4.4.: The absolute difference of the squared mass parameters and self-couplings of the real/imaginary part of the singlet computed at the top mass scale as a function of the SUSY matching scale. The parameters at the matching scale are: $\kappa = 2.2$, $\lambda = -0.7$, $\tan \beta = 17$, $v_s = 197$ GeV, $M_1 = 2706$ GeV, $M_2 = 1021$ GeV, $M_3 = 1723$ GeV, $T_\lambda = 2067$ GeV, $T_\kappa = 1865$ GeV.

Considering κ_S , the difference tends to zero near the SM scale because it is only an RGE generated effect and the couplings at m_t are tree-level parameters. However, the squared mass parameters are also affected by different tadpole corrections computed by SPHENO at m_t , which is why they differ even for a small RGE running. The relative difference generated by this effect is between 1-10% for the discussed example where a running over one order of magnitude is performed.

4.1.3.3. Fermion Sector

Similar to the scalar sector, the fermion interactions as well as mass terms have the general form in the EFT

$$\begin{aligned}
 \mathcal{L}_{\text{fermion}} = & Y_d^{\text{EFT}} q H^\dagger d - Y_u^{\text{EFT}} q H - Y_e^{\text{EFT}} l H e \\
 & - g_2^u \tilde{H}_u H^\dagger \tilde{W} - \frac{g_1^u}{\sqrt{2}} \tilde{H}_u H^\dagger \tilde{B} \\
 & - g_2^d \tilde{H}_d H \tilde{W} - \frac{g_1^d}{\sqrt{2}} \tilde{H}_d H \tilde{B} \\
 & - Y_S^u \tilde{S} \tilde{H}_u H^\dagger - Y_S^d \tilde{S} \tilde{H}_d H \\
 & - Y_{\tilde{S}} \tilde{S} \tilde{S} S - \frac{Y_{ud}}{\sqrt{2}} S \tilde{H}_u \cdot \tilde{H}_d \\
 & - \frac{M_{\tilde{g}}}{2} \tilde{g} \tilde{g} - \frac{M_{\tilde{B}}}{2} \tilde{B} \tilde{B} - \frac{M_{\tilde{W}}}{2} \tilde{W} \tilde{W} \\
 & + \text{h.c.},
 \end{aligned} \tag{4.14}$$

where the g_i^j and Y_i^j are YUKAWA couplings. Except $Y_{d,u,e}^{\text{EFT}}$, which are the SM-like YUKAWA couplings, all couplings are interpreted as free and independent input parameters. As in the usual NMSSM, an effective μ -term as well as a singlino mass is generated spontaneously through the VEV v_s of the singlet.

Comparison with the NMSSM Lagrangian yields the tree level relations valid at the matching scale

$$\begin{aligned}
 g_1^u &= g_1 \sin \beta, & g_2^u &= g_2 \sin \beta, \\
 g_1^d &= g_1 \cos \beta, & g_2^d &= g_2 \cos \beta, \\
 Y_{ud} &= \lambda, & Y_{\tilde{S}} &= \kappa, \\
 Y_S^u &= \lambda \sin \beta, & Y_S^d &= \lambda \cos \beta, \\
 Y_{e,d}^{\text{EFT}} &= \cos \beta Y_{e,d}^{\text{FULL}}, & Y_u^{\text{EFT}} &= \sin \beta Y_u^{\text{FULL}},
 \end{aligned} \tag{4.15}$$

$$M_{\tilde{B}, \tilde{W}, \tilde{g}} = M_{1,2,3},$$

where $Y_{d,u,e}^{\text{FULL}}$ are the YUKAWA couplings in the NMSSM superpotential. The mass matrices of the neutralinos and charginos in the split NMSSM are determined by the corresponding matrices of the NMSSM, described in Section 1.4.2.3, using the relations in Eq. (4.15). Also the diagonalization of the fermion sector is analogous to the procedure described in Section 1.4.2.3. Thus, we will use the same notation for the mixing matrices N , U and V . The actual diagonalization for all mass matrices with finite v_s and v is performed numerically by SPHENO.

4.2. One-Loop Matching of the Scalar Sector

In the following analytical expressions of the one-loop corrections to Eq. (4.6) are given. The full expressions are rather lengthy and can easily be reproduced with the new SARAH matching routines. Thus, only the leading one-loop contributions in the limit $g_1, g_2 \rightarrow 0$ are shown and are expanded for small/large values of $\tan \beta$. However, for the numerical analysis, the complete analytical results are used.

4.2.1. Quartic Couplings

The SM-like quartic coupling λ_H receives similar corrections as in the high-scale NMSSM, except that contributions from the higgsinos, gauginos and soft sfermion couplings A_i are absent. Thus, the leading contributions in the limit $\lambda \gg g_{1,2}$ are dominated by λ^4 terms

$$\begin{aligned}
 (4\pi)^2 \delta\lambda_H^{(1)} &\approx -12 \lambda^4 t_\beta^2 \frac{(t_\beta^2 - 1)^2}{(t_\beta^2 + 1)^4} \\
 &\quad - \frac{\lambda T_\lambda^2}{m_{SUSY}^2} \left\{ \begin{array}{l} 22\lambda t_\beta^{-2} \\ (\kappa + \frac{3}{4}\lambda) \end{array} \right\} + \frac{T_\lambda^4}{m_{SUSY}^4} \left\{ \begin{array}{l} 2 \\ 1 \end{array} \right\}, \quad \text{for } \left\{ \begin{array}{l} t_\beta \gg 1 \\ t_\beta \approx 1 \end{array} \right\},
 \end{aligned} \tag{4.16}$$

which are enhanced by a factor of $\tan \beta^2$. In addition to the absence of \hat{X}_t -terms, also the $Y_{t,u,d}$ -contributions vanish because a degenerate spectrum at the matching scale m_{SUSY} is

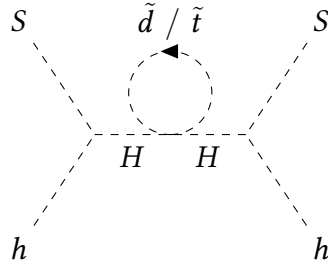


Figure 4.5.: Example of a $\tan \beta$ -enhanced/suppressed one-loop diagram involving a sbottom/stop loop and two heavy Higgs boson propagators.

considered, cf. Eq. (3.12). The m_{SUSY} -suppressed terms become important once a rather small matching scale $m_{SUSY} \approx |T_\lambda|$ is assumed.

The singlet-like quartic coupling λ_S is also dominated by diagrams that contain two quartic couplings and internal heavy Higgs bosons

$$(4\pi)^2 \delta\lambda_S^{(1)} \approx -4\kappa^2 \lambda^2 \left(\frac{t_\beta^2 - 1}{t_\beta^2 + 1} \right)^2 - \frac{4T_\lambda^2}{m_{SUSY}^2} \left\{ \kappa^2 \left[\frac{1}{6}(\kappa^2 - 3\lambda^2 - 3\kappa\lambda) \right] \right\} + \frac{T_\lambda^4}{m_{SUSY}^4} \left\{ \begin{matrix} 4 \\ -\frac{1}{6} \end{matrix} \right\}, \text{ for } \left\{ \begin{matrix} t_\beta \gg 1 \\ t_\beta \approx 1 \end{matrix} \right\}. \quad (4.17)$$

However, no $\tan \beta$ enhancement is found for $\lambda_S^{(1)}$. The shift in the quartic coupling λ_{SH} , which is responsible for the singlet-doublet mixing, is given by

$$(4\pi)^2 \delta\lambda_{SH}^{(1)} \approx -2\kappa \lambda^2 \left\{ \begin{matrix} -\kappa \\ (3\lambda - 2\kappa t_\beta) t_\beta^{-1} \end{matrix} \right\} - 2 \frac{T_\lambda^2}{m_{SUSY}^2} \left(\frac{t_\beta^2 - 1}{t_\beta^2 + 1} \right)^2 \left(t_\beta^{-2} Y_t^2 + t_\beta^2 (Y_d^2 + Y_\tau^2) \right) - \frac{T_\lambda^2}{m_{SUSY}^4} \left\{ \begin{matrix} 2T_\lambda^2 - 4T_\kappa^2 \\ 2T_\kappa^2 + \frac{T_\lambda^2}{4} + 2T_\lambda T_\kappa \end{matrix} \right\}, \text{ for } \left\{ \begin{matrix} t_\beta \gg 1 \\ t_\beta \approx 1 \end{matrix} \right\}, \quad (4.18)$$

which has an interesting $\tan \beta$ enhancement for the down-type sfermion YUKAWA couplings in the m_{SUSY}^{-2} suppressed terms while the stop contributions $\propto Y_t^2$ are $\tan \beta$ suppressed. The sfermion contributions are generated through diagrams of topology type SA4, like the one shown in Fig. 4.5.

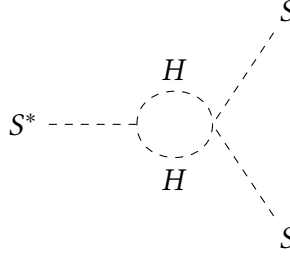


Figure 4.6.: The operator SSS^* is generated at one-loop order through corrections from the heavy Higgs boson H .

4.2.2. Trilinear Couplings

The trilinear singlet self-coupling is corrected at one-loop order by the leading term

$$(4\pi)^2 \delta\kappa_S^{(1)} \approx -2\kappa \lambda T_\lambda \left(\frac{t_\beta^2 - 1}{t_\beta^2 + 1} \right)^2 - \frac{1}{12m_{SUSY}^2} \left\{ \begin{array}{l} 6T_\kappa T_\lambda^2 \\ T_\lambda^2 (T_\kappa - 2T_\lambda) \end{array} \right\}, \text{ for } \left\{ \begin{array}{l} t_\beta \gg 1 \\ t_\beta \approx 1 \end{array} \right\}, \quad (4.19)$$

whereas the largest corrections to the coupling responsible for the $S - H$ mixing are

$$(4\pi)^2 \delta\kappa_{SH}^{(1)} \approx -\lambda T_\lambda \left\{ \begin{array}{l} \kappa \\ 3\lambda t_\beta^{-1} \end{array} \right\} + \frac{T_\lambda^2}{m_{SUSY}^2} \left\{ \begin{array}{l} 17T_\lambda t_\beta^{-1} \\ 2T_\kappa + \frac{9}{4}T_\lambda \end{array} \right\}, \text{ for } \left\{ \begin{array}{l} t_\beta \gg 1 \\ t_\beta \approx 1 \end{array} \right\}. \quad (4.20)$$

As expected, the one-loop trilinear couplings scale with $[\text{trilinear coupling}]^3 m_{SUSY}^{-2}$, because no threshold corrections from heavy fermions are present.

Additional operators are generated at the one-loop order, when integrating out the heavy Higgs doublet. For instance, the operator SSS^* is generated through the diagram Fig. 4.6, although it is not present in the original Lagrangian Eq. (4.5). However, since a CP-conserving model is considered, no additional operators to those in Eq. (4.12) can appear as this is already the most general CP-conserving potential for two real singlets. Thus, all new one-loop contributions, like the one in fig. Fig. 4.6, are already accounted for by directly matching the Lagrangian $\mathcal{L}(H, S_r, S_i)$ instead of $\mathcal{L}(H, S)$. This has been done by implementing a new SARAH model, `Sp1itSUSY_NMSSM`, which is based on Eqs. (4.5) and (4.14), and now part of SARAH's source code.

4.3. Numerical Analysis of the Split NMSSM Matching

The following sections perform a numerical analysis of the split NMSSM with a scalar sector matched at one-loop order to the NMSSM. The `SPHENO` code [11, 12] generated by SARAH [13] includes the matching conditions, the RGE running and computes the mass spectrum in the low-energy theory as well as cross-sections, branching fractions and decay rates of several processes. The output for a given set of numerical values of the input parameters, discussed in Section 4.1.2, is a spectrum file in the SLHA2 format [89].

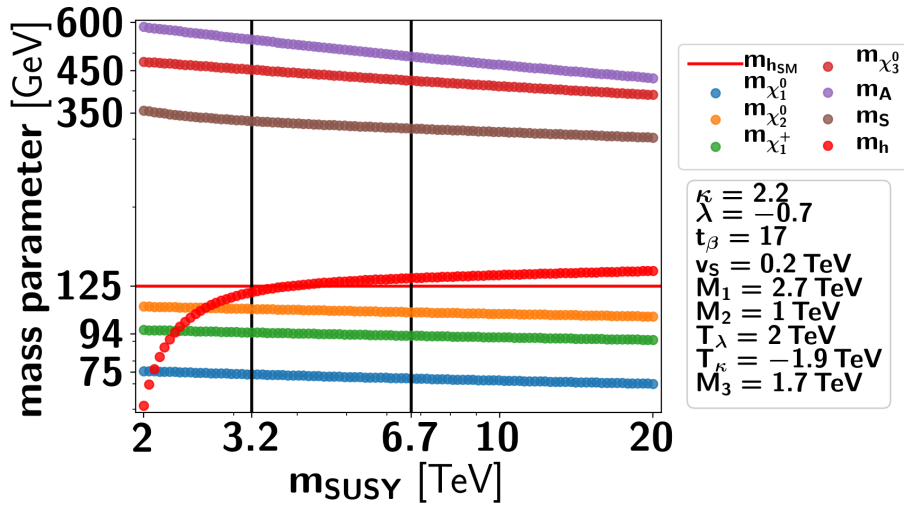


Figure 4.7.: Example of a split NMSSM mass spectrum. The red horizontal line marks 125 GeV whereas the area between the two vertical black lines is allowed by Higgs constraints (HIGGSBOUNDS). Masses ≥ 1 TeV are not shown for simplicity: $m_{\tilde{g}} \approx 1.7$ TeV, $m_{\chi_{2,4}^{\pm}, \chi_4^0} \approx 1$ TeV, $m_{\chi_5^0} \approx 2.7$ TeV in the area allowed by HIGGSBOUNDS.

The generated spectrum file contains all computed information of the low-energy theory and is passed to HIGGSBOUNDS [90], which compares the computed cross-sections and branching fractions against publicly available Higgs searches from the Large Electron Positron (LEP) collider, Tevatron and the LHC. Furthermore, MIRCOMEGAS [91] is used to calculate the relic density.

4.3.1. Example spectrum

Before examining the whole parameter space of the split NMSSM, an example spectrum is considered. All parameters are fixed to the values shown in Fig. 4.7 while only m_{SUSY} is varied from 2-20 TeV. In particular T_{λ} and T_{κ} are chosen to be ≈ 2 TeV. The purpose of this is to estimate the influence of the m_{SUSY} -suppressed terms, which become relevant if $T_{\lambda}, T_{\kappa} \approx m_{SUSY}$.

The dependence of the scalar and fermion masses lighter than one TeV on m_{SUSY} is shown in Fig. 4.7. In particular, the SM-like Higgs boson mass is very sensitive to m_{SUSY} for $m_{SUSY} < 3$ TeV compared to the other mass parameters. This is not only due to the running of λ_H (as in high-scale SUSY) but also due to the choice of $T_{\lambda} = 2$ TeV and the T_{λ}^2/m_{SUSY}^2 -terms in the tree-level relation of λ_{SH} which become important. In this regime the EFT approach of two well separated mass scales becomes questionable. Thus, we discard parameter points with $2 m_{SUSY} < T_{\lambda}, T_{\kappa}, v_s$ for the actual phenomenological study. The area enclosed by the two vertical black lines, where the m_{SUSY} -dependence of m_h is already flattened, is allowed by the HIGGSBOUNDS constraints.

4.3.1.1. Comparison: Tree-Level against One-Loop Matching

The effect of the NLO contributions calculated with the new SARAH interface w.r.t. the LO contributions can also give further guidance on the minimum choice of the matching scale. This is due to the fact, that all couplings (except λ_{SH}) do not receive m_{SUSY}^{-1} suppressed terms at LO but only from NLO threshold corrections.

For the comparison, only the perturbative order of the matching is varied while the mass spectrum at m_t is always computed at the one-loop order. The differences from LO to NLO matching conditions on the prediction of the quartic and trilinear couplings at m_t is shown in Figs. 4.8a and 4.8b while the resulting difference in the singlet-like, pseudoscalar and SM-like masses is shown in Fig. 4.8c. The experimentally allowed range $m_{SUSY} = \{3.2, 6.7\}$ TeV is considered only.

The quartic singlet self-coupling does neither receive large NLO corrections nor shows a strong dependence on the matching scale which is likely because the m_{SUSY}^{-4} -term has a different sign and less numerical suppression factors such that cancellations are possible. The SM-like coupling λ_H is $\tan \beta$ enhanced for terms which are not suppressed by m_{SUSY} (note that $t_\beta = 17$ is chosen) and thus is corrected at a level of 7% without a large dependence on the matching scale. Interestingly, the singlet-doublet coupling λ_{SH} receives large corrections for small m_{SUSY} which is due to the $\tan \beta$ enhanced m_{SUSY}^{-2} suppressed terms in Eq. (4.18). Thus, also the NLO corrections require at least $2m_{SUSY} > T_\lambda$.

The trilinear couplings in Fig. 4.8b have a rather weak dependence on m_{SUSY} . The singlet self-coupling has a positive correction of $\mathcal{O}(5\%)$ because $T_\kappa \approx -T_\lambda$ was chosen while the singlet-doublet coupling is barely changed w.r.t. the leading-order computation.

The resulting differences in the scalar mass predictions are shown in Fig. 4.8c. The scalar singlet and SM-like mass differences have a rough dependence on the matching scale for small m_{SUSY} and receive positive corrections at the $\mathcal{O}(2 - 4\%)$ level. The pseudoscalar mass is twice as heavy as the singlet mass and thus relatively robust against small changes of the matching scale. The shift on the singlet pseudoscalar mass m_A from an LO to NLO matching is about -4%.

In conclusion, NLO corrections have the ability to improve the mass predictions at the 1 – 10% level while care has to be taken if $m_{SUSY} \approx T_\lambda, T_\kappa$. All low-energy mass parameters should be chosen to be at least smaller than $2m_{SUSY}$ for the considered parameter point.

4.3.1.2. Relic Density Constraint

The impact of the matching scale on the prediction of the relic density Ωh^2 is shown in Fig. 4.9a where the horizontal line marks the central value of the experimental measurement. In the considered scan range, the neutralino mixing matrix elements fulfill $|N_{13}|^2 + |N_{14}|^2 = \{0.95, 0.96\}$ i.e. the LSP is higgsino-like. Thus, the running of the gauge couplings and Y_{ud} from m_t to m_{SUSY} are the dominant effects. A variation of less than 5% is observed in the region allowed by HIGGSBOUNDS. However, the theoretical uncertainty in the calculation of Ωh^2 performed with MIRCMEGAS is rather high and was found to be more than 20% [92] because only tree-level processes based on CALCHEP [93] are included.

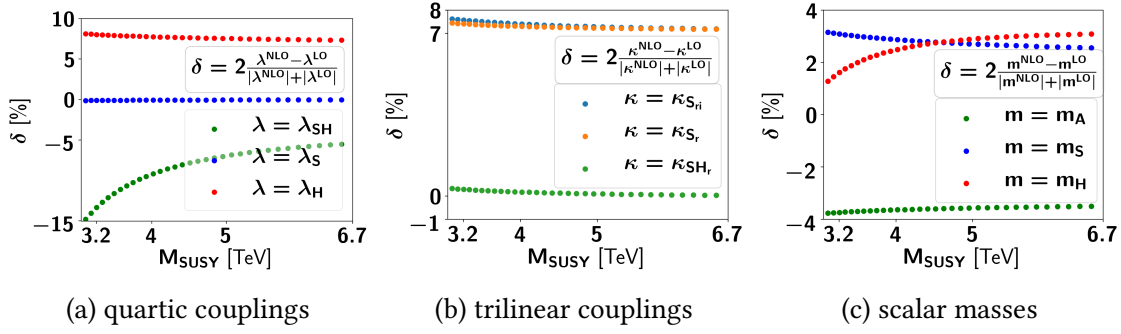


Figure 4.8.: Relative difference between leading and next-to-leading mass predictions. Parameters are chosen as in Fig. 4.7.

Thus, we allow for a variation of $\Omega h^2 = 0.12 \pm 0.08$ in the results generated by MICROMEGAS for all following scans.

4.3.1.3. Tree-Level Unitarity Constraints

Unitarity at tree-level constrains the smallest eigenvalue a_0 of the scattering matrix for a scalar state $a = \{1, 2\}$ with two scalars labeled by 1 and 2 into a scalar state $b = \{3, 4\}$ with two scalars 3 and 4,

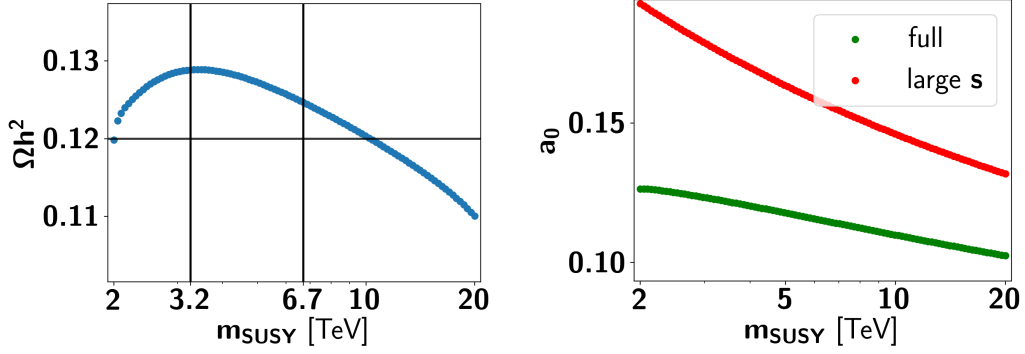
$$(a_0)_{ab} = \frac{1}{32\pi} \sqrt{\frac{4|\vec{p}_a||\vec{p}_b|}{2^{\delta_{12}}2^{\delta_{34}}s}} \int_{-1}^1 d(\cos \theta) \mathcal{M}_{ba}(\cos \theta), \quad (4.21)$$

where \vec{p}_i are the incoming/outgoing momenta in the centre-of-mass (CM) frame, s is the CM scattering energy, θ is the scattering angle between \vec{p}_a and \vec{p}_b and \mathcal{M}_{ab} is the FEYNMAN amplitude for the scattering process. Unitarity at tree level requires $Re(a_0)_{ab} < 1/2$. In the large s approximation $s \rightarrow \infty$, only 4-point interactions in the amplitude \mathcal{M}_{ba} are taken into account which leads to the constraint $|\mathcal{M}_{ba}| < 8\pi$ [94]. The impact of this approximation on the computation of the eigenvalues of the scattering matrix was studied in [94] and can differ significantly from a full computation involving trilinear couplings i.e. diagrams of the topology type T42. Such couplings are also generated in models with spontaneous symmetry breaking where quartic couplings are multiplied with potentially large VEVs. In this case, the amplitude may have the form

$$\mathcal{M}_{ba} \propto \frac{\lambda^2 v^2}{s - m^2}, \quad (4.22)$$

where λ is a quartic coupling, v is a (large) VEV and m a scalar mass. Thus, even if $m^2 \ll s$, it is possible that such contributions become important if $v^2 \propto \mathcal{O}(s)$. The computation of the full tree-level scattering matrix was implemented in SARAH/SPHENO [95] which is used in the following to determine the impact of the trilinear couplings present in the singlet extended Higgs boson sector of the EFT.

In Fig. 4.9b, the large s approximation is compared against the full computation with



(a) Relic density in the split NMSSM. The area between the two vertical black lines is allowed by HIGGSBOUNDS. The horizontal black line corresponds to the experimentally measured value. (b) Comparison of the smallest scattering eigenvalue in the large s approximation against the one of the full scattering matrix with $\sqrt{s_{\text{max}}} = 3$ TeV.

Figure 4.9.: Relic density (a) and tree-level unitarity (b) in the split NMSSM

the maximum scattering energy $\sqrt{s_{\text{max}}} = 3$ TeV using the same data sample as in the previous sections. The tree-level trilinear couplings $|T_\lambda|, |T_\kappa| \approx 2$ TeV are smaller than s if m_{SUSY} is large while at one-loop order the dependence on m_{SUSY} discussed in Section 4.3.1.1 is generated which can enhance the trilinear couplings for small values of m_{SUSY} . As expected, the full computation can significantly change the smallest scattering eigenvalue a_0 for small m_{SUSY} while it tends towards the result of the large s approximation for large m_{SUSY} .

A detailed study of the influence of the large s approximation on the unitarity constraint is performed in the next section.

4.3.2. Parameter Scan

To analyse the complete parameter space of the model, a random scan over all ten input parameters within the ranges given in Table 4.1 is performed. Parameter points that do not have a light scalar with mass $m = 125.09 \pm 2$ GeV are discarded while all other constraints are subsequently applied later on the generated data sample. Furthermore, all low-energy mass parameters must not be larger than $m_{\text{SUSY}}/2$ in order to keep the EFT uncertainty small. In addition, points with chargino masses smaller than their experimental lower bound from LEP of 94 GeV [2] as well as gluino masses smaller than 1.5 TeV are discarded.

4.3.2.1. Parameter Correlations after Matching

Before the different constraints are discussed, the correlations among the most important NMSSM input parameters are considered which are shown in scatter plots in Fig. 4.10. The orange points are excluded by HIGGSBOUNDS while white areas are unphysical (e.g. due to negative mass squares) and blue points fulfill the Higgs boson mass constraint in the range of ± 2 GeV. The correlation between λ and κ is shown in Fig. 4.10a, which is rather

parameter	scan range	parameter	scan range
λ	[-3, 3]	T_λ	[-3000, 3000] GeV
κ	[-3, 3]	T_κ	[-3000, 3000] GeV
$\tan \beta$	[1, 50]	$M_{1,2}$	[10, 3000] GeV
v_s	[0, 3000] GeV	M_3	[1000, 3000] GeV
		M_{SUSY}	[10^3 , 10^{16}] GeV

Table 4.1.: Scan ranges for the random scan over the NMSSM parameter space. All parameters are input at the matching scale m_{SUSY} .

weak and unaffected by the Higgs searches. A lower bound on $\lambda > 0.5$ exists in the range of $\kappa \approx 0$ which means that light singlinos require heavy higgsinos.

The dependence of T_λ on T_κ , shown in Fig. 4.10b, is uncorrelated for $T_\kappa < 0$ as it was chosen in the high-scale NMSSM, see Eq. (3.7). However, in the split NMSSM also positive T_κ are possible if T_λ is chosen to be non-zero.

The behaviour in the λ - $\tan \beta$ plane, Fig. 4.10c, is also very similar to the high-scale NMSSM i.e. low values of $\tan \beta$ enable larger values of λ . In the high-scale NMSSM we found for a degenerate spectrum in the decoupling parametrisation that $\lambda < 0.6$, cf. Fig. 3.3b, while in the split NMSSM $\lambda > 2$ is possible. The dependence of κ on $\tan \beta$, Fig. 4.10d, is complementary. Low values of $\tan \beta$ allow for $\kappa \approx 0$ only, otherwise the two parameters are uncorrelated.

The most important input parameter dependencies for the dark matter prediction are those of the dimensionless couplings on the singlet VEV, shown in Fig. 4.10e and Fig. 4.10f, because they determine the singlino/higgsino mass spectrum. The $v_s - \lambda$ plane has a white area for small v_s and λ from discarding points with $m_{\chi_1^\pm} < 94$ GeV. The exclusion limits from Higgs searches require λ to be rather small if v_s is assumed to be small in contrast to κ which must be large for small v_s because otherwise the singlet quartic coupling $\propto \kappa^2$ (and hence its mass) is too small.

4.3.2.2. Scalar Sector and Higgs Constraints

Since S is a gauge singlet, the observed tree-level decay $h_{125} \rightarrow ZZ$ is not possible for S if no mixing with the SM-like Higgs doublet is present. Thus, scenarios where the scalar with mass 125 GeV has a large singlet component, i.e. $\tan \theta \gg 1$, are likely to be excluded by Higgs boson measurements. This can be seen in the scatter plot in Fig. 4.11a, where the singlet-like mass is plotted against the mixing angle θ . The color of the points indicates the matching scale m_{SUSY} while grey points are excluded by HIGGSBOUNDS. Large SUSY scales allow for $\tan \theta^{\text{max}} \approx 1/2$ which corresponds to a maximum singlet admixture of 20%. This is only possible with m_{SUSY} near the GUT scale because the m_{SUSY}^{-2} -suppressed contributions to κ_{SH} and λ_{SH} are not too large such that all mass matrix elements are of similar size. Singlet-doublet decoupling, $\tan \theta \approx 0$, is only observed for TeV-scale SUSY breaking. This indicates that an RGE running over several orders of magnitude always

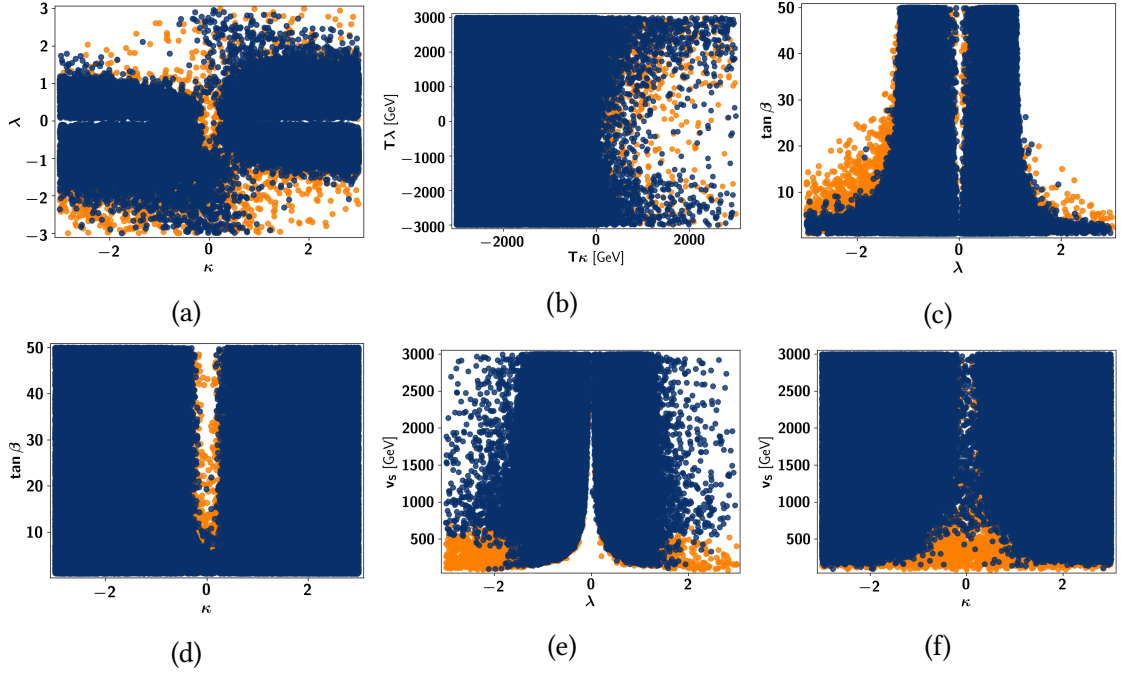


Figure 4.10.: NMSSM input parameters. Orange points are excluded by HIGGSBOUNDS.

introduces sizeable mixing effects i.e. relatively large λ_{SH} and κ_{SH} .

The mass of the singlet m_S as a function of the pseudoscalar singlet mass m_A is shown in Fig. 4.11b. In the considered parameter space, the singlet mass m_S scales from ≈ 200 GeV, near the current experimental constraints, up to 6 TeV which is above the energy-scale probed by current colliders. However, even for a TeV-scale CP-even singlet, the pseudoscalar can have a mass of only several GeV if the matching scale m_{SUSY} is not too small. Since the pseudoscalar is a singlet, it cannot be constrained through couplings to the Z -boson as they are only loop induced and naturally small. A possibility to constrain the pseudoscalar mass is through the invisible width of the SM-like Higgs boson $h \rightarrow AA$ which, however, was not considered here. The focus of this section is on the singlet as a DM mediator which is relatively independent on m_A for $m_A < 200$ GeV.

4.3.2.3. Tree-Level Unitarity Constraints

Tree-level unitarity checks are performed in the same manner as described in Section 4.3.1.3. The interesting region of \sqrt{s} is the scale of m_S and m_A in Fig. 4.11b, where contributions not covered by the large s approximation are important. Thus, we scan \sqrt{s} from 250 GeV (where SM Higgs boson propagators are important) to $m_S^{max} \approx 6$ TeV. The presence of poles, e.g. $s \approx m_S^2$, are handled by SPHENO [95], which ignores such corrections.

The prediction of the maximum smallest eigenvalue a_0^{full} as a function of the scalar and pseudoscalar mass in the full a_0 calculation (including trilinear couplings) is shown in Figs. 4.12a and 4.12b. The largest eigenvalues are found for $m_S \lesssim 3$ TeV and $m_A \lesssim 1.5$ TeV. This is the energy regime, for which the trilinear singlet coupling $\kappa_s \propto T_\kappa = \{-3, 3\}$ TeV

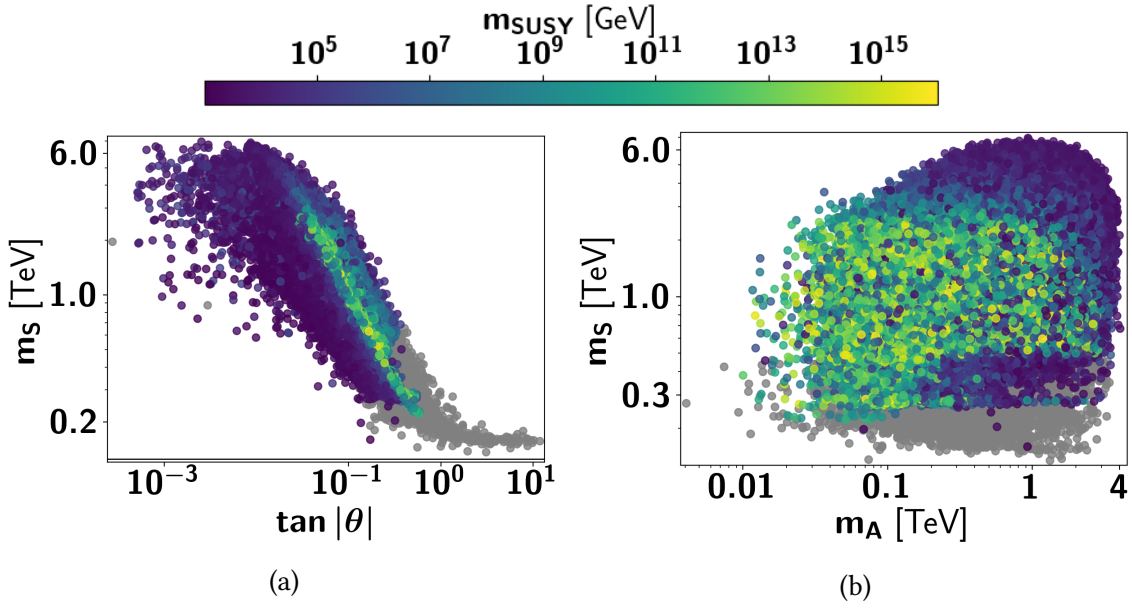


Figure 4.11.: Singlet scalar mass as a function of the mixing angle $\tan|\theta|$ (a) and the pseudoscalar mass (b). The color indicates the scale at which the matching to the NMSSM was performed. Grey points are excluded by HIGGSBOUNDS.

can be of $\mathcal{O}(1)$ compared to the singlet masses. Thus, tree-level contributions like

$$\mathcal{M}_{A,A \rightarrow S \rightarrow A,A} \propto \frac{T_\kappa^2}{s - m_S^2} \quad (4.23)$$

can contribute with large values to a_0^{full} , if s is not too large. The apparent threshold at $m_S \approx 5$ TeV is due to $s/t/u$ -channel resonances which are cut out by SPHENO.

The difference between the full a_0^{full} computation and the computation involving the large s approximation $a_0^{\text{large } s}$ is shown in Fig. 4.12c. The x-axis shows the scattering energy $\sqrt{s_{\text{best}}}$ for which a_0 is maximized. The largest deviations are observed in the region of the trilinear couplings $\sqrt{s_{\text{best}}} < 4$ TeV, while there is good agreement between the two approaches for large values of $\sqrt{s_{\text{best}}}$.

Furthermore, Figs. 4.12a to 4.12c also show the dependence on m_{SUSY} which is controlling the large values of a_0^{full} as well as the large deviations to $a_0^{\text{large } s}$. This is due to the trilinear couplings, which can be enhanced for small m_{SUSY} but are not accounted for in $a_0^{\text{large } s}$.

However, we do not find many cases where a parameter point is allowed in the $s \rightarrow \infty$ limit but forbidden in the finite s computation (or vice versa). In addition, the EFT uncertainty is larger for small m_{SUSY} . Higher-order corrections may predict smaller trilinear couplings and can shift the points with $a_0 > 1/2$ again below $1/2$. Thus, the tree-level unitarity constraint is satisfied in almost all regions of the considered split NMSSM parameter space.

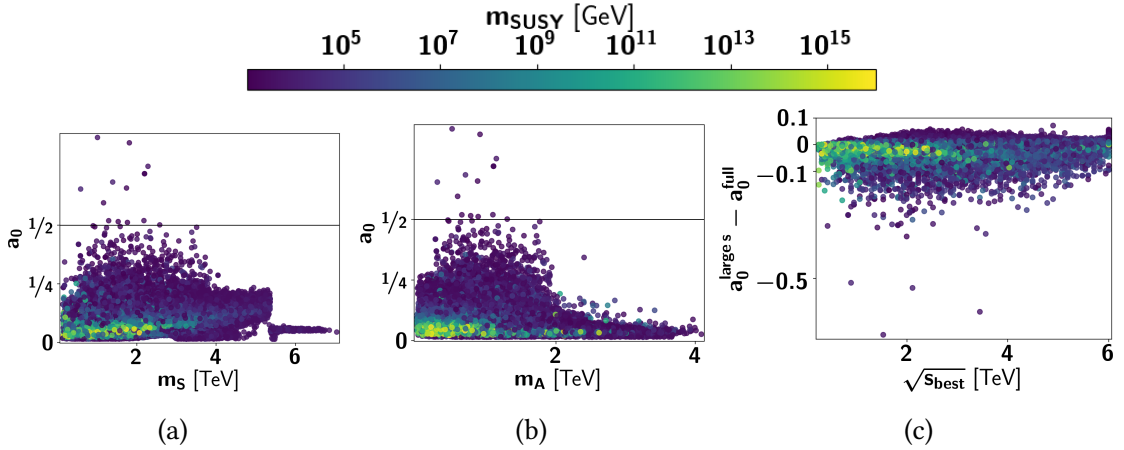


Figure 4.12.: Smallest scattering eigenvalue as a function of the matching scale and the (pseudo)scalar mass m_S (m_A). The right plot shows the difference between the smallest scattering eigenvalue in the large s approximation and the full tree-level computation depending on the scattering energy $\sqrt{s_{\text{best}}}$.

4.3.2.4. Low-Energy Constraint from the ρ -Parameter

The EFT of the split NMSSM does not contain light squarks. Thus, the only SUSY contributions to the ρ parameter are from the gauginos and higgsinos which give rise to electroweak corrections only. In contrast, stops/sbottoms would contribute with possible large mass splittings to the one-loop ρ parameter in Eq. (1.27) as well as with large QCD corrections at two-loop order. The effect of large mass splittings in the electroweakino sector is shown in Fig. 4.13a and b, where $\Delta\rho = \rho^{\text{NLO}} - 1$ is plotted against the relative mass difference of the two charginos (a) and the relative difference of the LSP mass and the heavier chargino mass (b). For the latter $M_1 > 2.5 \text{ TeV} > M_2$, μ_{eff} has been used because the bino cannot contribute to the ρ parameter due to its abelian nature.

No dependence on the mass splitting is observed and only a few points are outside the experimental uncertainty $\Delta\rho_{\text{exp}} = (3.9 \pm 1.9) \cdot 10^{-4}$ marked with the two horizontal lines in Fig. 4.13.

For the further analysis, no additional theoretical uncertainty is introduced but all points outside $\Delta\rho_{\text{exp}}$ are discarded.

4.3.2.5. Relic Density and Dark Matter Components in the Split NMSSM

The final goal is to find parameter spaces for singlet mediated singlino DM. For this purpose, the relic density dependence on the neutralino mixing elements is shown in Fig. 4.14a, to visualize if singlino DM is possible at all. The horizontal black lines mark the theoretical uncertainty, discussed in Section 4.3.1.2 around the central value of the measurement $\Omega h^2 = 0.12 \pm 0.08$. This area is exclusively shown in Fig. 4.14b.

The gaugino masses are driven by the four parameters M_1 , M_2 , $\tan\beta$ and m_{SUSY} (through the running of $g_{1,2}$), so that a rough estimate yields gaugino like DM if $M_{1,2} < v_s$. However, neutral gauginos do not directly couple to the Z boson because of the abelian $U(1)$ content. Annihilation between two gauginos is e.g. possible into two W bosons with a chargino in

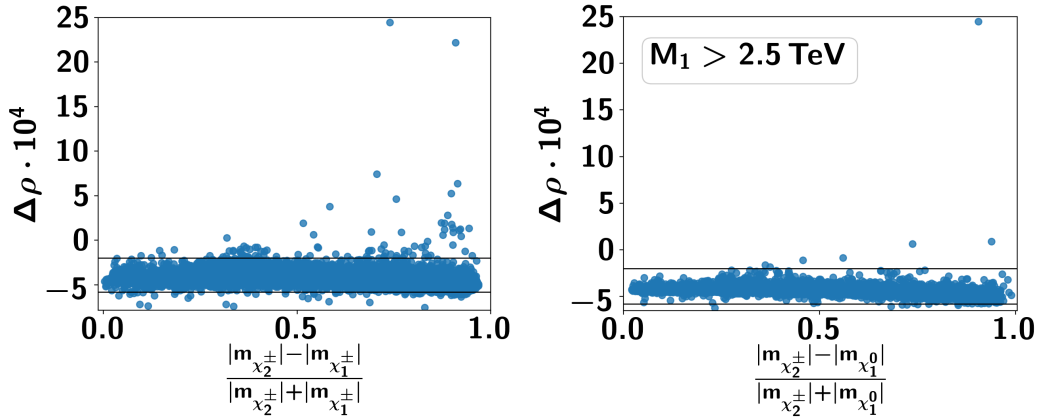


Figure 4.13.: The ρ -parameter prediction in the split NMSSM as a function of the chargino mass splitting (a) and the relative mass difference of the LSP and charged NLSP (b).

the u/t -channel. If the involved couplings are not large enough, pure gauginos easily lead to an overabundance as shown in Fig. 4.14.

The higgsino masses are controlled by v_s and λ and mix complementary to the gauginos since they share the same non-zero off-diagonal mass matrix elements. In particular, higgsinos have the possibility to co-annihilate into two SM Higgs bosons via t and u -channel exchange of the singlino. The annihilation into h_{SM} is relatively efficient as it can be seen in Fig. 4.15, where the relic density distribution is shown as a function of the LSP mass for the different LSP species (we require the corresponding mixing elements do indicate at least 90% of the corresponding field content in the LSP state). If the annihilation into the Higgs boson with a mass of 125 GeV becomes kinematically allowed, the higgsino prediction as well as the singlino prediction of Ωh^2 drop and start to increase with increasing LSP masses. However, resonant annihilation of pure higgsinos into the SM-like Higgs boson is not possible as this would violate $SU(2)$ invariance, i.e. there is no $\tilde{H}_u \tilde{H}_d H$ operator.

The singlet-component, plotted in green in Figs. 4.14 and 4.15, does not have the channels involving intermediate gauginos or charginos available. However, even without mixing, the singlino can annihilate into two SM-like Higgs bosons with a higgsino in the t/u -channel which is why the singlino-component has a similar shape as the higgsinos in Fig. 4.15. Resonant annihilation with a pure singlet in the s -channel is only possible into two higgsinos. If a singlet-doublet or singlino-higgsino admixture is present, annihilation into SM fields is possible as shown in Figs. 4.2a and 4.2b. However, the singlet mass is not an input parameter. Thus, resonant singlet exchange cannot be seen in Fig. 4.15 but must be investigated further which is the topic of the next section.

4.3.2.6. Resonant Singlino Dark Matter

From the previous discussion, one would expect that resonant singlino annihilation is possible starting from singlet masses of about 200 GeV as indicated by the lower-bound in Fig. 4.11c and the rich possibilities to accommodate light singlino LSP in the whole scan range in Fig. 4.15. However, projecting the singlino nature into the $m_{LSP} - m_S$ plane

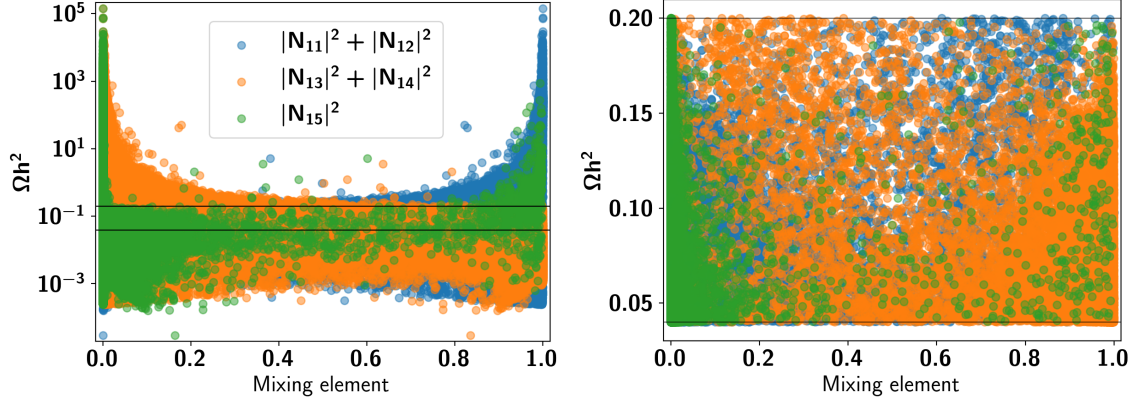


Figure 4.14.: The Relic density as a function of neutralino mixing elements. Blue, orange or green near to 1 correspond to gaugino-, higgsino- or singlino-like dark matter. The right plot zooms into the experimentally allowed region enclosed by the two black lines in the left plot.

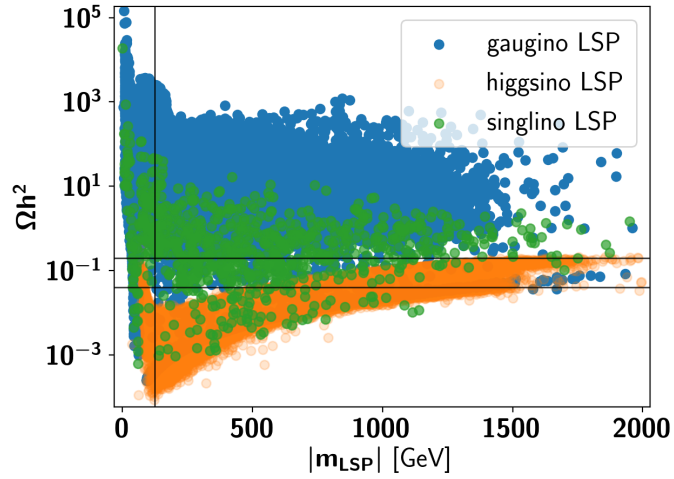
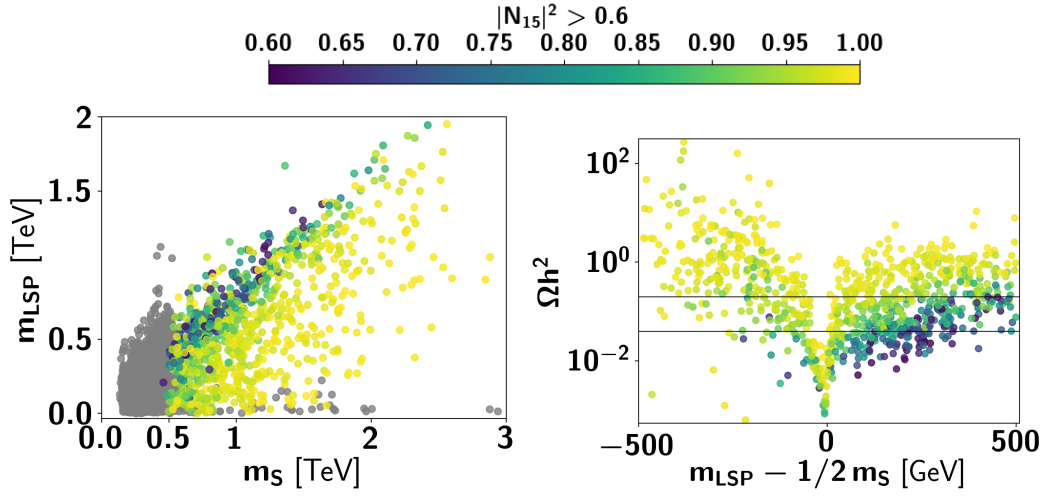


Figure 4.15.: The relic density as a function of the LSP mass for a gaugino-like LSP (blue, $|N_{11}|^2 + |N_{12}|^2 > 0.9$), higgsino-like LSP (orange, $|N_{13}|^2 + |N_{14}|^2 > 0.9$) and singlino-like LSP (green, $|N_{15}|^2 > 0.9$). The vertical line marks 125 GeV.



(a) The LSP mass as a function of the singlet mass and the singlino mixing component. Grey points are excluded by Higgs-BOUNDS. (b) The relic density as a function of the singlino-like LSP and the singlet-like mass. The area between the two black lines corresponds to the experimental constraint.

Figure 4.16.: Singlino-like dark matter. Only points with a singlino contribution to the LSP mass of at least 60% are shown.

yields a stronger lower-bound on the scalar singlet mass because v_s and κ cannot be small at the same time, as it was shown in the discussion of the input parameter correlations, cf. Fig. 4.10. This projection is given as scatter plot in Fig. 4.16a, where "singlino-like" DM is defined as $|N_{15}|^2 > 0.6$. The lower-bound on m_S is determined to ~ 500 GeV. If $m_{LSP} = 1/2 m_S$, a resonant s -channel annihilation can be achieved, starting from singlino masses of about 250 GeV.

The relic density as a function of $m_{LSP} - \frac{m_S}{2}$ is shown in Fig. 4.16 for singlino-like LSPs. As expected, a dip at zero indicates the high annihilation rate in this kinematic regime. Thus, it was shown that singlino-like dark matter can be achieved using the mechanism of resonant annihilation if the scalar superpartner of the singlino has a mass of at least 500 GeV.

4.3.3. Top-Down Versus Simplified Models: the Advantage of Matching

In Section 4.1.2 six input parameters concerning the split NMSSM scalar potential at the matching scale were counted (excluding scalar masses). However, the scalar potential of the low-energy EFT has six parameters as well

$$\tan \theta, v_s, \kappa_{SH}, \kappa_S, \lambda_S \text{ and } \lambda_H. \quad (4.24)$$

Thus, one may ask about the advantage of the matching because the number of parameters in the scalar sector is not reduced. If there is not advantage in the matching, the EFT may

be interpreted as a simplified model which is not matched to an UV completion but all parameters in Eq. (4.24) are input at the weak scale instead. The simplified model may then cover the whole parameter space as well (concerning the scalar sector) without being matched to a UV-completion. This question is addressed within this section.

In the EFT, the low-energy parameters counted in Eq. (4.24) are not an input at the electroweak scale but are expressed in terms of NMSSM parameters at the matching scale and undergo an RGE running. The NMSSM is a more fundamental theory since SUSY connects operators from the scalar, fermion and gauge sector.

Thus, the parameter space of a matched EFT can significantly differ from an simplified model. This is because experimental and theoretical constraints from e.g. the scalar sector are transmitted into the fermion sector and vice versa. To illustrate this connection, the three quartic couplings of the split NMSSM λ_{SH} , λ_S and λ_H are compared at the scale m_t . In Fig. 4.17a, the numerical results of the couplings, after the matching and the running to m_t was performed, are shown. Alternatively, we interpret the EFT as a simplified model and independently scan over all parameters in the effective Lagrangian without performing a matching but using the prior discussed constraints $m_h = 125 \pm 2$ GeV, $m_{\chi_0^\pm} > 94$ GeV and $m_{\tilde{g}} > 1.5$ TeV. The results of this scan in the $(\lambda_{SH}, \lambda_S, \lambda_H)$ -space are shown in Fig. 4.17b. The singlet-like quartic coupling λ_S is indeed identical in both approaches, since it concerns a pure BSM sector (i.e. κ^2). However, λ_H and λ_{SH} have completely different shapes in both approaches. In case of λ_H in the top-down approach, there is a deep connection to the weakly coupled gauge sector keeping it small for small values of λ . The presence of singlet F-terms in λ_H , is also connected to large $\lambda_{SH} \propto \lambda(\lambda - \kappa)$ which cannot always compensate each other to accommodate the correct Higgs boson mass and e.g. respect the mass constraint on charginos at the same time. This is not the case in the simplified model where scalar and fermion masses are independent parameters.

For completeness, the comparison between the two approaches is extended to the fermion sector in Fig. 4.18 where all YUKAWA couplings additional to the SM are shown. In contrast to the scalar sector, where spontaneous symmetry occurs, no predictions among the different parameters in the fermion sector are made in the simplified model. The matched prediction for the couplings $Y_s^d(Y_s^u)$ shown in the upper-left plot in Fig. 4.18 is aligned on the bisecting line at the matching scale but gets rotated clockwise through the stronger RGE running of Y_s^u . Likewise, the $Y_{ud}(Y_s)$ dependence in the upper-right plot (actually $\lambda(\kappa)$ at the matching scale) was already shown in Fig. 4.10a without the involved RGE running. The distribution is not changed but only scaled by a factor of $\sim 1/2$ through the RGE running. The YUKAWA couplings shown in the lower row of Fig. 4.18 are given by the SM gauge couplings and $\tan \beta$ at the matching scale which determine the shape of the right edge of the distributions. To explicitly demonstrate the effect of the RGE running, the values of the couplings at the matching scale are shown in red in the lower-right plot. The running of the YUKAWA couplings $g_{1,2}^{u,d}$ to m_t then deforms the shape of the parameter space to lower as well as larger values.

It was shown that the matching is crucial for determining the valid parameter space

of an EFT for a given UV completion. In addition, the RGE induced effects are not negligible and can change the shape in parameter distributions significantly.

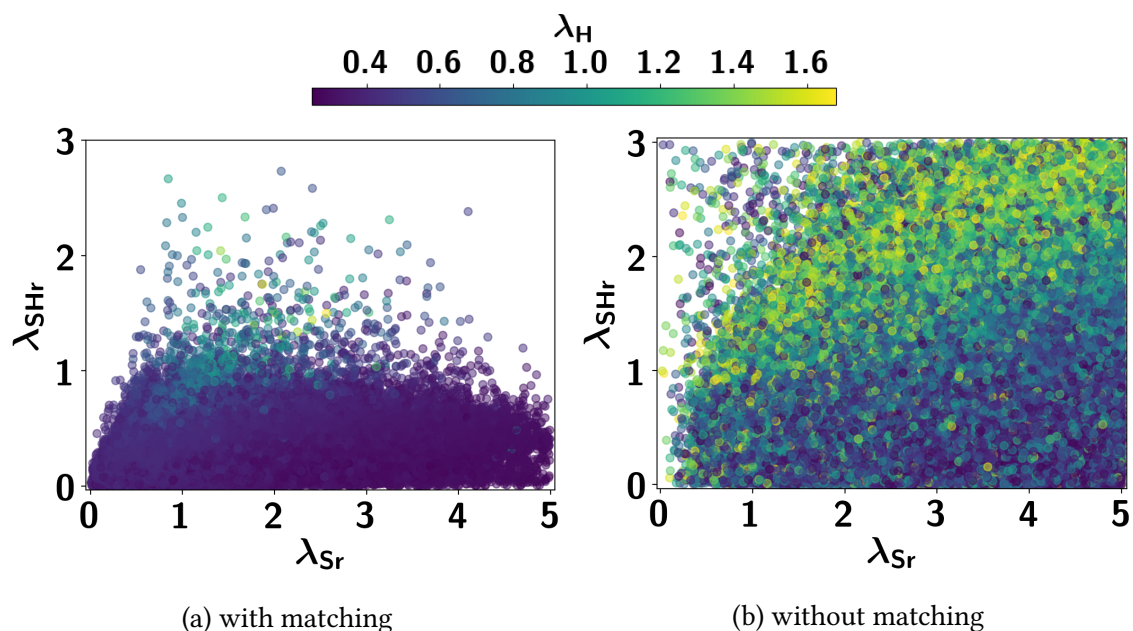


Figure 4.17.: Comparison between parameter scans in a top-down approach (a) and a simplified model (b) of the split NMSSM. The correlations between the three quartic couplings evaluated at m_t are shown. In (b) the couplings are input parameters at the weak scale while in (a) they are calculated through the matching conditions and undergo an RGE running.

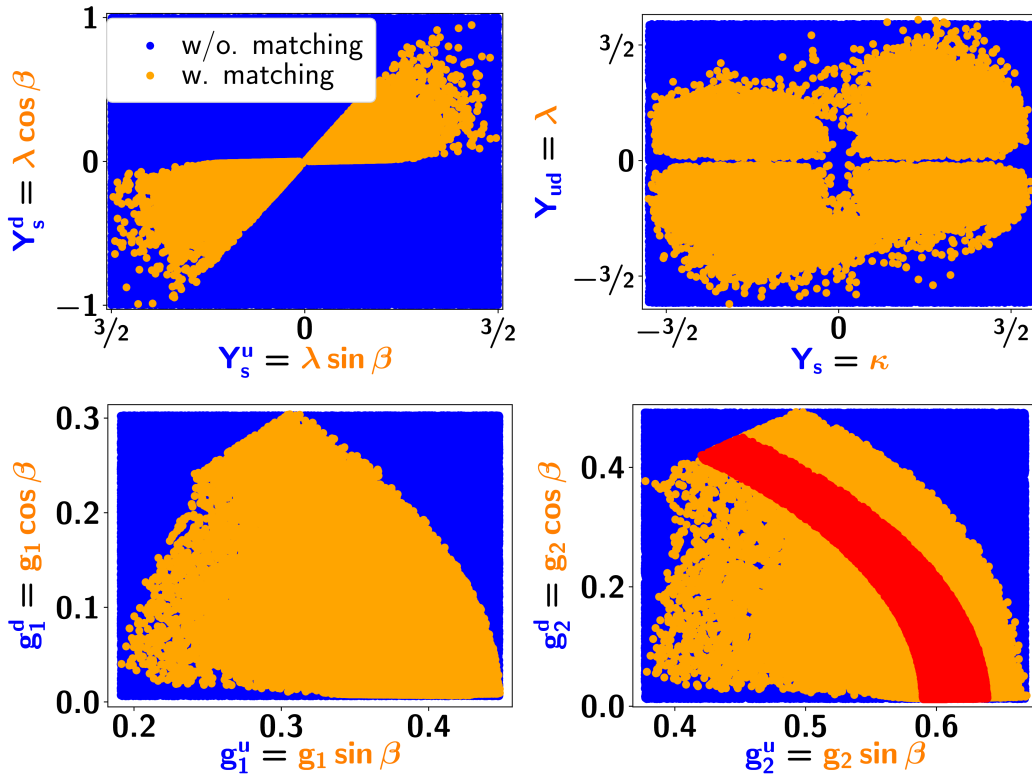


Figure 4.18.: Comparison between split NMSSM scans in the fermion sector with (orange) and without (blue) matching. All parameters values are given at the scale m_t while the red band in the lower-right plot marks values at the matching scale.

5. Summary and Outlook

Effective field theory techniques have been proven to be a powerful framework for the precise description of low-energy observables in the presence of large mass hierarchies. In contrast, fixed-order Higgs mass calculations in SUSY models suffer from large uncertainties starting at $\mathcal{O}(1 \text{ TeV})$ mass gaps. Thus, increasing lower bounds on colored scalar particle masses, naturally appearing in SUSY models, requires the use of EFTs in order to compete with the accuracy of current experiments.

At the same time, a landscape of complex BSM models demands for automation mechanisms of theoretical predictions. Computer programs such as SARAH/SPHENO [11, 13] have been developed in order to automatize the tree-level as well as higher-order calculations of mass spectra, decays, RGEs, theoretical constraints and low-energy observables at fixed-order. Thus, it is natural to extend such tools to include the use of EFT techniques in models with large mass hierarchies.

The focus of this work was to develop a generic method that allows to perform the matching of the scalar sectors of two arbitrary renormalizable QFTs at the one-loop order. The purpose of such a matching is to give precise predictions on scalar masses in theories with a large mass hierarchy and additional light scalars. The theoretical foundations for such a matching were reviewed in Chapter 1 with the focus on supersymmetric theories. The actual method and its implementation in the program code of SARAH was developed in Chapter 2. The correct separation of scales, belonging to the infra-red and ultra-violet parts of the theories to be matched, is crucial for the decoupling. This was explicitly demonstrated in a toy-model example in Chapter 2. Furthermore, the implementation includes all calculations necessary for the matching of supersymmetric models such as $\overline{\text{MS}} - \overline{\text{DR}}$ conversion and the calculation of gauge coupling threshold corrections of any renormalizable gauge theory.

The implementation was validated in Chapter 3 by comparing with results available in the literature. Two high-scale SUSY scenarios for the MSSM [9] and the NMSSM [10] as well as an effective 2HDM [8, 61] emerging from the MSSM were used for this purpose. In particular, the partial one-loop results for the NMSSM were completed and deviations of up to 2 GeV in the SM Higgs boson mass prediction have been found.

Non-minimal split SUSY was investigated in a dedicated study in Chapter 4. The split NMSSM was matched onto an EFT containing light fermions and one complex singlet, in addition to the SM fields. While the fermion sector was matched at tree-level, the new implementation has been used to perform a one-loop matching of the scalar sectors. A first phenomenological study, taking some theoretical as well as experimental constraints into account, found deviations of $\mathcal{O}(10\%)$ in the prediction of quartic couplings between tree-level and one-loop order matching. Variations in the scalar mass

predictions can also amount to several percent. The behaviour of trilinear couplings near the TeV-scale can be dangerous as potentially large higher-order corrections of the form [trilinear coupling] $\cdot m_{SUSY}^{-2}$ come into play.

The split NMSSM is relatively stable concerning the tree-level perturbative unitarity constraint, as it was shown in Section 4.3.2.3. Although the low-energy theory contains light $SU(2)$ doublets, no large deviations in the ρ -parameter have been found. However, Higgs boson searches constrain the CP-even singlet-like scalar to be heavier than ~ 250 GeV while the CP-odd singlet can be much lighter. Resonant singlino dark matter requires an appropriate singlet-doublet admixture as well as a singlino LSP which yields a lower bound on the scalar singlet mass of ~ 500 GeV and thus $m_{LSP} \approx 250$ GeV for resonant DM. In addition, the EFT of the split NMSSM has been interpreted as a simplified model at the weak scale demonstrating that such an effective model is not able to predict the same parameter correlations compared to its UV completion. In particular, comparisons between the scalar sectors have shown dramatic deviations between the two approaches even though the number of free parameters in the scalar sectors is equal. Taking the fermion sector into account, simplified models will always have more free parameters than SUSY models, which connect the fermion sector to the scalar sector. It was shown that this has dramatic consequences for the correlation among different YUKAWA couplings and thus influences e.g. DM searches.

However, the phenomenological study carried out in this thesis was motivated by a first dedicated application of the implemented matching routines and their numerical impact. Additional experimental as well as theoretical constraints may be included in future studies. The presence of potentially large trilinear couplings while requiring a small singlet mass may not always lead to a stable vacuum. Computer programs such as VEVACIOUS [96] are able to compute the global minima of extended scalar sectors. In addition, experimental constraints such as signal rates provided by e.g. HIGGSIGNALS [97] or direct detection of the LSP using MICROMEAS [91] could be considered as well. Future work may use these tools to constraint the split NMSSM parameter space further.

Furthermore, the method of matching scalar sectors presented in this thesis may be extended to the YUKAWA sector. In particular, this is necessary for a consistent matching when a tower of EFTs is considered. That is, if multiple matchings and RGE runnings are subsequently performed to account for more complex mass hierarchies. Therefore, the implementation of EFT towers is also reserved for future work.

Higher-order threshold corrections beyond the one-loop order are only known for specific models. The SM Higgs boson mass receives an additional shift from SUSY QCD corrections of up to $\mathcal{O}(2 \text{ GeV})$ in the high-scale MSSM for maximal stop mixing and relatively low matching scales while three and four-loop effects are in the sub-GeV range [6, 57]. The implementation of generic two-loop threshold corrections that include wavefunction renormalization effects as well as one-particle-reducible diagrams (not covered by the effective potential approach) is a possible but exhaustive task for the future.

A. Appendix

A.1. Topologies

In this appendix we provide a complete list of all possible one-loop topologies with 2, 3 and four external scalars which were discussed in Chapter 2.

A.1.1. Notation

For completeness, the notation already introduced in Chapter 2 is repeated in Fig. A.1. A topology is described by a string consisting of maximum five characters. It starts with the specification of the diagram type which can be tree-level (T), self-energy (S), WFR (W) or ordinary one-loop diagram (blank) followed by a letter specifying the involved loop integral defined in Appendix A.2. In the third place, the number of external fields is specified while the fourth digit indicates a 1PI (1) or 1PR (2) diagram type. The last digit is a counting index (blank means only one diagram of that type exists).

The external fields are always light scalars (dashed lines) while internal straight lines are placeholders for all kinds of propagators of different spin and mass.

A.1.2. Generic Tree-Level Graphs

A.1.2.1. Two-Point Function



Figure A.2.: The scalar propagator "T2" at tree-level.

A.1.2.2. Three-Point Function

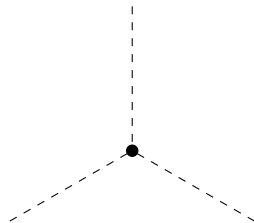


Figure A.3.: The only tree-level graph "T3" with 3 external scalars.

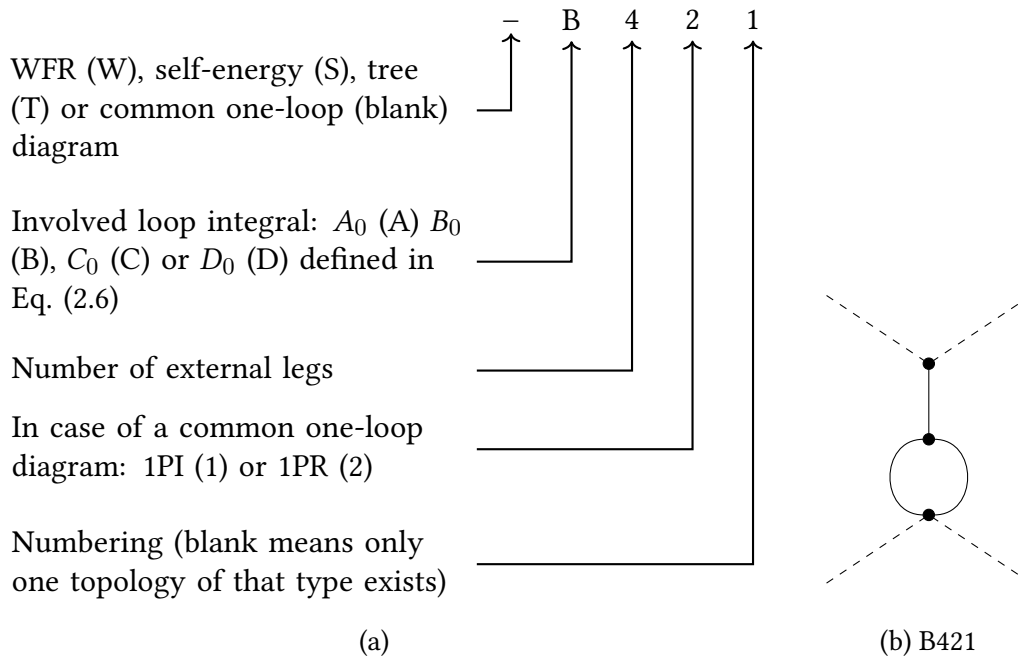


Figure A.1.: Notation on topologies shown in this appendix. The example expression explained in (a) corresponds to the topology shown in (b).

A.1.2.3. Four-Point Function

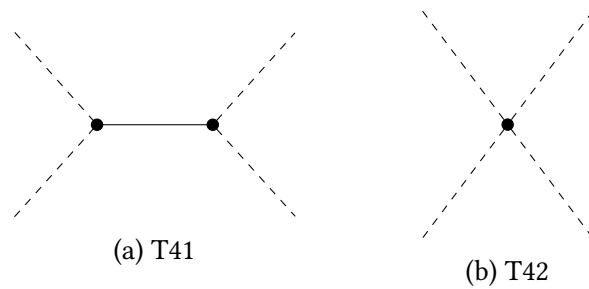


Figure A.4.: Tree-level graphs with 4 external scalars. The straight line can be a heavy scalar or a heavy vector boson.

A.1.3. Generic One-Loop Graphs

A.1.3.1. Two-Point Function

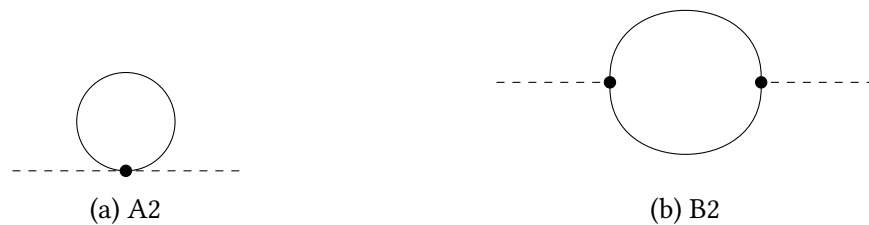


Figure A.5.: Scalar propagator topologies at the one-loop level.

A.1.3.2. Three-Point Function

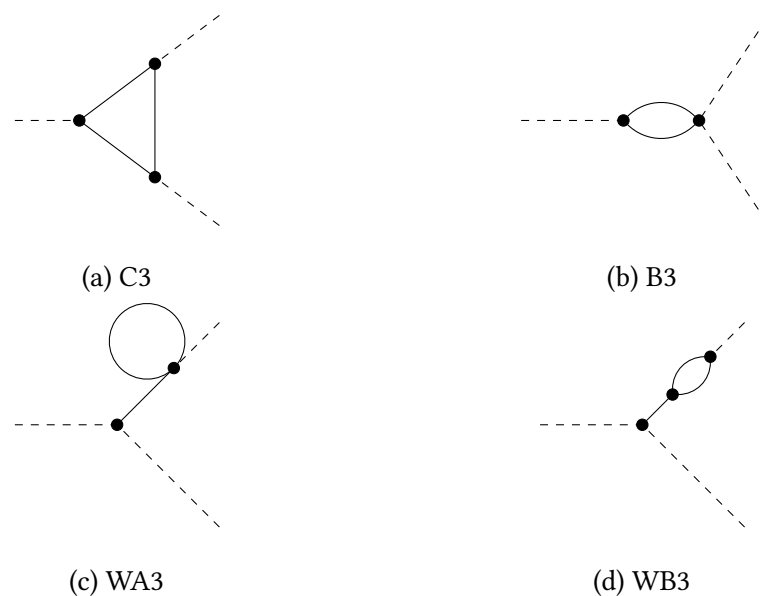


Figure A.6.: One loop three-point topologies. All diagrams which contain at least one heavy fermion, scalar or vector boson have to be computed. Diagrams (c)-(d) account for wave function renormalization constants. The notation used to describe the topologies is explained in Fig. A.1.

A.1.3.3. Four-Point Function

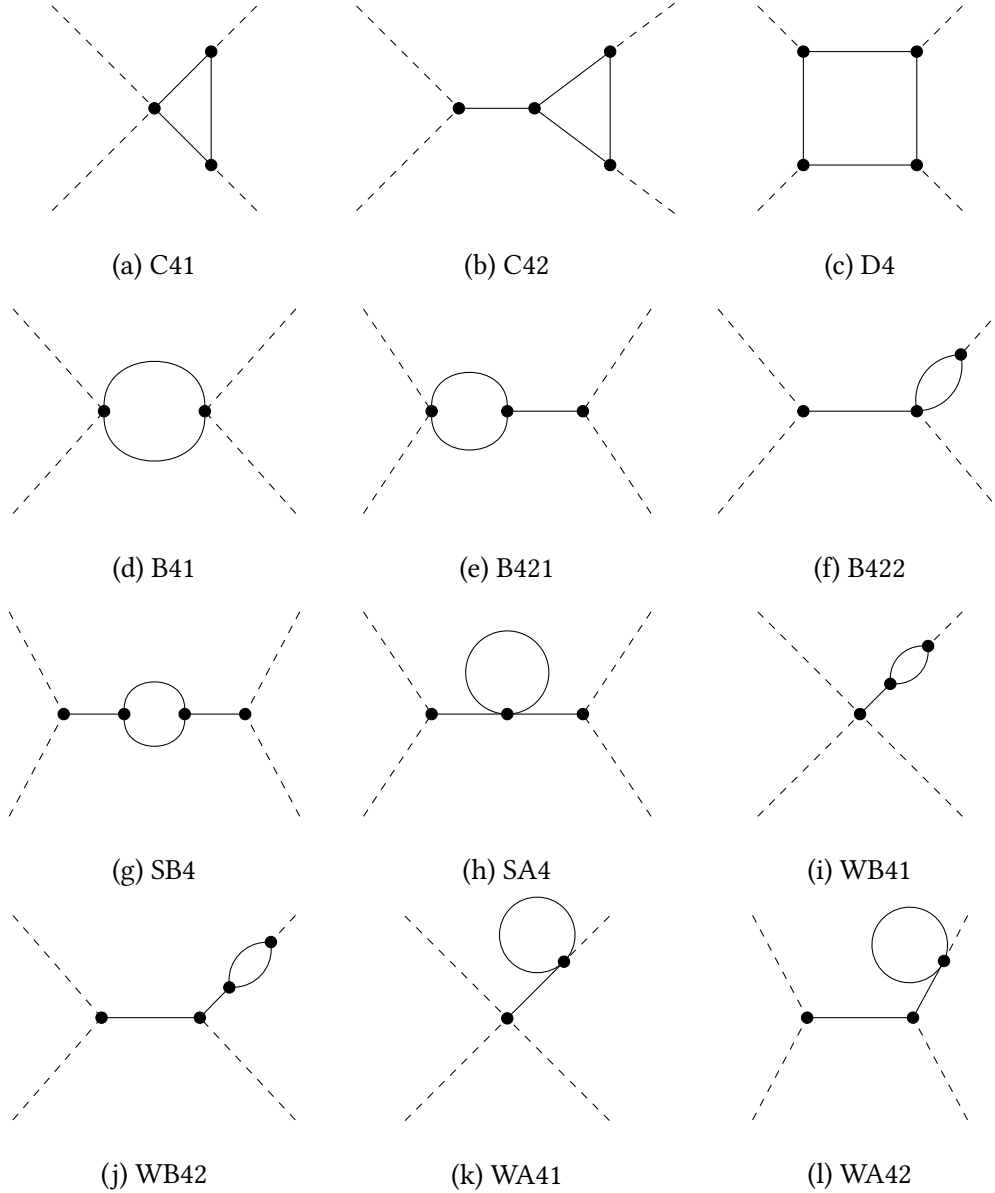


Figure A.7.: One loop four-point topologies. Topologies (i)-(l) account for wave function renormalization constants while (g)-(h) encode self-energy corrections of heavy fields. The notation used to describe the topologies is explained in Fig. A.1.

A.2. Loop Functions with vanishing External Momenta

In this appendix we give the analytical expressions for all loop functions used in the matching routines. In particular, we list the limits for all possible combinations of vanishing and equal masses.

A.2.1. Definition of the Loop Functions

For better readability, we repeat the definitions from Section 2.2. The common prefactor

$$\kappa_D = \frac{(2\pi Q)^{4-D}}{i\pi^2} \quad (\text{A.1})$$

and the integrand

$$I_n = \prod_{i=1}^n (q^2 - m_i^2)^{-1} \quad (\text{A.2})$$

simplify the definitions of the loop integrals

$$\begin{aligned} A_0(m^2) &= \kappa_D \int d^D q I_1 , \\ B_0(m_1^2, m_2^2) &= \kappa_D \int d^D q I_2 , \\ C_0(m_1^2, m_2^2, m_3^2) &= \kappa_D \int d^D q I_3 , \\ D_0(m_1^2, m_2^2, m_3^2, m_4^2) &= \kappa_D \int d^D q I_4 . \end{aligned} \quad (\text{A.3})$$

The integrand I_n is symmetric w.r.t to the masses and thus also the loop functions are symmetric w.r.t. their arguments. We define the following abbreviations for finite logarithmic terms

$$t_i \equiv \log \frac{m_i^2}{Q^2} \quad t_{ij} \equiv \log \frac{m_i^2}{m_j^2}, \quad (\text{A.4})$$

as well as for diverging terms

$$\begin{aligned} \Delta_t &\equiv \lim_{\epsilon_{match}^2 \rightarrow 0} \log \frac{\epsilon_{match}^2}{Q^2}, \\ \Delta_D &\equiv \lim_{\epsilon_{match}^2 \rightarrow 0} \frac{1}{-\epsilon_{match}^2}. \end{aligned} \quad (\text{A.5})$$

A.2.2. One- and Two-Point Integrals

The tadpole integral A_0 is given by

$$A_0(m^2) = m^2(1 - t) , \quad (\text{A.6})$$

$$A_0(0) = 0 , \quad (\text{A.7})$$

whereas the two-point integral B_0 is

$$B_0(m_1^2, m_2^2) = \frac{A_0(m_1^2) - A_0(m_2^2)}{m_1^2 - m_2^2} \quad (\text{A.8})$$

$$= 1 - t_2 - \frac{m_1^2}{m_1^2 - m_2^2} t_{12} , \quad (\text{A.9})$$

$$B_0(m^2, 0) = 1 - t , \quad (\text{A.10})$$

$$B_0(m^2, m^2) = -t , \quad (\text{A.11})$$

$$B_0(0, 0) = -\Delta_t . \quad (\text{A.12})$$

In addition, the tensor integral

$$B_1(m_1^2, m_2^2) = \frac{1}{p^2} p^\mu B^\mu = \frac{\kappa_D}{p^2} \int d^D q \, p q \left[(q^2 - m_1^2) (q + p)^2 - m_2^2 \right]^{-1} \quad (\text{A.13})$$

is not decomposed for vanishing external momenta by FORMCALC but needed for off-diagonal WFR factors with internal fermions. The analytical expression for arbitrary p^2 is given in Ref. [66]. In the limit of vanishing external momentum the B_1 -function reads

$$B_1(m_1^2, m_2^2) = -\frac{1}{4(m_1^2 - m_2^2)} \left[m_1^2 + m_2^2 - 2m_1^2 B_0(m_1^2, 0) + (4m_1^2 - 2m_2^2) B_0(m_1^2, m_2^2) \right] , \quad (\text{A.14})$$

$$B_1(m^2, 0) = -\frac{1}{4} \left(1 + 2B_0(m^2, 0) \right) , \quad (\text{A.15})$$

$$B_1(m^2, m^2) = \frac{1}{2} t , \quad (\text{A.16})$$

$$B_1(0, 0) = \frac{1}{2} \Delta_t . \quad (\text{A.17})$$

A.2.3. Triangle Integrals

The three-point function can be simplified with the definition

$$q_1 \equiv \frac{m_2^2}{m_1^2} \quad q_2 \equiv \frac{m_3^2}{m_1^2} , \quad (\text{A.18})$$

which yields

$$C_0(m_1^2, m_2^2, m_3^2) = \frac{B_0(m_1^2, m_3^2) - B_0(m_2^2, m_3^2)}{m_1^2 - m_2^2} \quad (\text{A.19})$$

$$= -\frac{q_1 t_{21} (q_2 - 1) + q_2 t_{32} (1 - q_1)}{m_1^2 (-1 + q_1)(q_1 - q_2)(-1 + q_2)}, \quad (\text{A.20})$$

$$C_0(m_1^2, m_1^2, m_2^2) = \frac{m_2^2 - m_1^2 + m_2^2 t_{12}}{(m_1^2 - m_2^2)^2}, \quad (\text{A.21})$$

$$C_0(m^2, m^2, m^2) = -\frac{1}{2m^2}, \quad (\text{A.22})$$

$$C_0(m_1^2, m_2^2, 0) = -\frac{t_{12}}{m_1^2 - m_2^2}, \quad (\text{A.23})$$

$$C_0(m^2, m^2, 0) = -\frac{1}{m^2}, \quad (\text{A.24})$$

$$C_0(m^2, 0, 0) = \frac{1}{m^2} - \frac{t}{m^2} + \frac{\Delta_t}{m^2}, \quad (\text{A.25})$$

$$C_0(0, 0, 0) = \frac{1}{2}\Delta_D. \quad (\text{A.26})$$

A.2.4. Box Integrals

Analogously we compute the four-point integral in all mass combinations

$$D_0(m_1^2, m_2^2, m_3^2, m_4^2) = \frac{1}{m_1^2 - m_2^2} \left(C_0(m_1^2, m_3^2, m_4^2) - C_0(m_2^2, m_3^2, m_4^2) \right), \quad (\text{A.27})$$

$$D_0(m_1^2, m_1^2, m_2^2, m_3^2) = \frac{1}{m_2^2 - m_3^2} \left(\frac{-m_1^2 + m_2^2 + m_2 t_{12}}{(m_2^2 - m_1^2)^2} + \frac{m_1^2 - m_3^2 - m_3^2 t_{13}}{(m_3^2 - m_1^2)^2} \right), \quad (\text{A.28})$$

$$D_0(m_1^2, m_1^2, m_2^2, m_2^2) = \frac{1}{(m_1^2 - m_2^2)^3} \left(-2m_1^2 + 2m_2^2 + (m_1^2 + m_2^2) t_{12} \right), \quad (\text{A.29})$$

$$D_0(m_1^2, m_1^2, m_1^2, m_2^2) = \frac{-m_1^2 + m_2^2 + 2m_1^2 m_2^2 t_{12}}{2m_1^2 (m_2^2 - m_1^2)^3}, \quad (\text{A.30})$$

$$D_0(m_1^2, m_1^2, m_1^2, m_1^2) = \frac{1}{6m_1^2}, \quad (\text{A.31})$$

$$(\text{A.32})$$

and with at least one vanishing mass (corresponding to a light field being part of the EFT),

$$D_0(m_1^2, m_2^2, m_3^2, 0) = \frac{(m_2^2 - m_3^2) t_{31} + (m_3^2 - m_1^2) t_{32}}{(m_1^2 - m_2^2)(m_1^2 - m_3^2)(m_2^2 - m_3^2)}, \quad (\text{A.33})$$

$$D_0(m_1^2, m_2^2, m_2^2, 0) = \frac{m_1^2 - m_2^2 + m_2^2 t_{21}}{m_2^2 (m_1^2 - m_2^2)}, \quad (\text{A.34})$$

$$D_0(m^2, m^2, m^2, 0) = \frac{1}{2m^2}, \quad (\text{A.35})$$

$$D_0(m_1^2, m_2^2, 0, 0) = \frac{t_2}{m_1^2 m_2^2} + \frac{t_{21}}{m_1^2 (m_1^2 - m_2^2)} - \frac{\Delta_t}{m_1^2 m_2^2}, \quad (\text{A.36})$$

$$D_0(m^2, m^2, 0, 0) = -\frac{2}{m^2} + \frac{t}{m^2} - \frac{\Delta_t}{m^2}, \quad (\text{A.37})$$

$$D_0(m^2, 0, 0, 0) = \frac{1}{m^2} - \frac{t}{m^2} + \frac{\Delta_t}{m^2} - \frac{\Delta_D}{2m^2}, \quad (\text{A.38})$$

$$D_0(0, 0, 0, 0) = -\frac{1}{6} \Delta_D^2. \quad (\text{A.39})$$

A.2.5. Derivatives of the One- and Two-Point Functions

Although already given in Eq. (2.18) we list the derivatives here for completeness

$$\partial A_0 = 0, \quad (\text{A.40})$$

$$\partial B_0(m_1^2, m_2^2) = \kappa_D \partial_p^2 \int d^D q \left((q+p)^2 - m_2^2 \right)^{-1} \left(q^2 - m_1^2 \right)^{-1} \Big|_{p^2 \rightarrow 0} \quad (\text{A.41})$$

$$= \frac{1}{2 (m_1^2 - m_2^2)^2} \left(m_1^2 + m_2^2 + \frac{2m_1^2 m_2^2 t_{21}}{m_1^2 - m_2^2} \right). \quad (\text{A.42})$$

Their mass limits are

$$\partial B_0(m^2, m^2) = \frac{1}{6m^2}, \quad (\text{A.43})$$

$$\partial B_0(m^2, 0) = \frac{1}{2m^2}, \quad (\text{A.44})$$

$$\partial B_0(0, 0) = -\frac{1}{6} \Delta_D. \quad (\text{A.45})$$

A.3. The SARAH Extension Manual

A.3.1. The SARAH NLO Matching Interface

This appendix describes the user interface to the matching routines available in SARAH from version 4.14.0.

A.3.1.1. Initialization

To initialize the routines, a MATHEMATICA kernel has to be started and the UV model must be initialized by SARAH,

```
In[1] <<SARAH`
In[2] Start["ModelName"]
In[3] InitMatching[Options]
```

The possible options for the initialization procedure are

- `Parametrisation` \rightarrow `$LIST`
 - Default: `{}`
 - Description: list of specific parametrisations of all model parameters
 - Example: `{vu \rightarrow v Sin[ArcTan[TanBeta]]}`
- `Assumptions` \rightarrow `$LIST`
 - Default: `{}`
 - Description: list of assumptions for parameters in the model in order to simplify the expressions
 - Example: `{v>0, TanBeta>0}`
- `SolveTadpoles` \rightarrow `$LIST`
 - Default: `{}`
 - Description: list of parameters which are obtained by the tadpole equations
 - Example: `{mHu2, mHd2}`
- `ReadLists` \rightarrow `$BOOL`
 - Default: `False`
 - Description: if set to `True`, the calculation of the vertices is skipped, but results stored in a previous session are used
- `InputFile` \rightarrow `$FileName`
 - Default: `False`
 - Description: can be used to define an input file containing all necessary informations

where `InputFile` has to be given if the SPHENO output is to be generated.

A.3.1.2. Interactive Mode

After the initialization and calculation of all mass matrices, involving the given simplifications and parametrisations, one can compute the leading order (LO) and next-to-leading order (NLO) corrections to an amplitude with the external fields given in the list `fieldlist` with the commands

```
In[1]      EFTcoupLO[fieldlist, Options]
In[2]      EFTcoupNLO[fieldlist, Options]
```

where the possible options are

- `Simplifications` \rightarrow `$LIST`
 - Default: `{}`
 - Description: list with additional simplifications in the current calculation beyond those already defined in `InitMatching`.
- `Topologies` \rightarrow `$LIST`
 - Default: `{}`
 - Description: list of topologies to include into the calculation. If empty, all topologies are used. Topologies are denoted as in Fig. A.1
 - Example: `{B[4][1], B[4][2][1], B[4][2][2]}` or equivalently `{B[4]}`
- `ExcludeFields` \rightarrow `$LIST`
 - Default: `{}`
 - Description: list of fields that are excluded when appearing as internal field
 - Example: `{Cha, Chi}` e.g. to exclude electroweakinos for a split SUSY scenario
- `GaugeThresholds` \rightarrow `$BOOL`
 - Default: `True`
 - Description: whether to include the contributions from gauge coupling thresholds to the amplitude
- `ShiftMSDR` \rightarrow `0/1/2/Automatic`
 - Default: `Automatic`
 - Description: whether to include the $\overline{\text{MS}}$ – $\overline{\text{DR}}$ conversion factors. 0: no, 1: inclusive, 2: exclusive, `Automatic`: decide between 1 and 0 depending on the type of considered model (SUSY or non-SUSY).
- `Debug` \rightarrow `$BOOL`
 - Default: `False`

- Description: multiplies each amplitude with a debug variable marking its topology and field insertions
- Example: `debug[B][4][1][hh[2], hh[1]]`
- `SimplifyResults` \rightarrow \$BOOL
 - Default: True
 - Description: whether to simplify the results using the given assumptions
- `ExplicitLoopFunctions` \rightarrow \$BOOL
 - Default: True
 - Description: whether to use the definitions in Appendix A.2 for loop functions. If set to `False`, the FORMCALC notation of the loop functions is used e.g. a $B_0(m_1^2, m_2^2)$ function is denoted by `B0i[bb0, 0, m1^2, m2^2]`.

A.3.1.3. Batch Mode

The complexity of the calculation requires a high level on reproducibility of the results. For this purpose it is possible to write input files that contain all necessary information for the matching to a given EFT model. This includes all information already discussed in the interactive mode. In addition, the correspondence between couplings in the low-energy model and amplitudes in the UV model, as they were for example given in Section 3.3 for a 2HDM matching, have to be defined. Also the generation of \LaTeX output, for an evaluation of expressions in a human readable format, can be controlled. The *batch mode* uses this input file and is started during the initialization

```
In[1] InitMatching[InputFile->"/path/to/Matching.m"]
```

where the content of `Matching.m` is e.g.

Matching.m

```

1 (* Defines a name for the current settings *)
2 $NameUV= "HighScaleMSSMLowMA";
3
4 (* Options equivalent to corresponding options of InitMatching *)
5 $ParametrisationUV = { vd-> epsUV, vu-> epsUV, B[\mu] -> epsUV^2};
6 $SimplificationsMatching={ conj[x_] -> x, ... };
7 $AssumptionsMatching={ TanBeta>0};
8 $SolveTadpolesUV = {mHd2, mHu2};
9
10 (* define the matching conditions *)
11 $MatchingConditions = {
12   Lambda1 -> -1/6 hh[1].hh[1].hh[1].hh[1],
13   Lambda2 -> -1/6 hh[2].hh[2].hh[2].hh[2],
14   Lambda3 -> -hh[1].hh[1].Hpm[2].conj[Hpm[2]],
15   Lambda4 -> hh[1].hh[2].Hpm[2].conj[Hpm[1]] +
      \(\leftrightarrow\) I*hh[1].Ah[2].Hpm[1].conj[Hpm[2]],

```

```

16   Lambda5 -> hh[1].hh[2].Hpm[2].conj[Hpm[1]] -
      ↪ I*hh[1].Ah[2].Hpm[1].conj[Hpm[2]],
17   Lambda6 -> -hh[1].hh[2].Hpm[1].conj[Hpm[1]],
18   Lambda7 -> -hh[1].hh[2].Hpm[2].conj[Hpm[2]]
19   };
20
21   (*Exclude light fields from being integrated out*)
22   $ExcludeFieldsMatching={hh,Ah,Hpm};
23
24   (* wheter to create TeX output *)
25   $EFTcouplingsToTeX = True/False;
26
27   (* additional TeX symbols *)
28   $AdditionalTeXsymbols={ Lambda1 -> "\\lambda_1", ... };

```

The variable `$MatchingConditions` is a list of matching conditions to be applied at the matching scale. In this example, we implemented the matching conditions for the effective 2HDM in a high-scale MSSM as in Section 3.3.

If `$EFTcouplingsToTeX` is set to `True`, a \TeX file is generated containing the results of all mass and rotation matrices as well as matching calculations. Additional \TeX symbols to those defined in the UV model can be defined in the `$AdditionalTeXsymbols` variable.

The results of the matching are stored in

$$\text{\$SARAH_Directory}/\text{Output}/\text{\$Model}/\text{EWSB}/\text{Matching}/\text{\$NameUV}$$

and can be used in other `MATHEMATICA/SARAH` sessions. The produced \TeX file

$$\text{MatchingConditions_}\text{\$Model_}\text{\$NameUV}.\text{tex}$$

can be compiled using a standard \LaTeX compiler.

A.3.1.4. SPheno Output

It is also possible to generate a `SPHENO` output using the analytical results. For this purpose, the command

```
In[1] ExportToSPheno[options]
```

exists which can be used after running the batch mode. If only the matching conditions in Form of `FORTTRAN` routines are demanded, no additional options need to be given. The output is given as `FORTTRAN` functions with a naming pattern

$$\text{EFTcoupling}\langle\text{counting number}\rangle$$

stored in the output directory mentioned above. An example function could look like

```

1 Real(dp) Function EFTcoupling1(g1,g2,TanBeta,Yd,Ye,Yu)
2 Implicit None
3 Complex(dp),Intent(in) :: Yd(3,3),Ye(3,3),Yu(3,3)

```

```

4 Real(dp),Intent(in) :: g1,g2,TanBeta
5 EFTcoupling1 = 1/4*(g1**2+g2**2)*(TanBeta-1)**2/(TanBeta+1)**2
6 End Function EFTcoupling1

```

These functions can be used in the FORTRAN output of the EFT model by specifying the boundary conditions at the matching scale in the file

SPheno/<Model>/Boundaries_<model>.f90

However, it is also possible to automatically adjust an existing SPheno.m file of a model to include these functions and generate the modified FORTRAN code with the MakeSPheno function as it is done in previous SARAH versions. For this purpose, the following options exist:

- EFTmode -> "ModelName"
 - Default: False
 - Description: name of the EFT model directory
 - Example: "SplitSUSY_NMSSM"
- SPhenoFile -> "FileName.m"
 - Default: "SPheno.m"
 - Description: .m SPheno file which is used as template
- MatchingScale -> \$Symbol
 - Default: UVscaleQ
 - Description: the matching scale to use
 - Example: MSUSY

This uses a SPheno.m file as template, and appends the boundary conditions as well as new parameter definitions to it. Also the FORTRAN functions are saved beside the new SPHENO input file and are used in there. Thus, there is no need to program FORTRAN code at all

SPheno.m

```

1 BoundaryHighScale = Join[BoundaryHighScale,{
2   {[ Lambda ],EFTcoupling1[g1,g2,TanBeta,Yd,Ye,Yu]}
3   }];
4 ...
5 SelfDefinedFunctions = {
6   ReadString[ToFileName[
7     $sarahCurrentMatchingDir,
8     "EFTcoupling1_SPhenoEFT_MSSM.f90" ]]
9   };

```

Furthermore, a new SPheno.m can be generated using information from variables set in the input file

Matching.m

```

1 (* ... Continue with Matching.m from above *)
2
3 $ExportToSPheno=True;
4 (*define the low-energy EFT model*)
5 $SPhenoEFTmodel="THDM-IInoZ2";
6 (*extra input parameters of the EFT model*)
7 $SPhenoMINPAR={
8   {1, m0},
9   {2, mGauginos},
10  {3, TanBeta},
11  {4, MuSUSY},
12  {5, Azero},
13  {6, MA}};
14 (*extra boundary conditions*)
15 $SPhenoBoundaryHighScale={};
16 $SPhenoBoundaryRenScale={
17   {M12, -MA^2 TanBeta/(1+TanBeta^2)}
18 };
19 (* Tadpole equations in the EFT model*)
20 $SPhenoTadpoles={M112,M222};
21 (* Which parameter to use for UVscaleQ *)
22 $SPhenoMatchingScale=m0;
23 (* Matching to the SM *)
24 $SPhenoRenScale=MA^2;
25 $SPhenoMatchingEWSB=Default[THDMI I];

```

where \$SPhenoEFTmodel defines the low-energy model. All other variables with the SPheno prefix have the same meaning as in the usual SPheno.m file, see Ref. [14]. The usage of \$ExportToSPheno=True automatizes the previously explained steps i.e. ExportToSPheno is already invoked with the correct options.

A.3.2. Reserved Variables

There are a couple of variables that should not be overwritten but can be used in various places

- epsUV
 - Type: Symbol
 - Description: is set to zero at the matching scale (e.g. one parametrize the VEVs with this)
- UVscaleQ
 - Type: Symbol
 - Description: default matching scale used in all loop functions

note that it can be important to use epsUV instead of directly setting e.g. the VEVs to zero because otherwise the tadpole conditions cannot be applied correctly.

A.3.3. Example Usage

A comprehensive example is located in the root directory of the new SARAH version. The MATHEMATICA notebook file `Example_matching.nb` contains the matching of the MSSM to an effective 2HDM described in Section 3.3 using the interactive as well as the batch mode.

Bibliography

- [1] F. Bloch and A. Nordsieck. “Note on the Radiation Field of the Electron”. In: *Phys. Rev.* 52 (2 1937), pp. 54–59. DOI: 10 . 1103/PhysRev . 52 . 54. URL: <https://link.aps.org/doi/10.1103/PhysRev.52.54>.
- [2] C. Patrignani et al. “Review of Particle Physics”. In: *Chin. Phys.* C40.10 (2016), p. 100001. DOI: 10 . 1088/1674-1137/40/10/100001.
- [3] Georges Aad et al. “Observation of a new particle in the search for the Standard Model Higgs boson with the ATLAS detector at the LHC”. In: *Phys.Lett.* B716 (2012), pp. 1–29. DOI: 10 . 1016/j . physletb . 2012 . 08 . 020. arXiv: 1207 . 7214 [hep-ex].
- [4] Serguei Chatrchyan et al. “Observation of a new boson at a mass of 125 GeV with the CMS experiment at the LHC”. In: *Phys.Lett.* B716 (2012), pp. 30–61. DOI: 10 . 1016/j . physletb . 2012 . 08 . 021. arXiv: 1207 . 7235 [hep-ex].
- [5] Albert M Sirunyan et al. “Search for natural and split supersymmetry in proton-proton collisions at $\sqrt{s} = 13$ TeV in final states with jets and missing transverse momentum”. In: *JHEP* 05 (2018), p. 025. DOI: 10 . 1007/JHEP05(2018)025. arXiv: 1802 . 02110 [hep-ex].
- [6] B. C. Allanach and A. Voigt. “Uncertainties in the Lightest CP Even Higgs Boson Mass Prediction in the Minimal Supersymmetric Standard Model: Fixed Order Versus Effective Field Theory Prediction”. In: (2018). arXiv: 1804 . 09410 [hep-ph].
- [7] G. F. Giudice and A. Romanino. “Split supersymmetry”. In: *Nucl. Phys.* B699 (2004). [Erratum: *Nucl. Phys.*B706,487(2005)], pp. 65–89. DOI: 10 . 1016/j . nuclphysb . 2004 . 11 . 048 , 10 . 1016/j . nuclphysb . 2004 . 08 . 001. arXiv: hep-ph/0406088 [hep-ph].
- [8] Gabriel Lee and Carlos E. M. Wagner. “Higgs bosons in heavy supersymmetry with an intermediate m_A ”. In: *Phys. Rev.* D92.7 (2015), p. 075032. DOI: 10 . 1103/PhysRevD . 92 . 075032. arXiv: 1508 . 00576 [hep-ph].
- [9] Emanuele Bagnaschi et al. “Higgs Mass and Unnatural Supersymmetry”. In: *JHEP* 09 (2014), p. 092. DOI: 10 . 1007/JHEP09(2014)092. arXiv: 1407 . 4081 [hep-ph].
- [10] Lucila Zarate. “The Higgs mass and the scale of SUSY breaking in the NMSSM”. In: *JHEP* 07 (2016), p. 102. DOI: 10 . 1007/JHEP07(2016)102. arXiv: 1601 . 05946 [hep-ph].

- [11] Werner Porod. “SPheno, a program for calculating supersymmetric spectra, SUSY particle decays and SUSY particle production at e^+e^- colliders”. In: *Comput. Phys. Commun.* 153 (2003), pp. 275–315. doi: 10.1016/S0010-4655(03)00222-4. arXiv: hep-ph/0301101 [hep-ph].
- [12] W. Porod and F. Staub. “SPheno 3.1: Extensions including flavour, CP-phases and models beyond the MSSM”. In: *Comput. Phys. Commun.* 183 (2012), pp. 2458–2469. doi: 10.1016/j.cpc.2012.05.021. arXiv: 1104.1573 [hep-ph].
- [13] F. Staub. “SARAH”. In: (2008). arXiv: 0806.0538 [hep-ph].
- [14] Florian Staub. “SARAH 4 : A tool for (not only SUSY) model builders”. In: *Comput. Phys. Commun.* 185 (2014), pp. 1773–1790. doi: 10.1016/j.cpc.2014.02.018. arXiv: 1309.7223 [hep-ph].
- [15] Andrzej J. Buras. “Weak Hamiltonian, CP violation and rare decays”. In: *Probing the standard model of particle interactions. Proceedings, Summer School in Theoretical Physics, NATO Advanced Study Institute, 68th session, Les Houches, France, July 28-September 5, 1997. Pt. 1, 2.* 1998, pp. 281–539. arXiv: hep-ph/9806471 [hep-ph].
- [16] Thomas Appelquist and J. Carazzone. “Infrared singularities and massive fields”. In: *Phys. Rev. D* 11 (10 1975), pp. 2856–2861. doi: 10.1103/PhysRevD.11.2856. URL: <https://link.aps.org/doi/10.1103/PhysRevD.11.2856>.
- [17] Burt A. Ovrut and Howard J. Schnitzer. “Gauge Theories With Minimal Subtraction and the Decoupling Theorem”. In: *Nucl. Phys.* B179 (1981), pp. 381–416. doi: 10.1016/0550-3213(81)90011-0.
- [18] Elisabeth K. Katehou and Graham G. Ross. “Decoupling in supersymmetric theories”. In: *Nuclear Physics B* 299.3 (1988), pp. 484–506. ISSN: 0550-3213. doi: [https://doi.org/10.1016/0550-3213\(88\)90546-9](https://doi.org/10.1016/0550-3213(88)90546-9). URL: <http://www.sciencedirect.com/science/article/pii/0550321388905469>.
- [19] Laurie M Brown. *Feynman’s Thesis — A New Approach to Quantum Theory*. WORLD SCIENTIFIC, 2005. doi: 10.1142/5852. eprint: <https://www.worldscientific.com/doi/pdf/10.1142/5852>. URL: <https://www.worldscientific.com/doi/abs/10.1142/5852>.
- [20] Brian Henning, Xiaochuan Lu, and Hitoshi Murayama. “How to use the Standard Model effective field theory”. In: *JHEP* 01 (2016), p. 023. doi: 10.1007/JHEP01(2016)023. arXiv: 1412.1837 [hep-ph].
- [21] Francisco del Aguila, Zoltan Kunszt, and Jose Santiago. “One-loop effective lagrangians after matching”. In: *Eur. Phys. J.* C76.5 (2016), p. 244. doi: 10.1140/epjc/s10052-016-4081-1. arXiv: 1602.00126 [hep-ph].
- [22] Michele Boggia, Raquel Gomez-Ambrosio, and Giampiero Passarino. “Low energy behaviour of standard model extensions”. In: *JHEP* 05 (2016), p. 162. doi: 10.1007/JHEP05(2016)162. arXiv: 1603.03660 [hep-ph].

-
- [23] Brian Henning, Xiaochuan Lu, and Hitoshi Murayama. “One-loop Matching and Running with Covariant Derivative Expansion”. In: *JHEP* 01 (2018), p. 123. DOI: 10.1007/JHEP01(2018)123. arXiv: 1604.01019 [hep-ph].
- [24] Sidney Coleman and Erick Weinberg. “Radiative Corrections as the Origin of Spontaneous Symmetry Breaking”. In: *Phys. Rev. D* 7 (6 1973), pp. 1888–1910. DOI: 10.1103/PhysRevD.7.1888. URL: <https://link.aps.org/doi/10.1103/PhysRevD.7.1888>.
- [25] R. Jackiw. “Functional evaluation of the effective potential”. In: *Phys. Rev. D* 9 (6 1974), pp. 1686–1701. DOI: 10.1103/PhysRevD.9.1686. URL: <https://link.aps.org/doi/10.1103/PhysRevD.9.1686>.
- [26] Stephen P. Martin. “Effective potential at three loops”. In: *Phys. Rev. D* 96.9 (2017), p. 096005. DOI: 10.1103/PhysRevD.96.096005. arXiv: 1709.02397 [hep-ph].
- [27] Thomas Hahn. “Generating Feynman diagrams and amplitudes with FeynArts 3”. In: *Comput. Phys. Commun.* 140 (2001), pp. 418–431. DOI: 10.1016/S0010-4655(01)00290-9. arXiv: hep-ph/0012260 [hep-ph].
- [28] Thomas Hahn, Sebastian Paßehr, and Christian Schappacher. “FormCalc 9 and Extensions”. In: *PoS LL2016* (2016). [J. Phys. Conf. Ser.762,no.1,012065(2016)], p. 068. DOI: 10.1088/1742-6596/762/1/012065. arXiv: 1604.04611 [hep-ph].
- [29] F. Englert and R. Brout. “Broken Symmetry and the Mass of Gauge Vector Mesons”. In: *Phys. Rev. Lett.* 13 (9 1964), pp. 321–323. DOI: 10.1103/PhysRevLett.13.321. URL: <http://link.aps.org/doi/10.1103/PhysRevLett.13.321>.
- [30] Jeffrey Goldstone, Abdus Salam, and Steven Weinberg. “Broken Symmetries”. In: *Phys. Rev.* 127 (1962), pp. 965–970. DOI: 10.1103/PhysRev.127.965.
- [31] P. W. Higgs. “Broken Symmetries and the Masses of Gauge Bosons”. In: *Physical Review Letters* 13 (Oct. 1964), pp. 508–509. DOI: 10.1103/PhysRevLett.13.508.
- [32] P. Sikivie et al. “Isospin breaking in technicolor models”. In: *Nuclear Physics B* 173.2 (1980), pp. 189–207. ISSN: 0550-3213. DOI: [https://doi.org/10.1016/0550-3213\(80\)90214-X](https://doi.org/10.1016/0550-3213(80)90214-X). URL: <http://www.sciencedirect.com/science/article/pii/055032138090214X>.
- [33] W. Buchmuller and D. Wyler. “Effective Lagrangian Analysis of New Interactions and Flavor Conservation”. In: *Nucl. Phys.* B268 (1986), pp. 621–653. DOI: 10.1016/0550-3213(86)90262-2.
- [34] B. Grzadkowski et al. “Dimension-Six Terms in the Standard Model Lagrangian”. In: *JHEP* 10 (2010), p. 085. DOI: 10.1007/JHEP10(2010)085. arXiv: 1008.4884 [hep-ph].

- [35] Emanuele Bagnaschi, Javier Pardo Vega, and Pietro Slavich. “Improved determination of the Higgs mass in the MSSM with heavy superpartners”. In: *Eur. Phys. J. C* 77.5 (2017), p. 334. doi: 10.1140/epjc/s10052-017-4885-7. arXiv: 1703.08166 [hep-ph].
- [36] Savas Dimopoulos and Howard Georgi. “Softly broken supersymmetry and SU(5)”. In: *Nuclear Physics B* 193.1 (1981), pp. 150–162. ISSN: 0550-3213. doi: [https://doi.org/10.1016/0550-3213\(81\)90522-8](https://doi.org/10.1016/0550-3213(81)90522-8). URL: <http://www.sciencedirect.com/science/article/pii/0550321381905228>.
- [37] Brian Batell, Gian F. Giudice, and Matthew McCullough. “Natural Heavy Supersymmetry”. In: *JHEP* 12 (2015), p. 162. doi: 10.1007/JHEP12(2015)162. arXiv: 1509.00834 [hep-ph].
- [38] Stephen P. Martin. “A Supersymmetry primer”. In: (1997). [Adv. Ser. Direct. High Energy Phys.18,1(1998)], pp. 1–98. doi: 10.1142/9789812839657_0001, 10.1142/9789814307505_0001. arXiv: hep-ph/9709356 [hep-ph].
- [39] John F. Gunion et al. “The Higgs Hunter’s Guide”. In: *Front. Phys.* 80 (2000), pp. 1–404.
- [40] S. Dawson. “The MSSM and why it works”. In: *Supersymmetry, supergravity and supercolliders. Proceedings, Theoretical Advanced Study Institute in elementary particle physics, TASI’97, Boulder, USA, June 2-27, 1997*. 1997, pp. 261–339. arXiv: hep-ph/9712464 [hep-ph].
- [41] Abdelhak Djouadi. “The Anatomy of electro-weak symmetry breaking. II. The Higgs bosons in the minimal supersymmetric model”. In: *Phys. Rept.* 459 (2008), pp. 1–241. doi: 10.1016/j.physrep.2007.10.005. arXiv: hep-ph/0503173 [hep-ph].
- [42] Yuri Shirman. “Introduction to Supersymmetry and Supersymmetry Breaking”. In: *Proceedings of Theoretical Advanced Study Institute in Elementary Particle Physics on The dawn of the LHC era (TASI 2008): Boulder, USA, June 2-27, 2008*. 2010, pp. 359–422. doi: 10.1142/9789812838360_0008. arXiv: 0907.0039 [hep-ph]. URL: <https://inspirehep.net/record/824631/files/arXiv:0907.0039.pdf>.
- [43] Sidney Coleman and Jeffrey Mandula. “All Possible Symmetries of the S Matrix”. In: *Phys. Rev.* 159 (5 1967), pp. 1251–1256. doi: 10.1103/PhysRev.159.1251. URL: <https://link.aps.org/doi/10.1103/PhysRev.159.1251>.
- [44] Rudolf Haag, Jan T. Lopuszanski, and Martin Sohnius. “All possible generators of supersymmetries of the S-matrix”. In: *Nuclear Physics B* 88.2 (1975), pp. 257–274. ISSN: 0550-3213. doi: 10.1016/0550-3213(75)90279-5. URL: <http://www.sciencedirect.com/science/article/pii/0550321375902795>.
- [45] Ulrich Ellwanger, Cyril Hugonie, and Ana M. Teixeira. “The Next-to-Minimal Supersymmetric Standard Model”. In: *Phys. Rept.* 496 (2010), pp. 1–77. doi: 10.1016/j.physrep.2010.07.001. arXiv: 0910.1785 [hep-ph].

- [46] P. A. R. Ade et al. “Planck 2015 results. XIII. Cosmological parameters”. In: *Astron. Astrophys.* 594 (2016), A13. doi: 10.1051/0004-6361/201525830. arXiv: 1502.01589 [astro-ph.CO].
- [47] Steven Weinberg. “The cosmological constant problem”. In: *Rev. Mod. Phys.* 61 (1 1989), pp. 1–23. doi: 10.1103/RevModPhys.61.1. URL: <https://link.aps.org/doi/10.1103/RevModPhys.61.1>.
- [48] Steven Weinberg. “Anthropic Bound on the Cosmological Constant”. In: *Phys. Rev. Lett.* 59 (22 1987), pp. 2607–2610. doi: 10.1103/PhysRevLett.59.2607. URL: <https://link.aps.org/doi/10.1103/PhysRevLett.59.2607>.
- [49] G’t Hooft. “Naturalness, Chiral Symmetry, and Spontaneous Chiral Symmetry Breaking”. In: *Recent Developments in Gauge Theories*. Ed. by G’t Hooft et al. Boston, MA: Springer US, 1980, pp. 135–157. ISBN: 978-1-4684-7571-5. doi: 10.1007/978-1-4684-7571-5_9. URL: https://doi.org/10.1007/978-1-4684-7571-5_9.
- [50] I. Jack, D. R. T. Jones, and K. L. Roberts. “Equivalence of dimensional reduction and dimensional regularisation”. In: *Zeitschrift für Physik C Particles and Fields* 63.1 (1994), pp. 151–159. ISSN: 1431-5858. doi: 10.1007/BF01577555. URL: <https://doi.org/10.1007/BF01577555>.
- [51] Steven Weinberg. “Effective gauge theories”. In: *Physics Letters B* 91.1 (1980), pp. 51–55. ISSN: 0370-2693. doi: [https://doi.org/10.1016/0370-2693\(80\)90660-7](https://doi.org/10.1016/0370-2693(80)90660-7). URL: <http://www.sciencedirect.com/science/article/pii/0370269380906607>.
- [52] Lawrence Hall. “Grand unification of effective gauge theories”. In: *Nuclear Physics B* 178.1 (1981), pp. 75–124. ISSN: 0550-3213. doi: [https://doi.org/10.1016/0550-3213\(81\)90498-3](https://doi.org/10.1016/0550-3213(81)90498-3). URL: <http://www.sciencedirect.com/science/article/pii/0550321381904983>.
- [53] Patrick Draper and Heidi Rzehak. “A Review of Higgs Mass Calculations in Supersymmetric Models”. In: *Phys. Rept.* 619 (2016), pp. 1–24. doi: 10.1016/j.physrep.2016.01.001. arXiv: 1601.01890 [hep-ph].
- [54] Henning Bahl et al. “Reconciling EFT and hybrid calculations of the light MSSM Higgs-boson mass”. In: *Eur. Phys. J. C* 78.1 (2018), p. 57. doi: 10.1140/epjc/s10052-018-5544-3. arXiv: 1706.00346 [hep-ph].
- [55] Henning Bahl and Wolfgang Hollik. “Precise prediction for the light MSSM Higgs boson mass combining effective field theory and fixed-order calculations”. In: *Eur. Phys. J. C* 76.9 (2016), p. 499. doi: 10.1140/epjc/s10052-016-4354-8. arXiv: 1608.01880 [hep-ph].
- [56] T. Hahn et al. “High-Precision Predictions for the Light CP -Even Higgs Boson Mass of the Minimal Supersymmetric Standard Model”. In: *Phys. Rev. Lett.* 112.14 (2014), p. 141801. doi: 10.1103/PhysRevLett.112.141801. arXiv: 1312.4937 [hep-ph].

- [57] R. V. Harlander et al. “The light CP-even MSSM Higgs mass resummed to fourth logarithmic order”. In: (2018). arXiv: 1807.03509 [hep-ph].
- [58] Peter Athron et al. “FlexibleSUSY 2.0: Extensions to investigate the phenomenology of SUSY and non-SUSY models”. In: *Comput. Phys. Commun.* 230 (2018), pp. 145–217. doi: 10.1016/j.cpc.2018.04.016. arXiv: 1710.03760 [hep-ph].
- [59] Florian Staub and Werner Porod. “Improved predictions for intermediate and heavy Supersymmetry in the MSSM and beyond”. In: *Eur. Phys. J. C* 77.5 (2017), p. 338. doi: 10.1140/epjc/s10052-017-4893-7. arXiv: 1703.03267 [hep-ph].
- [60] Javier Pardo Vega and Giovanni Villadoro. “SusyHD: Higgs mass Determination in Supersymmetry”. In: *JHEP* 07 (2015), p. 159. doi: 10.1007/JHEP07(2015)159. arXiv: 1504.05200 [hep-ph].
- [61] Martin Gorbahn et al. “The supersymmetric Higgs sector and $B - \bar{B}$ mixing for large $\tan \beta$ ”. In: *Phys. Rev. D* 84 (2011), p. 034030. doi: 10.1103/PhysRevD.84.034030. arXiv: 0901.2065 [hep-ph].
- [62] James D. Wells. “Implications of supersymmetry breaking with a little hierarchy between gauginos and scalars”. In: *11th International Conference on Supersymmetry and the Unification of Fundamental Interactions (SUSY 2003) Tucson, Arizona, June 5-10, 2003*. 2003. arXiv: hep-ph/0306127 [hep-ph].
- [63] Karim Benakli et al. “A Fake Split Supersymmetry Model for the 126 GeV Higgs”. In: *JHEP* 05 (2014), p. 113. doi: 10.1007/JHEP05(2014)113. arXiv: 1312.5220 [hep-ph].
- [64] S. V. Demidov, D. S. Gorbunov, and D. V. Kirpichnikov. “Split NMSSM with electroweak baryogenesis”. In: *JHEP* 11 (2016). [Erratum: JHEP08,080(2017)], p. 148. doi: 10.1007/JHEP11(2016)148, 10.1007/JHEP08(2017)080. arXiv: 1608.01985 [hep-ph].
- [65] S. V. Demidov and D. S. Gorbunov. “Non-minimal Split Supersymmetry”. In: *JHEP* 02 (2007), p. 055. doi: 10.1088/1126-6708/2007/02/055. arXiv: hep-ph/0612368 [hep-ph].
- [66] Stefan Liebler. “LHC phenomenology and higher order electroweak corrections with and without R-parity”. In: (2012).
- [67] Michael E. Peskin and Daniel V. Schroeder. *An Introduction to quantum field theory*. Reading, USA: Addison-Wesley, 1995. ISBN: 9780201503975, 0201503972. URL: <http://www.slac.stanford.edu/~mpeskin/QFT.html>.
- [68] Karina E. Williams. “The Higgs sector of the complex minimal supersymmetric standard model”. In: (2008).
- [69] G. 't Hooft and M. Veltman. “Scalar one-loop integrals”. In: *Nuclear Physics B* 153 (1979), pp. 365–401. ISSN: 0550-3213. doi: [https://doi.org/10.1016/0550-3213\(79\)90605-9](https://doi.org/10.1016/0550-3213(79)90605-9). URL: <http://www.sciencedirect.com/science/article/pii/0550321379906059>.

-
- [70] Sebastian A. R. Ellis and James D. Wells. “High-scale supersymmetry, the Higgs boson mass, and gauge unification”. In: *Phys. Rev. D* 96.5 (2017), p. 055024. DOI: 10.1103/PhysRevD.96.055024. arXiv: 1706.00013 [hep-ph].
- [71] Max F. Zoller. “Standard Model beta-functions to three-loop order and vacuum stability”. In: *17th International Moscow School of Physics and 42nd ITEP Winter School of Physics Moscow, Russia, February 11-18, 2014*. 2014. arXiv: 1411.2843 [hep-ph]. URL: <https://inspirehep.net/record/1327250/files/arXiv:1411.2843.pdf>.
- [72] Howard E. Haber and Ralf Hempfling. “The Renormalization group improved Higgs sector of the minimal supersymmetric model”. In: *Phys. Rev. D* 48 (1993), pp. 4280–4309. DOI: 10.1103/PhysRevD.48.4280. arXiv: hep-ph/9307201 [hep-ph].
- [73] M. Beneke, P. Ruiz-Femenia, and M. Spinrath. “Higgs couplings in the MSSM at large $\tan(\beta)$ ”. In: *JHEP* 01 (2009), p. 031. DOI: 10.1088/1126-6708/2009/01/031. arXiv: 0810.3768 [hep-ph].
- [74] A. Djouadi et al. “The post-Higgs MSSM scenario: Habemus MSSM?” In: *Eur. Phys. J. C* 73 (2013), p. 2650. DOI: 10.1140/epjc/s10052-013-2650-0. arXiv: 1307.5205 [hep-ph].
- [75] Henning Bahl and Wolfgang Hollik. “Precise prediction of the MSSM Higgs boson masses for low M_A ”. In: (2018). arXiv: 1805.00867 [hep-ph].
- [76] T. D. Lee. “A Theory of Spontaneous T Violation”. In: *Phys. Rev. D* 8 (1973). [516(1973)], pp. 1226–1239. DOI: 10.1103/PhysRevD.8.1226.
- [77] G. C. Branco et al. “Theory and phenomenology of two-Higgs-doublet models”. In: *Phys. Rept.* 516 (2012), pp. 1–102. DOI: 10.1016/j.physrep.2012.02.002. arXiv: 1106.0034 [hep-ph].
- [78] N. Arkani-Hamed et al. “Aspects of Split Supersymmetry”. In: *Nuclear Physics B* 709.1 (2005), pp. 3–46. ISSN: 0550-3213. DOI: <https://doi.org/10.1016/j.nuclphysb.2004.12.026>. URL: <http://www.sciencedirect.com/science/article/pii/S0550321304010259>.
- [79] M. Aaboud et al. “Search for direct top squark pair production in final states with two leptons in $\sqrt{s} = 13$ TeV pp collisions with the ATLAS detector”. In: *Eur. Phys. J. C* 77.12 (2017), p. 898. DOI: 10.1140/epjc/s10052-017-5445-x. arXiv: 1708.03247 [hep-ex].
- [80] Albert M Sirunyan et al. “Search for supersymmetry in events with a τ lepton pair and missing transverse momentum in proton-proton collisions at $\sqrt{s} = 13$ TeV”. In: (2018). arXiv: 1807.02048 [hep-ex].
- [81] A. M. Sirunyan et al. “Combined search for electroweak production of charginos and neutralinos in proton-proton collisions at $\sqrt{s} = 13$ TeV”. In: *JHEP* 03 (2018), p. 160. DOI: 10.1007/JHEP03(2018)160. arXiv: 1801.03957 [hep-ex].

- [82] Morad Aaboud et al. “Search for pair production of higgsinos in final states with at least three b -tagged jets in $\sqrt{s} = 13$ TeV pp collisions using the ATLAS detector”. In: *Submitted to: Phys. Rev.* (2018). arXiv: 1806.04030 [hep-ex].
- [83] Kingman Cheung et al. “Dark Matter in Split SUSY with Intermediate Higgses”. In: *JHEP* 04 (2015), p. 151. doi: 10.1007/JHEP04(2015)151. arXiv: 1411.7329 [hep-ph].
- [84] W. Kilian et al. “Split supersymmetry at colliders”. In: *Eur. Phys. J. C* 39 (2005), pp. 229–243. doi: 10.1140/epjc/s2004-02046-5. arXiv: hep-ph/0408088 [hep-ph].
- [85] Nima Arkani-Hamed et al. “Simply Unnatural Supersymmetry”. In: (2012). arXiv: 1212.6971 [hep-ph].
- [86] Ulrich Ellwanger and Cyril Hugonie. “The higgsino-singlino sector of the NMSSM: Combined constraints from dark matter and the LHC”. In: (2018). arXiv: 1806.09478 [hep-ph].
- [87] S.V. Demidov, D.S. Gorbunov, and D.V. Kirpichnikov. “Gravitational waves from phase transition in split NMSSM”. In: *Physics Letters B* 779 (2018), pp. 191–194. ISSN: 0370-2693. doi: <https://doi.org/10.1016/j.physletb.2018.02.007>. url: <http://www.sciencedirect.com/science/article/pii/S0370269318301096>.
- [88] Hyun Min Lee et al. “Discrete R symmetries for the MSSM and its singlet extensions”. In: *Nuclear Physics B* 850.1 (2011), pp. 1–30. ISSN: 0550-3213. doi: <https://doi.org/10.1016/j.nuclphysb.2011.04.009>. url: <http://www.sciencedirect.com/science/article/pii/S0550321311002331>.
- [89] B. C. Allanach et al. “SUSY Les Houches Accord 2”. In: *Comput. Phys. Commun.* 180 (2009), pp. 8–25. doi: 10.1016/j.cpc.2008.08.004. arXiv: 0801.0045 [hep-ph].
- [90] Philip Bechtle et al. “HIGGSBOUNDS-4: Improved Tests of Extended Higgs Sectors against Exclusion Bounds from LEP, the Tevatron and the LHC”. In: *Eur. Phys. J. C* 74.3 (2014), p. 2693. doi: 10.1140/epjc/s10052-013-2693-2. arXiv: 1311.0055 [hep-ph].
- [91] D. Barducci et al. “Collider limits on new physics within micrOMEGAs 4.3”. In: *Comput. Phys. Commun.* 222 (2018), pp. 327–338. doi: 10.1016/j.cpc.2017.08.028. arXiv: 1606.03834 [hep-ph].
- [92] Paul Bergeron, Pearl Sandick, and Kuver Sinha. “Theoretical Uncertainties in the Calculation of Supersymmetric Dark Matter Observables”. In: *JHEP* 05 (2018), p. 113. doi: 10.1007/JHEP05(2018)113. arXiv: 1712.05491 [hep-ph].
- [93] Alexander Belyaev, Neil D. Christensen, and Alexander Pukhov. “CalcHEP 3.4 for collider physics within and beyond the Standard Model”. In: *Comput. Phys. Commun.* 184 (2013), pp. 1729–1769. doi: 10.1016/j.cpc.2013.01.014. arXiv: 1207.6082 [hep-ph].

- [94] Manuel E. Krauss and Florian Staub. “Unitarity constraints in triplet extensions beyond the large s limit”. In: *Phys. Rev. D* 98.1 (2018), p. 015041. DOI: 10.1103/PhysRevD.98.015041. arXiv: 1805.07309 [hep-ph].
- [95] Mark D. Goodsell and Florian Staub. “Unitarity constraints on general scalar couplings with SARAH”. In: (2018). arXiv: 1805.07306 [hep-ph].
- [96] J. E. Camargo-Molina et al. “**Vevacious**: A Tool For Finding The Global Minima Of One-Loop Effective Potentials With Many Scalars”. In: *Eur. Phys. J. C* 73.10 (2013), p. 2588. DOI: 10.1140/epjc/s10052-013-2588-2. arXiv: 1307.1477 [hep-ph].
- [97] Oscar Stal and Tim Stefaniak. “Constraining extended Higgs sectors with HiggsSignals”. In: *PoS EPS-HEP2013* (2013), p. 314. arXiv: 1310.4039 [hep-ph].

Acknowledgements

Particle physics belongs to one of the most exciting research fields. Thus, I thank Prof. Dr. Mühlleitner for giving me the opportunity to work on this interesting and relatively new topic as well as for the kind integration into her workgroup. In particular, I want to thank Prof. Mühlleitner and my supervisor Dr. Staub for sending me to various research conferences to present my own work as well as to make new connections in the research community.

In addition, I want to thank my supervisor Dr. Staub for countless explanations on the topic, being patient with my ignorance, for the opportunity to contribute to the computer tool SARAH -which is the BSM flagship- and last but not least for the great time.

I'm also grateful for discussions within numerous working group meetings as well as with my room mates Jonas and Philipp. Special thanks go to Florian, Shruti, Stefan, Marcel and Jonas for proof-reading this thesis.

Besonderer Dank gilt meiner Familie, meinen Eltern Wolfgang und Anke sowie meiner Lebensgefährtin Natascha für die seelische und finanzielle Unterstützung, die meine bisherige akademischen Ausbildung erst ermöglicht hat.